

Digital converters for high speed coherent optical communication

Mahmood Abu-Romoh

Doctor of Philosophy

Aston University

March 2022

© Mahmood Abu- Romoh, 2022

Mahmood Abu-Romoh asserts his moral right to be identified as the author of this thesis.

This copy of the thesis has been supplied on condition that anyone who consults it is understood to recognise that its copyright belongs to its author and that no quotation from the thesis and no information derived from it may be published without appropriate permission or acknowledgement.

I would like to dedicate this thesis to my loving parents ...

Declaration

I hereby declare that except where specific reference is made to the work of others, the contents of this dissertation are original and have not been submitted in whole or in part for consideration for any other degree or qualification in this, or any other university. This dissertation is my own work and contains nothing which is the outcome of work done in collaboration with others, except as specified in the text and Acknowledgements. This dissertation contains fewer than 20,000 words including appendices, bibliography, footnotes, tables and equations and has fewer than 60 figures.

Mahmood Abu-Romoh
March 2022

Acknowledgements

I would like to extend my sincere gratitude to my supervisor, Prof. Wladek, for his unwavering support and guidance throughout my academic journey. Your expertise, encouragement, and motivation were invaluable in helping me complete this thesis.

I would also like to express my heartfelt thanks to all the friends and colleagues I met at Aston, who made my time here a truly enriching experience. Your support and camaraderie have been instrumental in shaping my knowledge and understanding of this field.

I would also like to express my appreciation to the examiners who have taken the time to carefully evaluate my thesis. Your constructive comments and feedback have been instrumental in improving the quality of my work.

Finally, I would like to dedicate this thesis to my parents Nidal and Rana, who have been a constant source of love, encouragement, and inspiration throughout my life. Your unwavering support and belief in me has been the driving force behind my success. I would also like to extend my love and gratitude to my brothers and sisters, Mohannad, Mais, Roaa and Mohammad, for their love and support. Last but not least, my loving fiancé Yomna, for her unwavering love and support from the moment we met. Your presence brings all the joy to my life.

Abstract

This thesis focuses on high speed digital converters in optical transmission systems. The study is divided into a literature review and three chapters, each exploring a specific aspect of digital converters, its characteristics and limitations and potential solutions for next generations of optical transceivers.

The thesis examines integral non-linearity (INL) in high-speed digital converters, particularly in coherent optical communication systems. The chapter provides an overview of INL, its metrics such as total harmonic distortion and signal-to-noise and distortion ratio, and their impact on DAC resolution measured through effective number of bits. Experimental measurements of INL are also presented and they show direct proportional correlation between INL and the effective number of bits (ENOB). Supported by experimental results, it has been shown that INL adds 0.15 dB loss for each 2 LSB increment in a B2B 256QAM/23 GBaud configuration.

The thesis explores the use of Artificial Neural Networks (ANNs) for compensating for non-linearity in digital converters. The chapter introduces Machine Learning, ANNs, and their application as pre-distorters to improve optical transmission system performance. It has been shown that ANNs are capable of recovering up to 75% of INL performance degradation in 64QAM/32GBaud configuration.

The thesis presents a detailed study of the digital resolution enhancement technique for low-resolution digital converters in optical transmission systems. The technique utilizes optimized quantization levels and advanced digital signal processing algorithms to mitigate quantization noise. Numerical simulations and experimental studies demonstrate the feasibility and efficacy of the DRE technique. They showed a mutual information improvement of up to 0.65 dB for a 64QAM/64GBaud with 4 bit DAC comparing to not using digital resolution enhancement.

In conclusion, this thesis provides evidence that the DRE technique is an effective solution for reducing quantization noise in low-resolution DACs and improving performance in optical transmission systems. The study highlights the importance of controlling INL and the potential of ANNs for non-linearity compensation.

Table of contents

List of figures	xiii
Nomenclature	xvii
1 Introduction	1
1.1 Background	1
1.2 Thesis structure	4
1.3 Thesis key contributions	5
1.4 List of publications	6
2 Coherent optical transceivers	7
2.1 Main building blocks of coherent optical transceivers	7
2.1.1 Digital converters	10
2.1.2 Mach-Zehnder Modulators	12
2.1.3 Lasers (LO & CW)	13
2.1.4 90 degree hybrids and photo diodes	14
2.2 DSP for coherent optical communication	17
2.2.1 I/Q imbalances compensation	19
2.2.2 Equalization	20
2.2.3 Timing recovery	24
2.2.4 Frequency and phase recovery (Carrier recovery)	24
2.2.5 Probabilistic constellation shaping	25
2.3 Spectral efficiency and up-scaling methods	26
2.4 Conclusion	28
3 Non-linearity in Digital to Analogue converters	31
3.1 Theory	31
3.1.1 The distinction between integral and differential non-linearity	32
3.1.2 Performance metrics (THD,SINAD and ENOB)	34

3.2	Practical INL measurements	37
3.2.1	Theory	37
3.2.2	Experimental measurements	40
3.2.3	Modelling	41
3.3	INL effect on ENOB	43
3.4	INL effect on coherent transmission	45
3.5	Conclusion	46
4	Neural networks for digital converters non-linearity compensation	49
4.1	Machine learning	51
4.1.1	Learning algorithms	51
4.1.2	Artificial neural networks	54
4.2	Artificial neural networks for INL compensation	59
4.2.1	Indirect learning	60
4.2.2	Analytical study and results	61
4.3	Conclusion	64
5	Digital resolution enhancer to enable low resolution digital to analogue converters	65
5.1	Digital resolution enhancer	70
5.1.1	Effective quantization noise	70
5.1.2	Dynamic quantization	72
5.2	Probabilistic constellation shaping	74
5.3	Analytical studies	75
5.3.1	Probabilistic shaping optimization	75
5.3.2	PCS gains for a 4 bit DAC with DRE	78
5.4	Experimental studies	79
5.5	Conclusion	81
6	Conclusion and future work	83
6.1	Conclusion	83
6.2	Future work	84
	References	87

List of figures

1.1	Internet traffic growth expectations according to cisco forecast	2
2.1	Ways to increase the spectral efficiency in coherent optical communication systems	8
2.2	Block diagram of conventional optical coherent transmitter	10
2.3	Simplified DAC operation on analogue symbols	11
2.4	The transfer function of zero order hold DAC	12
2.5	A schematic diagram of a dual arm Mach-Zehnder modulator and a graphical illustration for the phase and in-phase modulation of a 16-QAM	13
2.6	Signal spectrum after optical demodulation using a (a) intradyne receiver (b) homodyne receiver	15
2.7	Block diagram of conventional optical coherent receiver	16
2.8	Optical coherent transmission system non-idealities	18
2.9	Conventional DSP chain in a coherent receiver	19
2.10	Gram-Schmidt orthogonalization procedure	20
2.11	Constellation diagram for samples before and after applying adaptive filtering using constant modulus algorithm	23
2.12	Constellation diagram for samples before and after applying adaptive filtering using Decision Directed Least Mean Square algorithm	24
2.13	The relationship between transceiver's SNR and achievable information rate	26
2.14	A graphical comparison of assigned probability of occurrence for constellation points in a) a uniform 16-QAM (b) a probabilistically shaped 16-QAM	27
3.1	A simple binary weighted current switching DAC with N bits resolution . .	32
3.2	Transfer function for an ideal 3 bits DAC	33
3.3	Types of INL in DACs	36
3.4	The spectrum of harmonics and spurs generated at the output of a digital converter with a single sinusoid f_C input	37

3.5	Sinusoidal histogram test mechanism	39
3.6	Illustration for sine wave PDF difference of actual and ideal digital converter	40
3.7	A comparison of the euclidean distance between two adjacent constellation points in 256, 64 and 16-QAM	41
3.8	Block diagram for SHT applied on Electrical back to back 8 bits/ 92 GSamples/s DAC/ADC setup	42
3.9	INL measured for all codes in a real commercial 8 bits/ 92 GSamples/s DAC/ADC using SHT	42
3.10	INL model constructed based on experimental results	43
3.11	A comparison between model added INL and measured INL by applying SHT	44
3.12	A comparison of different harmonics magnitudes for different INL variations	45
3.13	ENOB degradation for different INL values	46
3.14	An experimental optical back to back setup for a coherent optical transmission system	47
3.15	The effect of different INL values on OSNR vs mutual information performance for a 256-QAM configuration	47
4.1	Visual illustration for two types of supervised learning: classification and regression	52
4.2	Visual illustration for K-means clustering method	53
4.3	Illustration for sine wave PDF difference of actual and ideal digital converter	53
4.4	Schematic of an artificial neuron with n inputs	55
4.5	Performing classification by an artificial neural network with linear and non-linear activation function	56
4.6	Linear activation function	57
4.7	Sigmoid and hyperbolic tangent activation functions	58
4.8	ReLU activation function	59
4.9	The INL pre-distorter's indirect learning structure	61
4.10	Block diagram for the optical back to back transmission system used the simulation study including pre-distorter and INL model	62
4.11	BER vs OSNR curves for 64 QAM, 32 GBaud and 32 QAM, 32 GBaud with 5 bits resolution DAC in two scenarios (a) INL = 2 LSB (b) INL = 4 LSB	63
4.12	Constellation diagram comparison to illustrate the effect of applying ANN pre-distorter to 64 QAM, 32 GBaud signal under INL = 4 LSB	63
5.1	The theoretical channel capacity vs SNR relationship	69

5.2	Simplified block diagram for an optical transmission system to illustrate the combine channel impulse response $h_c(n)$ components	72
5.3	Schematic diagram to illustrate the dynamic quantization problem	73
5.4	Trellis diagram for a dynamic quantization problem	74
5.5	Block diagram for the optical back-to-back transmission system used in the experimental and simulation study including probabilistic shaping and digital resolution enhancement	76
5.6	A heat map shows the performance in terms MI for different SNR vs PCS factors. The scale bar ranges from 0 to 1 where 0 corresponds to lowest achievable MI and 1 corresponds to highest achievable MI at each SNR. . .	77
5.7	Performance in terms of MI versus channel SNR for simulated 64-Gbd/64-QAM modulation in different scenarios with DRE compared to Shannon's limit (black) and uniform modulation w/o DRE (red).	78
5.8	Performance improvement reflected in recovered constellations after applying DSP at receiver side. The improvement is due to applying DRE in two different scenarios. (a) Uniform 64GBd/64-QAM without applying DRE, (b) Uniform 64-GBd/64-QAM with applying DRE, (c) Probabilistically shaped 64-GBd/64-QAM without applying DRE, (d) Probabilistically shaped 64-GBd/64-QAM with applying DRE.	80
5.9	Performance in terms of MI versus channel SNR for experimental 64-Gbd/64-QAM modulation in different scenarios with DRE compared to Shannon's limit (black) and uniform modulation w/o DRE (red)	80

Nomenclature

Greek Symbols

j unit imaginary number $\sqrt{-1}$

Acronyms / Abbreviations

ADC Analogue to digital conversion/converter

ANN Artificial neural network

ASE Amplified spontaneous emission

AWGN Additive white Gaussian noise

B2B Back to back

BER Bit error rate

CD Chromatic dispersion

CMA Constant modulus algorithm

CMOS Complementary metal oxide semiconductor

CW Continuous wave

DAC Digital to analogue conversion/converter

DCI Data center interconnect

DD-LMS Decision directed least mean square

DNL Deferential Non-Linearity

DNL Differential non linearity

DP Dual polarization

DQ Dynamic quantization

DQPSK Differential phase shift keying

DSP Digital system processing / processor

DWDM Dense wavelength division multiplexing

EAM Electron-absorption modulator

EDFA Erbium doped fibre amplifier

ENOB Effective number of bits

FEC Forward error correction

FIR Finite impulse response

FS Full scale

FWM Four wave mixing

GSOP Gram-Schmidt orthogonalization procedure

HQ-VOD High quality video on demand

IM/DD Intensity modulation and direct detection

INL Integral Non-Linearity

IoT Internet of things

ISD Information spectral density

ISI Inter-symbol interference

LASER light amplification by stimulated emission of radiation

LO Local oscillator

LSB Least significant bit

MAP Maximum a posteriori probability

MF Matched Filter

MIMO Multiple input multiple output

ML Machine learning

MMSE Minimum mean square error

MSE Mean square error

MZM Mach-Zehnder modulator

OOK On Off keying

OPEX Operating expenses

OPLL Optical phase locked loop

PBC Polarization beam combiner

PBS Polarization beam splitter

PCS Probabilistic constellation shaping

PD PhotoDiode

PMD Polarization mode dispersion

PO Phase offset

PSD Power spectrum density

QAM Quadrature amplitude modulation

QPSK Quadrature shift keying

ReLU Rectified Linear Unit

RF Radio frequency

RLS Recursive least square

RMS Root mean square

RRC Root raised cosine

SE Spectral efficiency

SINAD Signal to noise and distortion ratio

STR Square law timing recovery

TIA Trans-impedance amplifier

VoIP Voice over IP

WDM Wavelength division multiplexing

Chapter 1

Introduction

1.1 Background

It's undoubtedly a fact that the world is moving expeditiously towards more dependency on internet based applications. According to forecasts, the Global monthly internet traffic, which is an explicit indication of the global data consumption, is expected to roughly reach the level of 280 Exabytes ($1\text{Exabyte} = 10^6\text{Terabytes}$) by the end of year 2021. This expectation clearly shows that comparing to 2016, the internet global traffic will be tripled in 2021 driven by all of the bandwidth hungry applications and services such as voice over IP (VoIP), high quality Video on demand (HQ-VOD), Virtual and Augmented reality with immersive graphics, internet of things (IoT) devices and abundant multimedia sharing platforms [1]. As over than 95% of the VoIP and data traffic between countries and continents and almost 100% of the internet traffic are transferred at some point via optical fibres [2], increasing the throughput rate of optical communication systems became extremely desirable to cope with global needs. Since the advent of optical communication systems, supported by the demonstration of the first LASER by Theodore H. Maiman in the early sixties and the introduction of suitable optical fibre fabrication processes which could minimise the extrinsic losses in the medium to an acceptable level for transmission, optical transceivers and optical transmission lines went through a few radical changes which significantly increased the maximum throughput and allowed for better exploitation for the optical extensive bandwidth [3] [4]. For instance, the invention of Erbium Doped Fibre Amplifier (EDFA) was one of the breakthroughs which significantly extended the maximum reach of optical communication systems. Modern long reach optical communication systems underwent several remarkable changes in the last three decades which significantly increased the overall capacity of these systems as shown in fig 1.1. One of the latest distinguishable advances in optical transceivers' architecture is the shift from the conventional simple ON-OFF keying (OOK) scheme based

on intensity modulation and direct detection (IM/DD) to Quadrature shift keying (QPSK) based on coherent detection. This leap started by firstly introducing the so called “Self-coherent detection” or what is known as “Differential phase shift keying” (DQPSK) which utilizes the orthogonal in-phase and quadrature components of the signal into doubling the information spectral density (ISD) from 1 b/s/Hz to 2 b/s/Hz comparing to OOK IM/DD [5]. To extract the In-phase and quadrature components from the received DQPSK signal, the receiver simply compares the current received symbol with the deliberately delayed previous received symbol which gives a clear indication of the value of the I and Q components of the current symbol. Despite the fact that DQPSK introduced a significant improvement to the system in term of better utilisation of the available bandwidth compared to the conventional OOK IM/DD, one extra attribute of the optical field hasn’t been taken into consideration which is the light’s polarization.

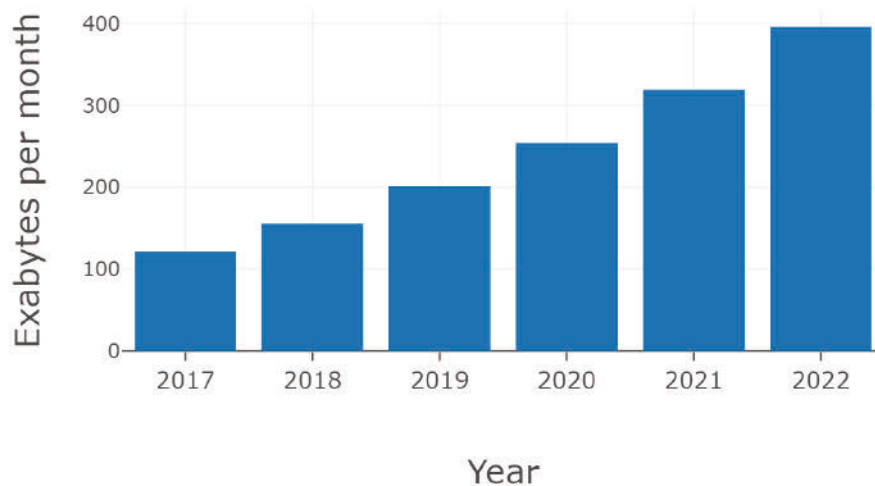


Fig. 1.1 Internet traffic growth expectations according to cisco forecast [6]

Full optical coherent detection communication systems arrived later to achieve higher ISD by exploiting the dual polarization nature of light. The first implementation of a dual polarization (DP) based system has been introduced in 2005 and called DP-QPSK [7]. The main difference between DP based systems and DQPSK systems is that the first type employs an external laser at the receiver side as a local oscillator (LO) to retrieve the implicit information in polarizations while the latter one doesn’t require any LOs since the signal is mixed by itself at the receiver side. There is no doubt that implementing a dual polarization based system requires additional components such as optical hybrids, local

oscillators and additional photodiodes. However, the aforementioned costs are reasonable taking into consideration the higher achievable bit rate and the robustness against channel noise comparing to self-coherent detection scheme.

The advent of faster, more reliable and energy efficient digital system processors (DSPs) supported by high speed digital to analogue converters (DACs) and analogue to digital converters (ADCs), which showed significant improvements due to the big leap in the field of CMOS designing and fabrication, stretched the optical transceivers capabilities. DSPs illustrated their strength by offering cost effective solutions to estimate and compensate for wide variety of channel impairments and transceiver noises, distortions and bandwidth limitations. The first application for DSP in optical transceivers was to compensate for chromatic dispersion (CD) [8], [9] and polarization mode dispersion (PMD) [10] then it extended to mitigate and compensate for other effects such as frequency offset (FO), IQ impairments, phase offset (PO), Components bandwidth limitations, Polarization rotation and many others. The introduction of DSP in optical communication systems was an absolute breakthrough since it effectively assisted in achieving high optical signal to noise ratio (OSNR) versus bit error rate (BER) gains which opened the door for designers to achieve higher baud rates and utilize higher cardinality modulation formats to reach bit rates up to 600Gbits/s per transceiver [11]. Notwithstanding the high maturity which optical DSPs have reached in a short period of time, there are still many limitations which obstruct the maximum optical achievable throughput of approaching Shannon's capacity limit. One of these limitations lies on the operational frontiers in electronic components in both optical transmitters and receivers beside the electrical to optical convertors (Mach-Zehnder modulators) non-idealities.

Since the scope of this research will extensively focus on digital convertors' resolution, timing accuracy, synchronization and bandwidth as some of the main limitations in modern optical communication systems, it worth emphasising that digital convertors' limited bandwidth combined with the frequency roll off effect of RF drivers act as limiting factor for the maximum achievable bit rate. On the other hand, digital convertors' resolution is the main limitation for utilising higher cardinality modulation formats. Taking into consideration that fabricating more compact, faster ADC/DAC chips with higher resolution might not be as cost effective as before especially that fabricating denser CMOS chips will require more advanced lithography methods and will be confronted by the necessity of minimising the power dissipation in transistors for lower than 8 nm chips . Moreover, good isolation methods will be required to prevent any crosstalk which imposes another challenge to be considered. Not mentioning the physical limitation of minimising the gates' size to the atomic level which might induce different quantum effects [12]. All of these difficulties will certainly

increase the net cost of next generations of ADC/DAC chips, hence, the cost of future optical transceivers. In light of the aforementioned facts, it's vitally important to apply an in-depth study on the current DAC/ADC limitations in optical communication systems to address the possible trade-offs which can be considered in designing and fabricating. Moreover, it's also beneficial to find the optimum DSP methods to compensate for the ADC/DAC limitations and exploit their available capabilities to the max.

1.2 Thesis structure

The remaining 5 chapters are organized as follows :

Chapter 2 presents the fundamental building blocks of an optical coherent transceiver. The variety of electrical and optical components which takes a part of the transmission system have been described and their underlying physical and mathematical models have been discussed. The chapter has focused on the sources of noise and distortion in a typical coherent transceiver. Moreover, the DSP chain which compensates for transmission those non-idealities has been explained. Finally, The concept of spectral efficiency and different approaches of up scaling it have been illustrated.

Chapter 3 goes in-depth by discussing digital converters as one of the essential building blocks of any coherent optical transceiver. In this chapter, digital converters performance assessment metrics such as integral non-linearity (INL), signal to noise and distortion ratio (SINAD) and effective number of bits (ENOB) and their mathematical representation have been explained. The chapter focuses on INL as one of the major ENOB static contributors. The chapter introduces the sinusoidal histogram test (SHT), one of the widely used methods to measure INL in digital converts. The underlying theoretical aspect of it has been explained. SHT has been used in this thesis to experimentally measure the INL for a practical pairs of DAC/ADC. An INL model has been built by interpolating the measured values and used later to assist different INL effects on ENOB. Additionally, the effect of different INL values vary from 0 to 10 LSB has been studied on a 256 QAM , 23 GBaud configuration.

Chapter 4 discusses the variety of machine learning techniques and their integration in modern high speed coherent optical transceivers. The chapter focuses on artificial neural networks as one of the easy-to-employ and promising solutions for some of the non-linearity problems in coherent optical transceivers. In this chapter, the utilising of Indirect learning method using multi layers neural network to compensate of digital converter's non-linearity is numerically studied. The study explores the performance enhancement of applying this solution in multiple scenarios and different INL values.

Chapter 5 investigates the possibility of using low resolution DACs in high speed optical transceivers. The chapter focuses on digital resolution enhancers as the most promising technique to compensate for the high quantization noise induced by low resolution DACs. The theory behind digital resolution enhancement technique based on Viterbi algorithm is discussed and verified using analytical and experimental test. Additionally, the joint test of digital resolution enhancement with probabilistic shaping has been conducted to find out the maximum achievable gain of using digital resolution enhancement in modern optical transceivers.

Chapter 6 summarizes the work presented in chapter 3, 4 and 5, highlights the main findings and conclusions and provides an outline for possible future work and research directions. Hence, expediting the production of higher speed and more power efficient transceivers by developing DSP and machine learning based algorithm to compensate for digital converter impairments and non-idealities.

1.3 Thesis key contributions

The contribution of this thesis lies in its extensive study of digital converters in coherent optical communication systems. The study explores different aspects such as Signal-to-Noise and Distortion Ratio (SINAD) and Effective Number of Bits (ENOB), and provides a detailed analysis of these metrics. One of the unique contributions of this thesis is the focus on digital converter non-linearity for the first time. The study investigates the effect of non-linearity on the overall performance of the system and provides a reliable Integral Non-Linearity (INL) model for future studies.

Another major contribution of this thesis is the proposed solution to compensate for the effect of non-linearity in digital converters using neural network-based techniques. This study is expected to help in using higher modulation formats and increasing the spectral efficiency in future optical communication systems.

In addition, the thesis explores the possibility of using low resolution digital to analogue converters to support energy critical applications while minimizing power consumption without sacrificing performance. This is enabled by a technique called digital resolution enhancement, which is studied in detail in this thesis. The study also uses probabilistic shaping to achieve the maximum gain when using digital resolution enhancement.

Numerical and practical studies were performed to validate the proposed solutions and techniques. The results of these studies provide significant insights into the use of digital converters in coherent optical communication systems and the impact of non-linearity and digital resolution enhancement on system performance.

Overall, the contribution of this thesis lies in its comprehensive study of digital converters in coherent optical communication systems, and the proposed solutions to overcome the challenges faced in the use of these converters. The results of this study will be of great value to researchers and practitioners in the field of optical communication systems, and will provide a foundation for further research and development in this area.

1.4 List of publications

- **M. Abu-Romoh**, P. Skvortcov, T. Zhang, T. T. Nguyen, I. Phillips, and W. Forysiak, "Experimental study of the effect of integral nonlinearity in 8-bits resolution DACs on 256-QAM," in OSA Advanced Photonics Congress (AP) 2020 (IPR, NP, NOMA, Networks, PVLED, PSC, SPPCom, SOF), 2020, SpTu2I.5. **Chapter 3**
- **M. Abu-Romoh**, S. Sygletos, I. D. Phillips and W. Forysiak, "Neural-network-based pre-distortion method to compensate for low resolution DAC nonlinearity," 45th European Conference on Optical Communication (ECOC 2019), 2019. **Chapter 4**
- T. T. Nguyen, T. Zhang, **M. Abu-Romoh**, and A. Ellis, "Artificial Neural Network-Based Compensation for Transceiver Nonlinearity in Probabilistic Shaping Systems," in Optical Fiber Communication Conference (OFC) 2020, 2020, W2A.44. **Chapter 4**
- **M. Abu-Romoh**, T. T. Nguyen, Y. Yoffe, I. Phillips and W. Forysiak, "Numerical study on the combination of Probabilistic Shaping and Digital Resolution Enhancer for high baud rate optical communications," 2020 European Conference on Optical Communications (ECOC), 2020. **Chapter 5**
- **M. Abu-Romoh**, T. T. Nguyen, P. Skvortcov, Y. Yoffe, I. Phillips, T. Drenski, W. Forysiak "Experimental verification of 64-Gbd/64-QAM interworking of probabilistic shaping with a digital resolution enhancer," 2021 Optical Fiber Communications Conference and Exhibition (OFC). **Chapter 5**
- P. Hazarika, **M. Abu-Romoh**, M. Tan, L. Krzczanowicz, T. T. Nguyen, M. A. Iqbal, I. Phillips, P. Harper, M. Li, and W. Forysiak, "Impact of Chromatic Dispersion in Discrete Raman Amplifiers on Coherent Transmission Systems," in Optical Fiber Communication Conference (OFC) 2021, 2021, Th1A.14.

Chapter 2

Coherent optical transceivers

2.1 Main building blocks of coherent optical transceivers

As pointed out in the introduction, the main difference between the old WDM-OOK based systems and the modern optical coherent WDM systems is that the first ones rely exclusively on the amplitude variation of the signal to encode information while the second ones utilize the three attributes of the optical field which are amplitude, phase and polarization. The first method, WDM OOK, is known by its simplicity since a single photo detector can detect the amplitude variation based on the square law due to the proportional relationship between the generated current and the square of the instantaneous optical field ($I \propto |E|^2$). On the other hand, optical coherent WDM based systems detect the in-phase, quadrature and two polarizations states of the received signal, hence display higher complexity in design not only at the receiver side but also at the transmitter side. However, they clearly demonstrate higher ISD, flexibility and robustness against noise which make them preferable over any other contender in high speed transmission applications. Scalability is one of the pivotal and highly demanded feature in any communication system. A highly scalable system reflects positively on low CaPex and lower upgrading costs on service providers. There are three scalability dimensions in a coherent WDM based system as shown in fig 2.1. Each direction introduces a different set of challenges and constrains which need to be overcome to attain higher utilization for the deployed optical fibre cables. For instance, higher number of channels require better and more advanced amplification schemes with wider effective bandwidth, low overall noise figure and flat gain [13] [14]. Utilizing higher modulation formats requires better SNR profile and well designed and manufactured digital converters with high resolution and high ENOB [15]. Higher modulation formats tend to be more susceptible against phase noise [16] which require stringent CW and LO linewidth requirements and more sophisticated DSP algorithms. Due to the limited bandwidth, coherent

optical transceivers are capable of supporting limited baudrates. This bandwidth can be extended using variety of pre-emphasis and pre-compensation techniques to inverse the frequency roll off [17] [18]. However, extended the baudrate in this way comes at the cost of SNR degradation. Fabricating and manufacturing next generations of MZMs, DACs, ADCs and RF lines with wider bandwidth can be a better solution without sacrificing SNR [19] [20]. However, they come at the cost of higher fabricating and designing cost. The current record for industrially adopted coherent transmission is 100 GBauds and 64 probabilistically shaped QAM which supports a rate of 800 GBits/s per channel [21].

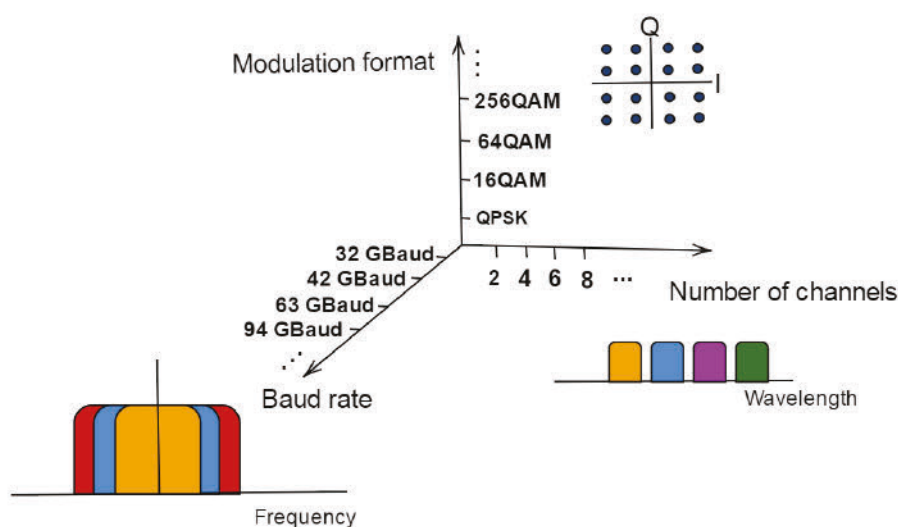


Fig. 2.1 Ways to increase the spectral efficiency in coherent optical communication systems

The DSP architecture of a conventional coherent optical transmitter is shown in fig 2.2. The main stages of optical coherent transmission can be listed as:

- Mapping: the digital processor arranges the bits' sequence into their complex counterparts (Symbols) corresponding to the chosen modulation format (i.e QPSK, 16-QAM, 32-QAM). The flexibility of coherent transmitters is strongly displayed in the ability of choosing arbitrary modulation formats without the necessity to change any part of either the transmitter or the receiver architecture. However, the manifest trade-off between the modulation format's level and the optical signal to noise ratio (OSNR) requirement should be taken into consideration. As a rule of thumb, higher modulation formats require higher OSNR to achieve the same maximum reach mainly due to the increasing vulnerability for higher modulation formats against noise and distortion.

-
- I/Q splitting: to adjust the signal for the next stages of transmission, each symbol (complex value) is split into in-phase component (I component) and quadrature component (Q component) and fed separately into the DACs.
 - Pulse shaping: to achieve the highest spectral efficiency of a single WDM channel, a digital pulse shaping filter is applied to the signal before inserting it to the DAC. Digital pulse shaping plays a crucial role in achieving high spectral efficiency and reducing inter-symbol interference. It involves the manipulation of digital signals to shape the waveform before modulation and transmission. The roll-off factor determines the width of the transition band in a shaped pulse. It is defined as the ratio of the bandwidth occupied by the signal to the symbol rate of the signal. The roll-off factor has a direct impact on the inter-symbol interference and the spectral efficiency of the communication system. A lower roll-off factor results in a more gradual transition band and less inter-symbol interference (ISI). However, it also reduces the spectral efficiency of the system as more bandwidth is occupied by the signal. On the other hand, a higher roll-off factor results in a sharper transition band and increased spectral efficiency, but also leads to higher inter-symbol interference. To eliminate ISI, the receiver uses a filter that is matched to the pulse shape used at the transmitter, in order to maximize the signal energy and reduce the interference from neighboring symbols. This technique is called "matched filtering" [22].
 - Digital to Analogue conversion (DAC): to convert the signal from its digital form to a sufficient analogue form to drive the Mach Zehnder modulators (MZM), 4 DACs are essentially needed. Each DAC will convert one of the following sequences (X_I, X_Q, Y_I, Y_Q) where X Y refer to the dual polarizations and I Q refer to the in-phase and quadrature components of the signal, respectively. DACs are crucially important parts of the system specially if high modulation formats are utilized (ie. 16-QAM, 32-QAM, 64-QAM) since they facilitate the usage of pre-emphasis techniques and pulse shaping on transmitted signal. It worth mentioning that some of the early DP-QPSK demonstrations showed that it's possible to transmit DP-QPSK signal without using DAC by directly driving the MZMs using digital signals [23]. However, that comes in the expense of sacrificing the merits of applying pulse shaping and pre-emphasis.
 - Electrical to optical conversion: The nearly smooth analogue DACs' output will be carried by RF links to drive two dual arms MZMs. Each dual arms MZM modulates a single polarization of a continuous wave (CW) laser beam. The laser beam is previously split into two polarization by a polarization beam splitter (PBS) and fed into the MZM. Each arm of any of the MZMs is delayed by $\pi/4$ of the other arm to modulate the

in-phase and quadrature components. The optical output of the two dual arms MZMs is combined using polarization beam combiner (PBC) and transmitted over the optical fibre link.

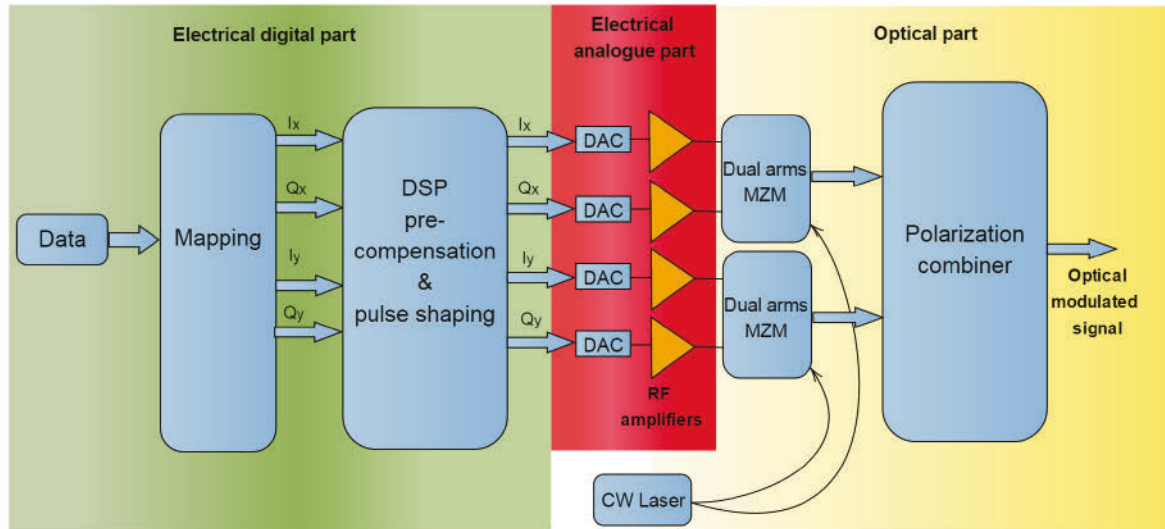


Fig. 2.2 Block diagram of conventional optical coherent transmitter

2.1.1 Digital converters

For the sake of clarity, a mathematical illustration for the transmission process of a single complex symbol of one of the polarizations can be modelled as follow. Assuming that the mapped single base-band complex symbol is:

$$d(t) = I(t) + jQ(t) \quad (1)$$

Where I and Q are the in-phase and Quadrature components respectively. To attain a full digital to analogue conversion, 4 sub DACs are needed. Each sub DAC is responsible of converting either the in-phase or the quadrature symbols of one polarization. As shown in fig 2.3, the digital to analogue conversion process is consisted of three main stages. First stage is resampling where the input signal is resampled to match DAC's sampling rate. If the baud rate is lower than the sampling rate ($f_{input} < f_s$), upsampling is applied to the input sequence. On the other hand, donwsampling is applied when the baud rate is greater than the sampling rate ($f_{input} > f_s$). It's more common to choose a sampling rate greater to minimise the ISI affecting the signal. Notwithstanding, transmission with less than 1 sample per symbol has

been done before with sufficient equalization schemes to mitigate the effect of extra ISI [24]. Second stage is quantization where all symbols are rounded up to the closest quantization level. The quantization process introduces a quantization error which can be approximated to a white noise [25]. The higher the resolution, the less quantization noise imposed and better performance transmission system can achieve. The last stage of DAC operation is zero order hold in which each sample is held constant for T_s period of time. T_s is the inverse of the sampling frequency and is controlled by an internal or external clock. The hold process is usually triggered by a clock rising or falling edge event. ZOH is one of the simplest and most common reconstruction functions in conventional DACs which has been studied in depth in multiple occasions [26] [27].

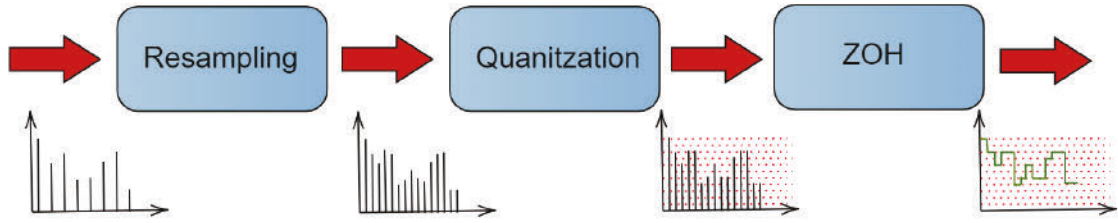


Fig. 2.3 Simplified DAC operation on analogue symbols

Assuming a sampling time of T_s , the mathematical representation of ZOH transfer function in time domain is

$$h(t) = \text{rect} \left(\frac{t - \frac{T_s}{2}}{T_s} \right) \quad (2)$$

Which translates into a *sinc* function in the frequency domain by applying Fourier transform as shown

$$H(f) = e^{-2\pi f T_s} \left(\frac{\sin(\pi f T_s)}{\pi f T_s} \right) = e^{-2\pi f T_s} \text{sinc}(f T_s) \quad (3)$$

As illustrated in fig 2.4, spectral replicas of the base-band signal in each Nyquist zone is a natural byproduct of the digital to analogue conversion process. Those replicas are affected by the ZOH transfer function and the what remains of the images appear on the DAC output. An analogue anti-aliasing filter is usually deployed to remove those images [28].

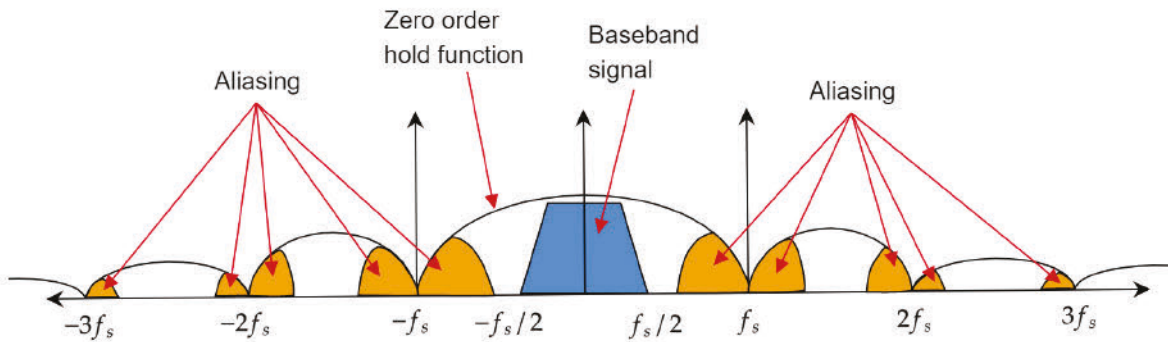


Fig. 2.4 The transfer function of zero order hold DAC

2.1.2 Mach-Zehnder Modulators

Modulation is embedding information by manipulating one of the attributes of a physical carrier. This attribute can be amplitude, phase, frequency or any other characteristic which can be clearly detected and distinguished for different levels by a receiver at the other end of the link. Similarly, in coherent optical communication systems, the formerly modulated electrical signal is converted into the optical domain using a designated optical modulator. Optical modulation can be carried out using direct or indirect modulation schemes. Direct modulation is the simplest and most straightforward type where the electrically modulated stream of data controls the drive current of the laser. Hence, the output laser power varies with the variation of the fed-in stream of data. Direct modulation is one of the earliest methods used in optical communication systems due to its simplicity and cost efficiency [29]. Despite its robustness against distortion, direct modulation is limited by laser resonance frequency, chirp and laser non-linearity [30]. Direct modulation commonly relies on the amplitude and dismisses all the other attributes of the optical carrier which significantly limits the SE of the system.

In contrast, indirect modulation doesn't interfere with the light wave generation process. Light is generated independently by a CW laser then modulated externally by external optical modulators. A variety of external modulators with different underlying operational mechanisms and properties are used in modern coherent optical communication systems. For instance, EAM modulators make use of the light absorption property of specific semiconductors controlled by an external voltage. Applying an external voltage to the semiconductor changes the light absorption property of the material which either makes it transparent or an absorption medium, hence, the light emitted by a CW laser can be easily modulated by controlling the light intensity. An accompanied change in the refractive index

is expected which result into phase changes. Eventhough, chirp effect is present in EAM modulators, the severity of chirp is very limited comparing to a direct modulator.

Another type of external modulators widely used in high speed coherent optical communication systems is MZMs. MZMs make use of a unique property of some materials such as $LiNbO_3$ and InP with a varying refractive index [31][32][33]. This variation is artificially induced by an external voltage source and accounts for a phase variation in the propagating light wave. Hence, phase modulation can be easily achieved. This variation can also be reflected on the intensity by utilising the principle of interference. As its known, wave interference can be constructive or destructive ,thus, a dual arms MZM interferometer is sufficient for a single polarization amplitude modulation as shown in fig 2.5. V_1 and V_2 are the amplitude modulation voltages and V_3 is the phase modulation voltage as depicted.

When the optical carrier is modulated using MZMs, the transmitted symbol will be up converted by multiplying it by $e^{j\omega_{Tx}(t)t+\theta_{Tx}(t)}$ which is the up-conversion component of the carrier and the resultant expression will be

$$d(t)_{upcomv} = d(t)e^{j\omega_{Tx}(t)t+\theta_{Tx}(t)} \quad (4)$$

Where f_{Tx} is the carrier's frequency and θ_{Tx} is the carrier's phase.

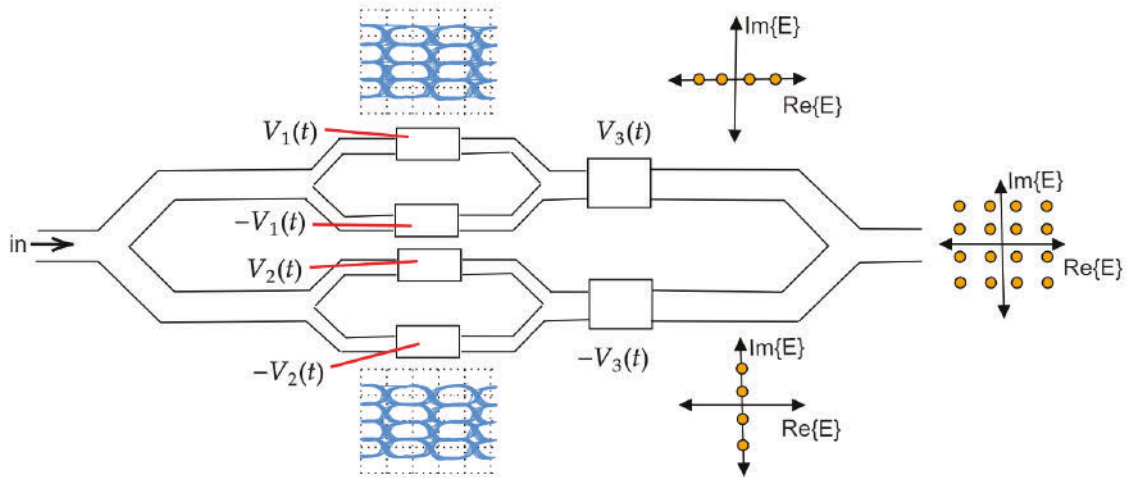


Fig. 2.5 A schematic diagram of a dual arm Mach-Zehnder modulator and a graphical illustration for the phase and in-phase modulation of a 16-QAM

2.1.3 Lasers (LO & CW)

As the case with all telecommunication channels, the transmitted signal will be affected by the channel's response which is generally modelled as an additive white Gaussian noise (AWGN).

This assumption is valid for long reach optical communication links since the dominant type of noise in these links is the Amplified Spontaneous Emission (ASE) which is an additive white Gaussian type of noise [14]. Additionally, other effects such as chromatic dispersion (CD), polarization mode dispersion (PMD), polarization rotation, Kerr nonlinearity, four waves mixing (FWM) and other types of nonlinearities can affect the signal, however, they won't be focused on at this stage for the sake of simplicity. Based on what have been mentioned, the received signal will be expressed as follow.

$$d(t)_{received} = d(t)_{upconv} + n_{ASE} \quad (5)$$

Where n_{ASE} is the ASE white Gaussian noise. To retrieve the symbol at the receiver side, the signal is required to be down converted which is typically done by mixing it with a another laser's beam (Local oscillator "LO") which has a down conversion exponential of $e^{-j2\pi f_{Rx}(t)t + \theta_{Rx}(t)}$ where f_{Rx} is the LO's frequency and θ_{Rx} is the LO's phase. The difference between the carrier's frequency and the LO's frequency is expressed as follow.

$$f_{IF} = f_{Tx} - f_{Rx} \quad (6)$$

Where f_{IF} is what known as the "intermediate frequency" or frequency offset and should be totally nulled using an optical phase locked loop (OPLL) in homodyne receivers or it can be compensated for using DSP offset estimation and compensation techniques in intradyne receivers. The difference between a spectrum of an optically demodulated signal in an intradyne and homodyne receiver is depicted in fig 2.6. Additionally, there is also the phase difference which is expressed as.

$$\theta_{IF} = \theta_{Tx} - \theta_{Rx} \quad (7)$$

This difference can also be solved by OPLL correction in homodyne receivers or by DSP carrier phase recovery techniques in heterodyne receivers. However, DSP techniques showed superiority over OPLLs due to their speed, low complexity and power efficiency [34]. It worth mentioning that sometimes the combination of DSP frequency offset compensation and phase recovery is called by "Carrier recovery".

2.1.4 90 degree hybrids and photo diodes

DSP is one of the core elements of any coherent optical communication system to recover the transmitted data back to its original form. Enabling DSP requires a few steps of conversion such as optical down conversion, optical-to-electrical conversion and analogue to digital

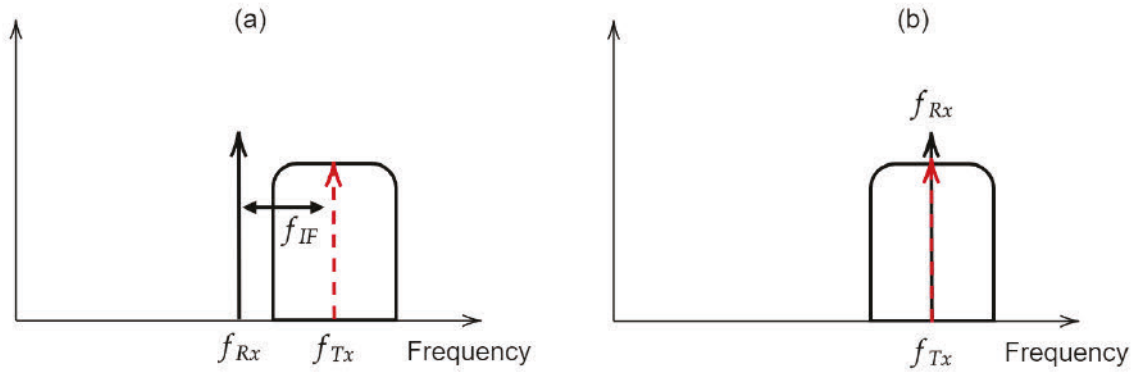


Fig. 2.6 Signal spectrum after optical demodulation using a (a) intradyne receiver (b) homodyne receiver

conversion. As previously discussed, optical modulation and up-conversion is performed at the transmitter side using MZMs. The signal is usually upconverted to occupy the C-band of optical spectrum which extends from 1530-1565 nm and sometimes the L and S bands which extend from 1565 nm to 1625 nm and 1460-1530 nm, respectively [35]. At the receiver side, 90 degrees hybrids are responsible of mixing the free running LO with the incoming modulated signal. Thereupon, designated photo-detectors convert the incoming time varying optical power into corresponding variations of electrical signal which then amplified using TIA amplifiers. Lastly, the amplified electrical analogue form of the signal is converted into a digital form by a set of 4 sub ADCs.

Photo-diodes are considered as one of the simplest, fastest and most effective photo-detectors. Their amplitude response is $I \propto |E|^2$ according to the square law, where I is the output current and E is the incident electric field. Detection can be performed using photodiodes as single ended or balanced configuration as shown in fig 2.7. Both configurations are sufficient for optical coherent systems, however, the balanced configuration provides a better SNR. It worth mentioning that photodiodes exclusively detects the variation of intensity, however, phase information are preserved due to mixing the incoming signal with LO.

The mathematical representation

$$E_s(t) = \sqrt{P_s} e^{j(\omega_s(t)t + \theta_s(t))} e^{j\theta_{n_s}(t)} d_s(t) \quad (8)$$

is a model that represents the signal transmission in fiber-optic communication systems. The complex signal envelope, $E_s(t)$, represents the waveform of the signal that is transmitted through the fiber-optic.

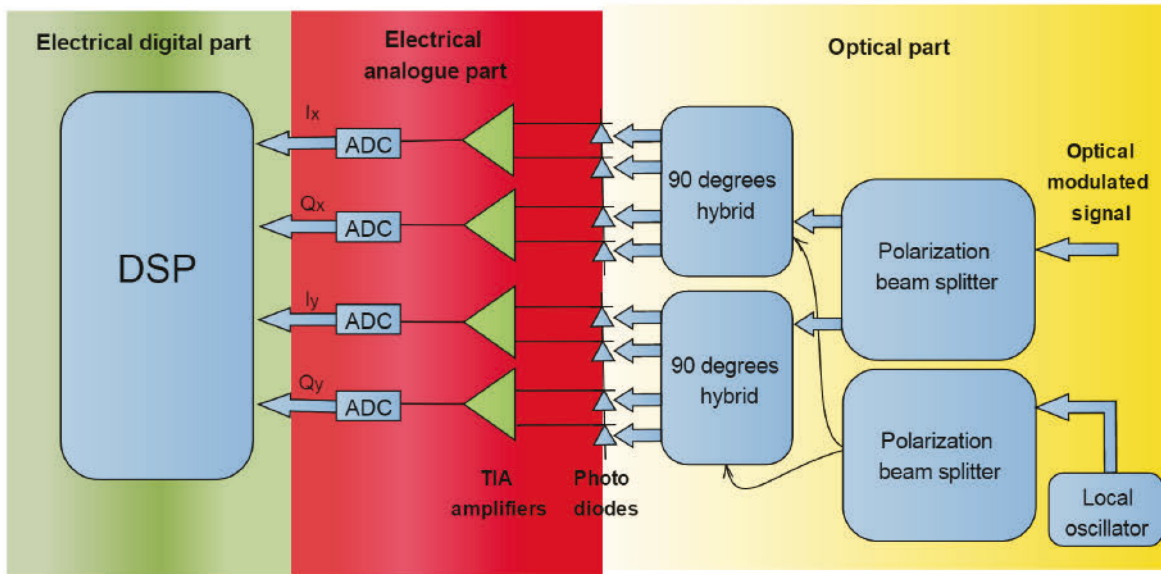


Fig. 2.7 Block diagram of conventional optical coherent receiver

The signal envelope is a combination of several components, including the square root of the signal power, $\sqrt{P_s}$, the carrier wave, $e^{j(\omega_s t + \theta_s(t))}$, the noise component, $e^{j\theta_{ns}(t)}$, and the digital pulse shaping waveform, $d_s(t)$.

The carrier wave represents the main signal component, with its frequency and phase determining the information carrying capacity of the signal. The noise component, on the other hand, represents unwanted disturbance in the signal that can impact the signal quality and performance. The digital pulse shaping waveform is used to shape the signal into a specific form that can be transmitted effectively through the fiber-optic communication system.

Since some of the coherent detection aspects have been slightly discussed, it worth overviewing the main practical coherent receiver detection and recovery blocks. The architecture for heterodyne optical receiver will be exclusively discussed since it's the most widely used type of optical receivers nowadays. Its architecture is depicted in the block diagram in fig 2.7 and each block is discussed consequently as follow.

- Polarization splitting: Both of the received signal and the LO beam are split by two polarization beam splitters (PBS) to two orthogonal polarizations X and Y as a prior stage before mixing.
- Phase diverse coupling (In-phase and quadrature separation): a pair of 90° optical hybrids are used to mix the X polarization components of the received signal and the

LO and the Y polarization components of the received signal and the LO separately as shown in fig 2.7.

- Detection: a set of four balanced photo detectors is used to extract the I and Q components of both polarizations. The output of the aforementioned stage can be given as [36]:

$$\begin{bmatrix} I_x \\ Q_x \\ I_y \\ Q_y \end{bmatrix} \propto \begin{bmatrix} Re \{ E_x E_{LO}^* \} \\ Im \{ E_x E_{LO}^* \} \\ Re \{ E_y E_{LO}^* \} \\ Im \{ E_y E_{LO}^* \} \end{bmatrix} \quad (9)$$

Where E_x denotes to the incident electrical field of the x polarization, E_y denotes to the incident electrical field of the y polarization and E_{LO} denotes to the incident electrical field of the LO beam. The main advantage of the balanced photo detector arrangement is the merit of suppressing the unwanted direct detection part from the output of the 90° optical hybrids as can be noticed from the detailed derivation in the reference [36].

- Electrical amplification: The four electrical components will pass through four trans-impedance amplifiers (TIA) to magnify the output to a suitable level for Digital conversion.
- Analogue to Digital Conversion (ADC): The input signal is digitised accordingly by four separate ADCs. ADCs' resolution is crucial to minimise the induced quantization noise and increase the accuracy of symbol decisions.
- Digital signal processing (DSP): As mentioned at the introduction, DSP offers many cost-effective solutions to compensate for many of non-idealities introduced by the transmitter, receiver and channel. The conventional DSP techniques in optical coherent systems are over-viewed in the next sub section.

2.2 DSP for coherent optical communication

Due to the wide variation of non-idealities in optical coherent systems, numerous DSP algorithms have been introduced to solve multiple possible scenarios. As a way to merge the most common non-idealities in optical coherent systems in one place, a diagram has been drawn to illustrate these non idealities in fig 2.8.

As soon as the signal is digitized by ADCs it undergoes a chain of DSP operations to “purify” it from all the impurities imposed from different sources before reaching the final

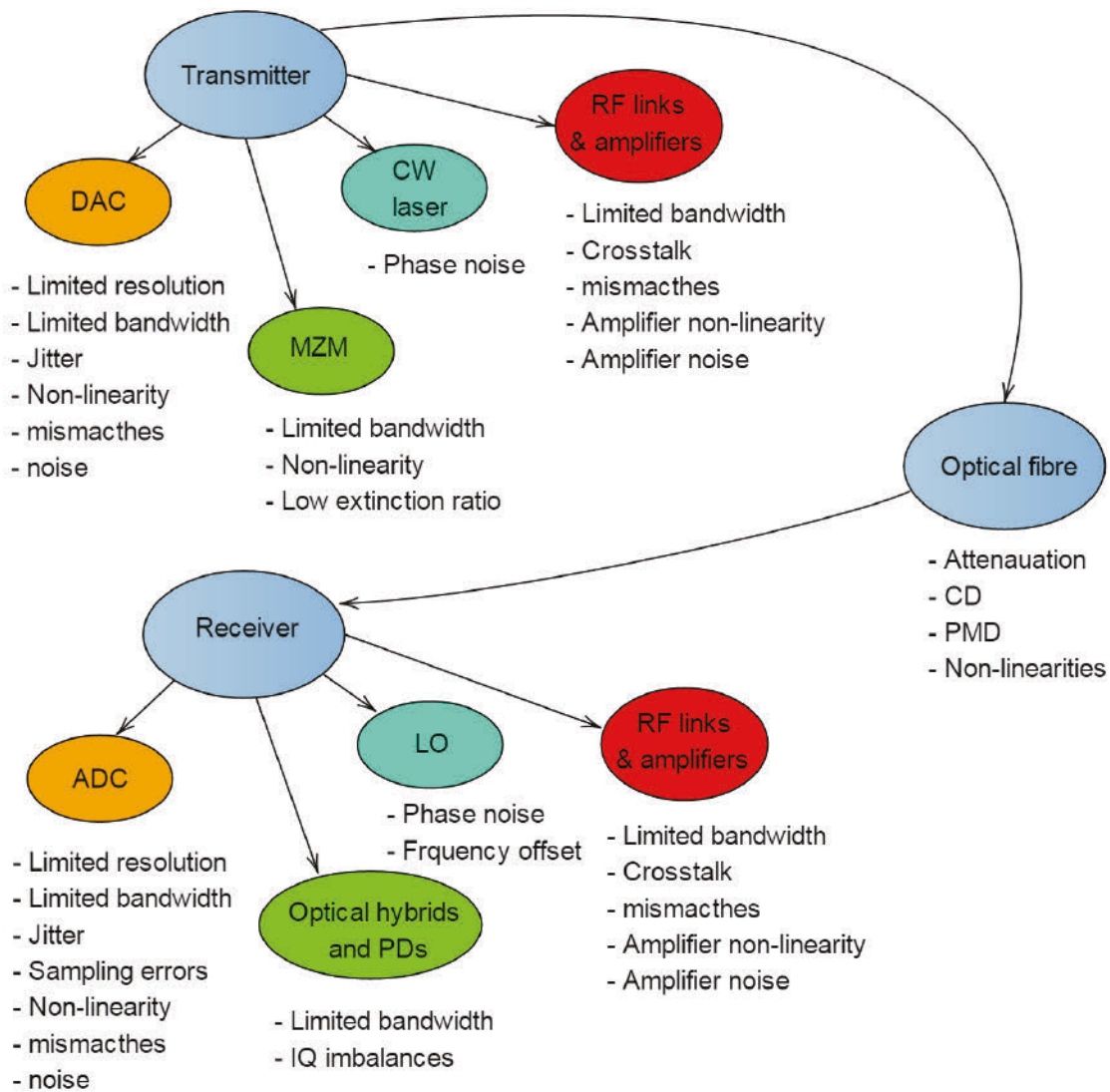


Fig. 2.8 Optical coherent transmission system non-idealities

stage which is the symbol decision. The accuracy of the decision is directly correlated to the quality of all the preceding DSP operations in eliminating these impurities. The conventional sequence of DSP operations is shown in fig 2.9. These operations will consequently be highlighted according to that conventional sequence.

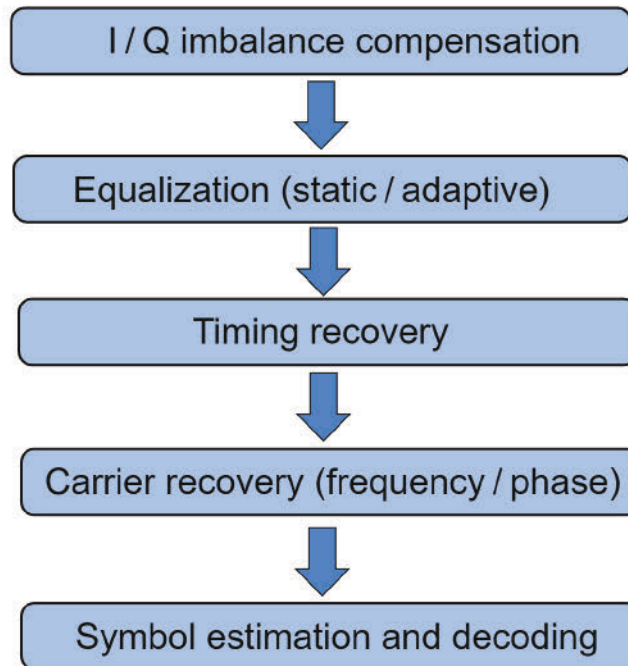


Fig. 2.9 Conventional DSP chain in a coherent receiver

2.2.1 I/Q imbalances compensation

In theory, I and Q should be orthogonal to each other. In other words, they should differ by exactly 90° . This quadrature difference insures a zero correlation between them which prevents any interference or leakage. As a second restriction, I and Q should be strictly timely synchronised with each other. As known, the I and Q components are converted from digital to analogue then modulated separately to the optical domain then multiplexed before transmission. Hence, they will go through different RF lines and pass through different DACs and MZM. The asymmetry in paths causes timing difference between the I and Q components. This phenomenon is known as IQ skew mismatch. Additionally, the amplitude of both I and Q channels should be the same to obtain the right constellation diagram which is not always the case. So, IQ quadrature error, IQ skew and IQ gain mismatches can be considered as the

main IQ imbalances in optical transceivers. Each one of the aforementioned mismatches has different sources and different methods proposed to compensate for its effects. The most straightforward one to correct is the gain mismatch and it's traditionally corrected by automatic gain controlled trans-impedance amplifier [37]. For IQ skew compensation, different calibration techniques have been introduced and can be reviewed from the reference [38]. For IQ quadrature error, Gram-Schmidt orthogonalization procedure (GSOP) is one of the well-known traditional DSP techniques which is used in recovering the orthogonality between the in-phase and quadrature samples by removing the correlation. It simply measures an optimum set of orthogonal vectors based on a comparison with a reference vector as shown in fig 2.10. This technique showed strong potential in correcting all the IQ quadrature mismatched imposed by the receiver, however, it doesn't do well in correcting IQ quadrature errors imposed by the transmitter especially if it is followed by a frequency offset. This draw-back can be explained by the convergence scheme of GSOP which tends to converge whenever the constellation approaches a circular shape and this condition can easily be affected by the frequency offset component $e^{j\omega t}$ [37] [39]. A full compensation for the transmitter's IQ quadrature mismatch is still a solid area of research [40].

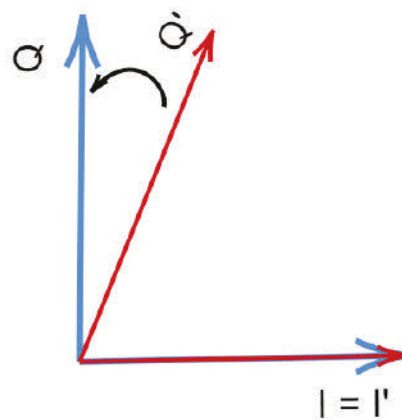


Fig. 2.10 Gram-Schmidt orthogonalization procedure

2.2.2 Equalization

The main purpose of equalization is to remove the linear impairments such as chromatic dispersion (CD) and polarization mode dispersion (PMD). As it's known, both dispersions are lossless which means that they corrupt the signal's phase response but don't show any effect on the magnitudes of the power spectral density (PSD) elements. It has been shown that

it's more beneficial to divide the equalization into two different steps due to the difference in CD's and PMD's natures [41]. Typically, CD is a slowly changing type of dispersion which requires a single FIR filter with large number of taps to equalise while PMD is a dynamic and fast changing type of dispersion which requires multiple small adaptive filters which can update their taps continuously to track the changes.

Static equalization

The transfer function of the CD can be expressed as [42]

$$G(z, \omega) = \exp\left(-\frac{j\omega^2\beta_2z}{2}\right) \quad (10)$$

Where ω is the angular frequency, β_2 is the parameter of the group delay dispersion and z is the fiber link length. To extract the FIR filter taps values which are needed to equalise for CD, the inverse Fourier transform is applied to $G(z, \omega)$ and the resultant formula is.

$$h_c(z, t) = \frac{1}{\sqrt{-2\pi j\beta_2z}} \exp\left(-\frac{jt^2}{2\beta_2z}\right) \quad (11)$$

which represents the impulse response of a single-mode optical fiber in a fiber-optic communication system. The impulse response, $h_c(z, t)$, describes the response of the optical fiber to an impulse or delta function input.

In this equation, the term $\frac{1}{\sqrt{-2\pi j\beta_2z}}$ represents a normalization constant, which ensures that the impulse response has unit energy. The term $\exp\left(-\frac{jt^2}{2\beta_2z}\right)$ represents the frequency-dependent phase shift caused by the optical fiber, similar to the transfer function described in Equation 10.

The impulse response of the optical fiber is an important characteristic that provides information about the behavior of the fiber-optic communication system in response to impulse inputs. By analyzing the impulse response, engineers can determine the time-domain behavior of the system and design effective strategies to minimize the impact of dispersion and other factors that can degrade the signal quality and performance.

As it's shown, the formula is unbounded which means that it requires an unrealistic FIR filter with infinite number of taps. To make the FIR design applicable, two types of impulse response truncation have been proposed

1. Time domain truncation: It shows a good performance for short distances but high complexity in long reach links and higher modulation formats.

-
2. Frequency domain truncation: It shows a good performance for less complexity for longer distances and easier implementation [43].

As a way to ease some of the processing requirements at the receiver. The Matched filter (MF) can be associated with the static equalizer at the same stage. Hence, the CD equalizer will have the combined following frequency response.

$$H_{total}(\omega) = H_{RRC}(\omega)H_c(z, \omega) \quad (12)$$

Where H_{RRC} is the frequency response of the RRC matched filter and H_c is the frequency response of the CD equaliser.

Adaptive equalization

It's true that a static CD equaliser combined with MF remove any CD and ISI elements added to the signal. However, some residual CD and ISI components can still be presented in the signal even after static equalisation is applied. Here comes the necessity for further equalisation. The second stage of equalisation is performed using short adaptive filters not only to remove the effect of PMD but also to eliminate any residual CD and ISI. A 2X2 MIMO structured adaptive filter or what is called as "butterfly shape adaptive filter" is commonly utilized for this purpose in correspondence to the dual polarization nature of the carrier. The four filters taps' weights are updated using an adaptive algorithm to minimise the error which is usually measured as a mean squared error (MSE). PMD equalizers generally fall under two main categories, the first one is what's known as data aided equalizers. This category of equalisers assign periodically inserted training sequences to estimate the channel's response. Based on the estimation, the receiver updates its adaptive filters taps to apply an inverse of the channel's response. As how straightforward this method seems, one main disadvantage makes it not as popular as the second method of equalisation which will eventually be mentioned. This drawback is the additional overhead requirement to insert the training sequence which will decrease the overall spectral efficiency of the transmission system. As an alternative, the so called "blind equalization" is used by utilising some properties of the transmitted modulation format to estimate the mean square error (MSE) and minimise it. To avoid complication, the detailed adaptive equations won't be mentioned in this report, however, they can be seen in reference [20]. The three main adaptive algorithms are:

1. Constant modulus Algorithm (CMA): CMA is one of the famous algorithms for equalising PMD which can operate with a full blind mode. It's well suited for constant modulus formats such as QPSK and a variety of PSK formats, however, it can be used but can't exactly converge to zero error when high cardinality QAM formats

are used such as 16 QAM, 32 QAM or 64 QAM. The main principle of CMA is to minimise the amplitude fluctuations of the received samples compared to the average amplitude taken for all of the received samples as shown in fig 2.11. This method deals with samples' phase component as a marginalised quantity which makes it immune to phase and frequency offsets. This property makes it suitable to be applied before any frequency or phase offset compensation unlike other algorithms.

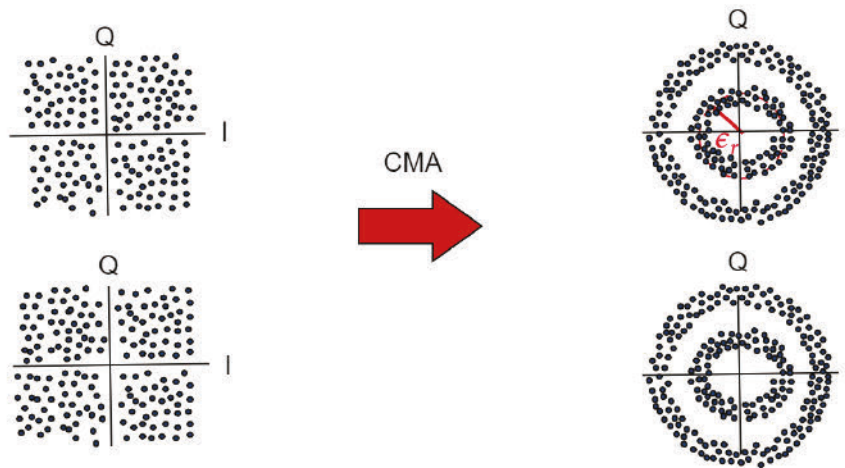


Fig. 2.11 Constellation diagram for samples before and after applying adaptive filtering using constant modulus algorithm

2. Decision Directed Least Mean Square (DD-LMS): in DD-LMS the error is calculated by comparing the output of the adaptive filter x_o with the symbol after decoding $D\{x_o\}$ as shown in fig 2.12. The DD-LMS technique shows better performance when dealing with high levels of QAM formats, however, it faces a few implementation drawbacks. Firstly, it can't operate in a full blind mode since all of the first decisions will be wrong and can't be relied on to apply the algorithm. That's why it's usually applied with a sequence of training symbols to initiate the equalizer or accompanied by CMA at the start of the operation. The second drawback is the accumulated latency since the decisions are made after the carrier recovery and frequency estimation stages which will add up to the tap weights update time.
3. Recursive Least-Squares Algorithm (RLS): RLS shows a faster convergence and higher accuracy comparing to LMS but that comes in the expense of higher computational requirements. Several papers studied the performance of RLS in adaptive equalization in details [44][45]

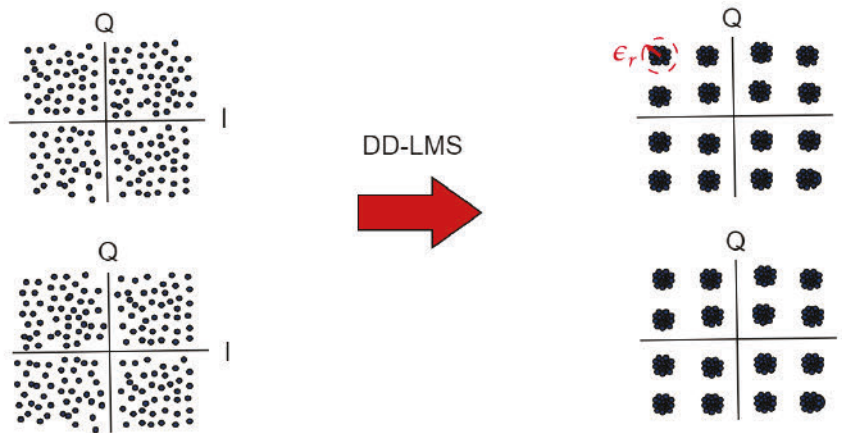


Fig. 2.12 Constellation diagram for samples before and after applying adaptive filtering using Decision Directed Least Mean Square algorithm

2.2.3 Timing recovery

The minimisation of inter-symbol interference (ISI) in any communication system is directly related to the accuracy of synchronisation between the transmitter's and receiver's clocks. As it's well known that the zero ISI point in a well synchronised transceiver occurs at the decision instances, any deviation from these instances will cause an observable ISI added to the sampled signal and its severity relies on many factors, one of them is the roll off factor of the pulse shaping [12]. The deviation in sampling instances is called a clock jitter and it's caused by many sources. Moreover, the sampling phase should be optimised to locate the sampling instants at the peak of the received symbol to obtain the highest SNR possible. The digital process of correcting clock jitter and optimising sampling phase is called timing recovery. Such as many impairments, the clock can be digitally recovered using different DSP methods. One of the widely used ones in all types of digital communications due to its simplicity is Gardner's method [46]. As Gardner's method can be considered as a feedback method, square law timing recovery (STR) is a widely used feed-forward method in optical communication due to the absence of delay [47].

2.2.4 Frequency and phase recovery (Carrier recovery)

An ideal optical carrier is expected to have a constant amplitude, frequency and phase. However, due to the nature of optical sources and the impracticability of constructing an ideal coherent optical transmission system, deviations and fluctuations are always expected. As

previously discussed, LO and CW lasers are not frequency locked. Hence, a frequency difference is presented at the received signal. Mathematically, the frequency shift is represented by a multiplication of the received signal and frequency shift term $e^{j\Delta f}$. Visually, the frequency shift appears on the constellation diagram as a constellation rotation. Similarly, phase noise is usually incorporated due to laser LO and CW linewidths [48] which also appears as a constellation shift. Mathematically, the phase noise is represented by multiplying the phase noise term $e^{j\Delta\theta}$. A sequence of phase and frequency estimation and compensation algorithms are applied as a part of the DSP chain at the receiver side to recover the signal. This process is called carrier recovery. Carrier recovery can be conducted in blind or pilot aided manner. In other words, carrier recovery can be conducted blindly without the need for any overheads or pilot symbols to assist the algorithm.

2.2.5 Probabilistic constellation shaping

The upper bound of the achievable information rate for a communication link in presence of AWGN has been theoretically defined by Claude Shannon in [49]. Shannon's limit has a prolonged history of being used as a standard reference for all telecommunication systems. The closer the performance gets to Shannon's limit, the closer the system is to be ideal. Uniform constellation shapes such as QPSK, 16-QAM and 64-QAM are commonly used in commercial coherent optical communication systems due to their resilience against noise and distortion and its ability to transmit high number of bits per symbol. Uniform constellation shapes are capable of transmitting integer number of bits for each symbol. For instance, 16-QAM constellation is consisted of 16 points drawn on a plane. Each one of those points represents a unique symbol of 4 bits. All symbols have equal probability of occurrence which results into an entropy of 4 bits/symbol.

The optimum choice of modulation format immensely rely on the SNR supported by the transmission system as shown in fig 2.13. Higher SNRs are capable of supporting higher modulation formats, hence, higher bit rates. However, the supported SNR is generally limited by transceiver's components and channel's parameters. Despite the choice of modulation format, the SNR gap between Shannon's limit and uniform modulation formats always exists. This SNR gap presents an opportunity for further exploitation of the capacity. One of the suggested techniques to bridge the SNR gap is to introduce a set of new constellation shapes with better granularity. This can be achieved by manipulating the probability of occurrence of a conventional QAM modulation using an added DSP block called distribution matcher prior to the FEC encoder [50]. Redistributing the probability of occurrence by transmitting more of the lower energy symbols (inner symbols) than higher energy symbols (outer symbols) as illustrated in fig 2.14 shows better performance at certain SNR levels comparing to uniform

QAM constellation. This performance improvement can relate to higher resilience against noise due to the avoidance of outer constellation points which are commonly most effected by noise. Probabilistic constellation shaping (PCS) can achieve up to 1.53 dB shaping gain under additive white Gaussian noise (AWGN) in certain transmission conditions [51]. PCS is well known for its rate adaptivity. In other words, the data rate can be controlled by changing the PCS factor while keeping modulation format, FEC rate the same. This feature makes PCS a strong candidate to be an essential part of future flexible and high speed optical transceivers. PCS will be discussed in more depth in **Chapter 5**.

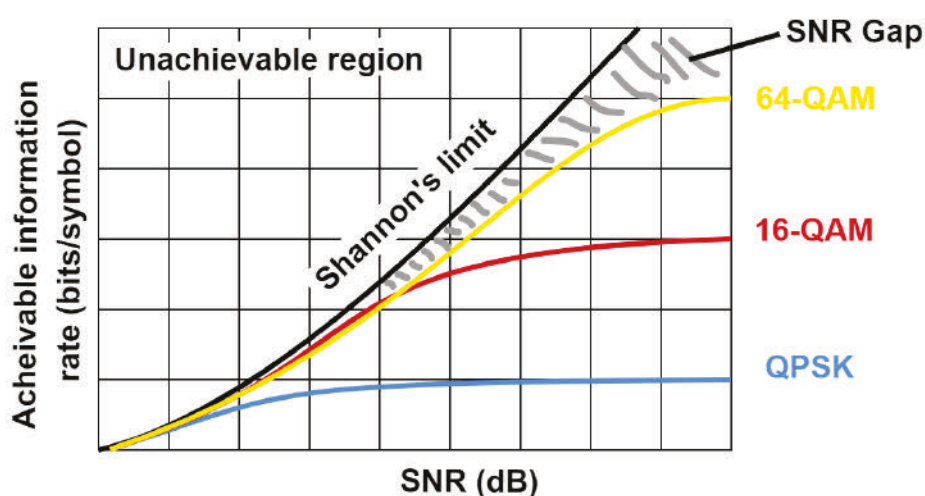


Fig. 2.13 The relationship between transceiver's SNR and achievable information rate

2.3 Spectral efficiency and up-scaling methods

Spectral efficiency (SE) is a decisive indication of how effectively the available channel bandwidth is exploited in transmission. The higher the spectral efficiency, the higher the total achievable bit rate or the less components needed to achieve a specific net bit rate which consequently leads to a lower deployment costs and higher cost efficiency. The simple expression below can be used to quantify the spectral efficiency

$$SE = \frac{R_s \log_2(M)}{\Delta f (1+r)} \quad (13)$$

Where R_s is the symbol rate or can be called as the baud rate and measured in symbol/second, Δf is the frequency spacing between adjacent WDM channels and measured in Hz, M is the number of unique constellation points and r is the redundancy resulted from

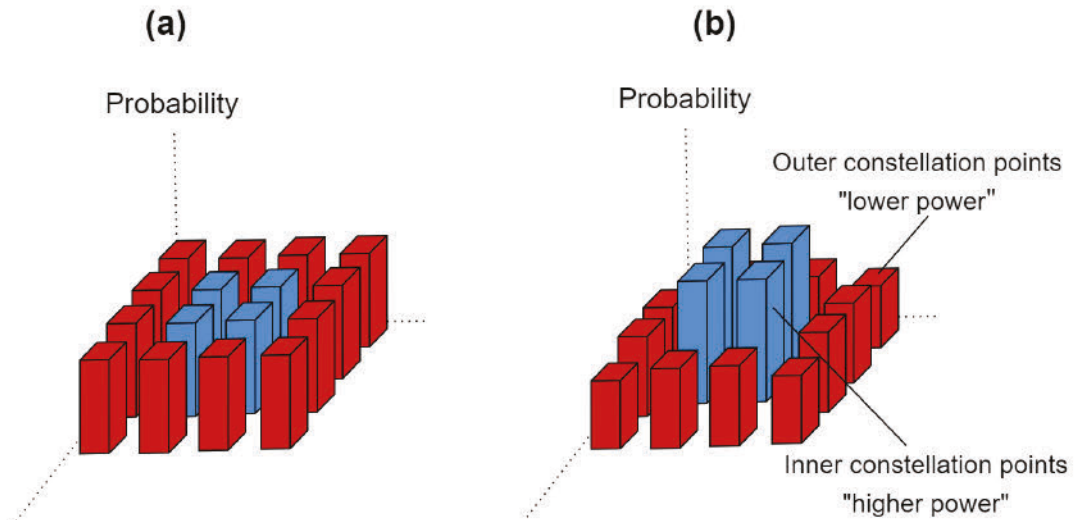


Fig. 2.14 A graphical comparison of assigned probability of occurrence for constellation points in a) a uniform 16-QAM (b) a probabilistically shaped 16-QAM

the forward error correction (FEC) code [42]. As it can be interpreted from the SE equation, there are 4 ways of increasing the SE and these ways are:

1. Increasing the symbol rate R_s : Increasing the symbol rate (Baud rate) is one of the most obvious ways to increase the spectral efficiency in any telecommunication system. A decrement in the signal to noise ratio (SNR) comes as a direct response of increasing the baud rate and fixing the signal's power according to Shannon's law. Moreover, transmitting higher baud rates applies more pressure on the electronic and optical components of the system which have their own bandwidth limitations. These bandwidth limitations act like a low pass filter in some of the components such as the ADC and DAC and act like as nonlinear distorters in other components such as RF amplifiers. In both of the cases, the transmitted signal will be constrained by these components' physical limitations.
2. Higher modulation formats M : Another way of achieving higher SE is by encoding more bits into each symbol. This is achieved by utilising higher modulation formats such as (32QAM, 64QAM, and 128QAM) instead of the conventionally used QPSK and 16QAM. Utilising higher modulation formats will make the decoding and decision making process more vulnerable for errors considering that more constellation points will be packed in the same constellation area. In other words, the Euclidean distances between adjacent constellation points will dramatically minimise which make it harder

for the receiver to distinguish between these points in the presence of noise. Increasing OSNR will assist the receiver in making correct decisions however this will come at the expense of more nonlinearities due to the optical fibre interaction with high power pulses.

3. Less spaces between WDM subcarriers δf : Narrowing WDM subcarriers to each other will definitely support the compactness of the spectrum and allow for higher number of subcarriers to be inserted. On the other hand, careful consideration should be taken to assure that subcarriers don't overlap or that will cause an extremely unwanted cross talk.
4. Shortening the forward error correction (FEC) overhead: FEC is one of the methods which aims to correct receiver's decisions at the expense of redundancy. The FEC scheme utilizes additional overheads in correcting the falsely detected bits. As ITU-T recommends RS(255,239) FEC codes which usually require 7% overhead for dense WDM (DWDM) networks, other researches discussed adding longer overheads to increase the maximum reach of the optical link [47] [52]. Definitely, as the FEC overhead length increases, the entropy decreases which means less SE.

2.4 Conclusion

The main building blocks of a coherent optical transceiver are mapping, I/Q splitting, pulse shaping, Mach-Zehnder modulation, digital conversion and digital signal processing. These components work together to transmit and receive optical signals with high speed and spectral efficiency in modern optical communication systems. The scalability of these systems is a crucial factor in their design, and there are several dimensions that can be considered to increase their performance. The number of utilized channels, modulation format, baudrate are the three main dimensions to consider for scalability. DSP architecture of a conventional coherent optical transmitter is complex and requires careful consideration of the trade-off between modulation format, baudrate and SNR. Despite the challenges, coherent optical transceivers have demonstrated higher ISD, flexibility, and robustness against noise compared to older WDM-OOK based systems, making them a preferred choice in high speed transmission applications.

The digital to analogue conversion process in coherent optical transceivers is a crucial step in the data transmission. The process is composed of three main stages : resampling, quantization, and zero order hold. The zero order hold function introduces spectral replicas of the base-band signal that need to be removed by an analogue anti-aliasing filter. This chapter

presented the mathematical representation of zero order hold transfer function and its effect on the spectral replicas of the base-band signal in the digital to analogue conversion process. It also discussed two types of optical modulators used in coherent optical communication systems, direct modulation and indirect modulation. Among the indirect modulators, the Mach-Zehnder Modulators (MZMs) were explored in detail, including its operational mechanism, properties, and its effect on the transmitted symbol. The up-conversion component of the carrier was also derived to provide a comprehensive understanding of the modulation process. The discussion in this chapter highlights the importance of understanding the underlying modulation mechanisms and their impact on the performance of the optical communication systems.

The chapter has provided an overview of the DSP techniques applied in coherent optical communication systems. The goal of these techniques is to eliminate linear impairments such as CD and PMD that occur in the fiber link transmission. To achieve this, equalization is performed in two stages; the first stage being a static equalization process and the second stage being an adaptive equalization process. The static equalization involves the use of a MF combined with a CD equalizer to remove CD and ISI components. The adaptive equalization process employs a 2X2 MIMO structured adaptive filter or "butterfly shape adaptive filter" to remove any residual CD and PMD effects. There are two main categories of PMD equalization: data-aided and blind equalization. Data-aided equalization requires the insertion of training sequences to estimate the channel's response, while blind equalization uses the properties of the transmitted modulation format to estimate the MSE and minimize it. Three main adaptive algorithms are used for PMD equalization: CMA, DD-LMS and RLS.

Timing recovery , frequency and phase recovery and probabilistic constellation shaping are important elements in modern digital communication systems. Timing recovery is the process of correcting clock jitter and optimizing the sampling phase to minimize ISI. Gardner's method is one of the most widely used technique for timing recovery due to its simplicity. Frequency and phase recovery, also known as carrier recovery, is the process of correcting the frequency and phase deviations in a received signal caused by deviations and fluctuations in the optical source and transmission system. Carrier recovery can be conducted blindly or with the use of pilot symbols. Probabilistic constellation shaping (PCS) is a technique used to improve the performance of a communication system by manipulating the probability of occurrence of the symbols in a conventional QAM modulation. PCS can achieve up to 1.53 dB shaping gain under AWGN which makes it an essential part of modern optical transceivers.

Chapter 3

Non-linearity in Digital to Analogue converters

3.1 Theory

The ubiquitous presence of non-linearity in optical and electrical subsystems impose an immense number of challenges for high speed coherent optical communication systems. The complexity of non-linearity arises from the fact that most forms of non-linearity can not be compensated for by using conventional linear DSP methods. This would usually make them harder to deal with and computationally expensive to solve. Therefore, non-linearity and its variations in optical communication systems have been always a fertile ground for research and investigations. For instance, IQ-MZM transfer function non-linearity, over driven RF amplifier induced non-linearity and Kerr non-linearity have been studied in several occasions. While, a few of them attracted more attention than others, one type of non-linearity has been completely neglected despite its potential effect on future generations of coherent optical transceivers which might rely on higher modulation formats to maximise their SE. Similar to most electro-optical components of the system, digital converters have their own non-linearity which are accounted for in ENOB calculations. Non-linearity is one of many other sources of noise and distortion which have distinctive behavioural nature in digital converters. Those unique behavioural natures allow them to be classified under two main categories. The first category is signal-dependent or frequency dependent. They can also be called as "dynamic ENOB contributors" which implies that they are the ones accountable for ENOB variation over range of input signal frequencies. The two main examples for dynamic ENOB contributors are time jitter and digital converter's frequency response. Those contributors have been modelled in [53] represented as

$$\begin{aligned}
ENoB(f) = & ENoB_{DC} - \frac{1}{2} \log_2 \left(1 + 6(2^{ENoB_{DC}} \pi f \sigma_{tj})^2 \right) \\
& + \log_2 |H(f)| - \frac{1}{2} \log_2 \left[\frac{1}{f_B} \int_0^{f_B} |H(v)|^2 dv \right]
\end{aligned} \tag{14}$$

It can be clearly noted that the main frequency dependent terms of the equation are the second term on the RHS of eq (1) which includes the jitter σ_{tj} and the third term on the RHS of eq (1) which accounts for the frequency response $|H(f)|$. While, the final term on the RHS of eq (1) is a representation of the correction factor or what's referred to as processing gain. Processing gain is a result of an internal digital filter applied to signal which does not occupy the full Nyquist bandwidth. Applying the digital filter suppresses the out of band noises and distortions and enhances SNR which consequently improves the overall ENOB. $ENoB_{DC}$ in eq (1) includes all static impairments such as non-linearities, thermal noise and other frequency independent noise. $ENoB_{DC}$ is usually measured at low input frequencies since it's expected to be dominant in these regions.

3.1.1 The distinction between integral and differential non-linearity

Integral non-linearity (INL) and differential non linearity (DNL) are the two forms of non-linearity in digital converters. Prior to reviewing the distinction between them, it's extremely important to understand the underlying mismatches in circuit-level structure which result in this phenomena. Despite the wide variety of DAC topologies [15] such as thermometer [54], R2R ladder [55] and segmentation, most DACs employed in high speed optical transmission descend from a current steering architecture. Fig 3.1 shows a simplified circuit diagram for a binary weighted current steering DAC. A D_N of switches control N number of current sources to convert the binary digital input to an analogue output.

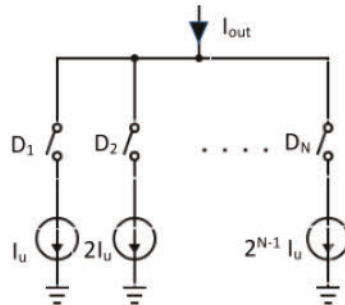


Fig. 3.1 A simple binary weighted current switching DAC with N bits resolution

The output current for any specific input code will be a summation for output of all activated current sources and is calculated by the following equation

$$I_{\text{out}} = D_N (2^{N-1}I_u) + \dots + D_2(2I_u) + D_1I_u. \quad (15)$$

Fig 3.2 represents the resultant transfer function of a hypothetical ideal DAC with 3 bits resolution. Each level of the vertical axes resembles a unique current value which is a fraction of the DAC's full scale (maximum current) while the points on the transfer function line show which digital code (input) does that analogue current (output) corresponds to. The output difference between two successive digital inputs is called least significant bit (LSB). LSB is the smallest output step in a digital converter. For instance, the 1 LSB in the hypothetical DAC presented in fig 3.2 is 0.2V.

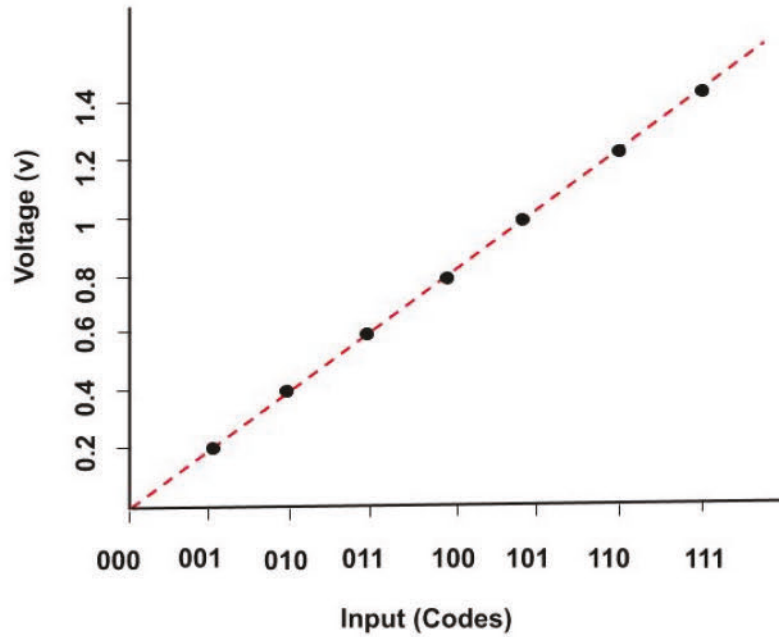


Fig. 3.2 Transfer function for an ideal 3 bits DAC

A current steering DAC ideally has identical current sources (sub DACs) with a similar output. However, due to internal circuit non-idealities and mismatches, a deviation from the expected output current for each input digital code is highly anticipated [56]. This deviation can take different forms and can range from a slight anomaly to a severe diversion. For instance, missing codes, which affect the monotonicity of the transfer function would be considered as a severe impairment while slight difference between a point on the real transfer function line and its ideal counterpart can be considered as a slight anomaly. Other types of

errors such as gain and offset errors can also be displayed on the transfer function however they won't be discussed in details in this chapter.

Two types of non-linearities, INL and DNL, can be realized form a digital converter transfer function. INL can simply be defined as the maximum deviation between an ideal and a real transfer function line. INL can take different shapes based on the topology of the digital converter. For instance, The S shape showed in fig 3.3a is common in high speed digital converters for coherent optical communication systems while the bow shape showed in fig 3.3b is common in other types of digital converters. Different shapes have different harmonic properties. For instance, the 3rd is dominant in an S shaped INL digital converter while the 2nd harmonic in bow shaped INL digital converter. Harmonics always appear on the spectral analyzer as integer multiples of the fundamental frequency. Assuming a fundamental sinusoidal signal with frequency f_c , the 2nd will be located at $2f_c$ and the 3rd harmonic will be located at $3f_c$ etc.

As previously explained, the difference between two successive outputs is 1 LSB. In a real case scenario, that difference might be more or less than 1 LSB and that difference is refered to as DNL. DNL can be negative, positive or zero and it is measured for each two successive outputs individually. INL for point m can be derived from DNL bu computing its comulative sum

$$INL[m] = \sum_{i=1}^{m-1} DNL[i] \quad (16)$$

3.1.2 Performance metrics (THD,SINAD and ENOB)

An illustration for a typical output spectrum for a digital converter is shown in fig 3.4. The fundamental sinusoidal signal f_c usually has the highest power. The noise floor is a combination of quantization noise, thermal noise and any electronic emitted noises. Any distinct pulse above the noise floor level can be either a harmonic or a spur. As previously explained, harmonics are a byproduct of non-linearity in a digital converter. However, spurs have other origins such as interleaving mismatches and clock signal leakages. Harmonics and spurs power can be expressed in dB as absolute power or in dB_c as a relative power to the fundamental signal. For example, the power of harmonic k is calculated as

$$P_k[dB_c] = 10 \log \left(\frac{P_k}{P_c} \right) \quad (17)$$

Where P_c is the power of fundamental and P_k is the power of the harmonic k . Total harmonic distortion is one of the standard metrics to assess the performance of a digital converter. Well

designed digital converter is expected to have a low THD while a high THD is an indication for high non-linearity. THD can be calculated as

$$THD[dB_c] = 10\log \left(\frac{\sum_{k=2}^N P_k}{P_c} \right) \quad (18)$$

Where N is the total number of harmonics taken into account. The difference between highest harmonic and fundamental signal is called spurious free dynamic range. High quality digital converters with low non-linearity are expected to have high SFDR.

Likewise, another paramount metric for digital converters is signal to quantization noise ratio. $SQNR$ can be calculated as

$$SQNR[dB] = 10\log \left(\frac{P_c}{P_Q} \right) \quad (19)$$

Where P_Q is the quantization noise power or the quantization variance. According to Bennett's approximations [25], $SQNR$ can be expressed as

$$SQNR(dB) = 6.02N_b + 1.76dB - PAPR(dB) + 3dB \quad (20)$$

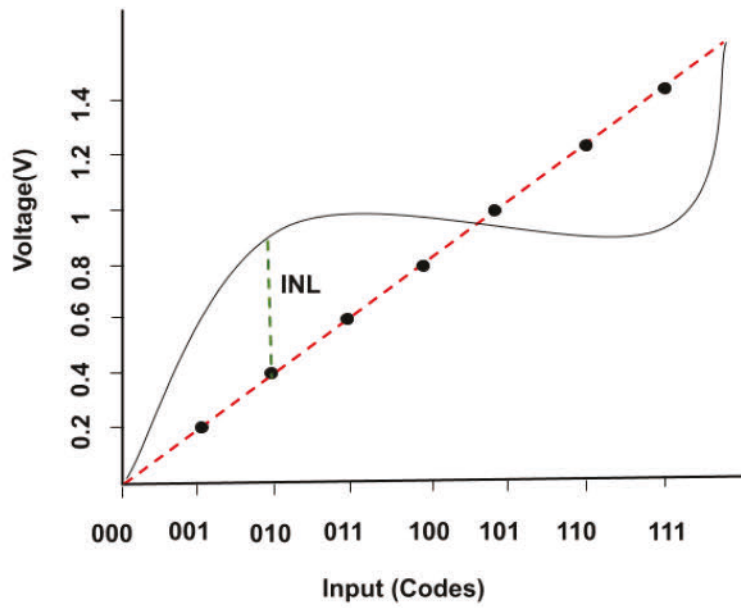
Where N_b is the number of resolution bits and $PAPR$ is the peak to average power ratio for the input signal. In the case of a sine wave form input, $PAPR = 3$. As it can be noticed, the two main variables in defining the $SQNR$ are the number of resolution bits and the $PAPR$ of the input signal.

$SINAD$ on the other hand can be calculated as

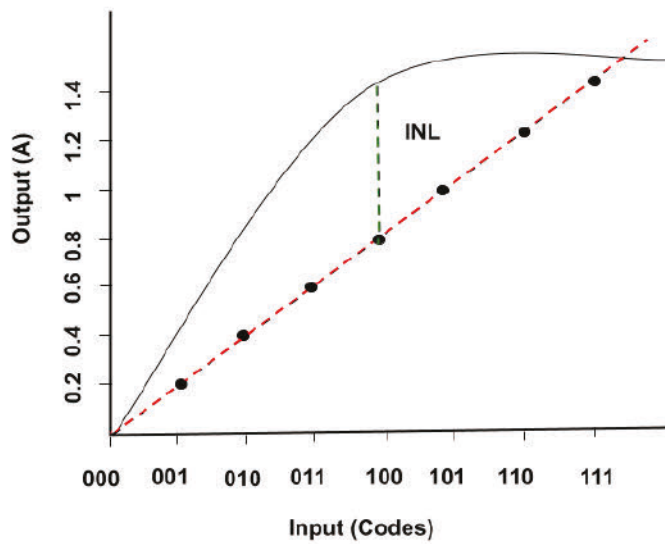
$$SINAD[dB] = 10\log \left(\frac{P_c}{P_N + THD} \right) \quad (21)$$

Both $SINAD$ and $SQNR$ take into account the quantization noise, however, $SINAD$ is a more comprehensive and adequate measure due to the harmonic distortion and other noises being included as shown in equation 21. As the bit resolution could be derived from the $SQNR$ equation, an equivalent definition is derived by replacing $SQNR$ in equation 20 with $SINAD$ is called effective number of bits

$$ENOB = \frac{SINAD - 1.76dB - PAPR(dB) + 3dB}{6.02} \quad (22)$$



(a) S shaped INL



(b) Bow shaped INL

Fig. 3.3 Types of INL in DACs
M. Abu-Romoh, PhD Thesis, Aston University, 2022

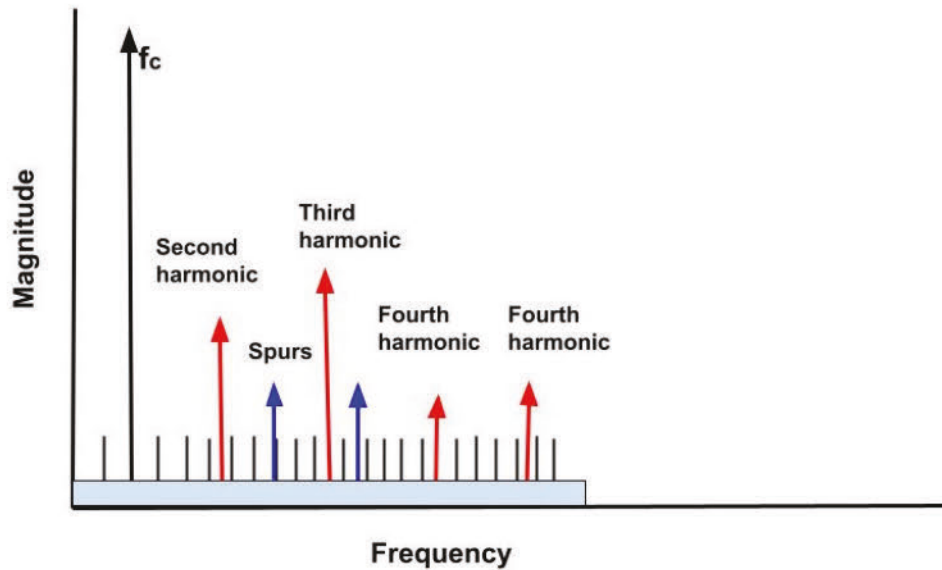


Fig. 3.4 The spectrum of harmonics and spurs generated at the output of a digital converter with a single sinusoid f_c input

As it can be noticed, ENOB is a quantity which implicitly includes quantization noise and distortion, thus, gives an overview of the resolution and linearity of a digital converter. This feature made it one of the most widely used expressions in defining the digital converter's performance [57].

3.2 Practical INL measurements

3.2.1 Theory

The histogram test is one of the classical methods to measure INL in digital converters. According to IEEE standards, a histogram test can be conducted by either a linear ramp or a sinusoidal signal [58]. The generation of a clear sine wave is usually simpler and more straightforward than other forms of wave, hence, the sinusoidal histogram test is the commonly used for INL measurements. An integer number of sinusoidal periods is generated, the waveform is captured by an ADC and the code density is measured [59] as shown in fig 3.5. Code density will later be compared to the expected code density for an ideal sinusoidal signal to estimate DNL and INL. An ADC with N resolution would have 2^N codes and each code has a code width of $F_s/2^N$ where F_s is the full scale of the ADC. If the input sinusoidal signal is

$$V = A \sin(\omega t + \phi) + d \quad (23)$$

where A is sine wave amplitude, ω is the angular frequency, ϕ is the initial phase and d is the offset. The probability density function of the sine wave can be calculated accordingly as

$$p(V) = \frac{1}{\pi \sqrt{A^2 - (V - d)^2}} \quad (24)$$

non-linearity tests normally require a long sequence of data points to ensure that all bins have been sufficiently exercised and tested. Additionally, the sine wave frequency is wisely chosen in such a way that the ratio of the sinusoidal and sampling frequency is a rational number of prime numerator and denominator [60]. Respecting this criterion is essential to ensure asynchronous sampling which eliminates the effect of phase noise on non-linearity test measurements [61]. Fig 3.5 is an illustration for a SHT applied on a sinusoidal signal. As can be seen from the shown histogram, codes at the two ends of the occupied range of the digital converter have higher probability of occurrence comparing to codes located on the middle of the range. For instance, H[0] and H[8] are expected to have higher code count comparing to H[3].

DNL can be calculated by knowing the amplitude and frequency of the input sinusoidal signal, constructing an equivalent ideal sine wave and directly comparing the PDFs of the actual and ideal wave. The PDF of any single input point of the sine wave is calculated as illustrated in equation 24. The probability of occurrence of a single digital converter bin is derived by integrating equation 24 over the bin size. In an ideal case scenario, bin n would have a size of $[(n-2^{N-1}) - (n-1-2^{N-1})]$.

Hence, the probability of occurrence of a sinusoidal over a bin is expressed as

$$P(n) = \frac{1}{\pi} \left[\arcsin \left(\frac{F_S \times n - 2^{N-1}}{A \times 2^N} \right) - \arcsin \left(\frac{F_S \times n - 1 - 2^{N-1}}{A \times 2^N} \right) \right] \quad (25)$$

equation (25) calculates the probability of occurrence of a sinusoidal signal in a specific bin based on the characteristics of the digital converter. It takes into account the bin code number (n), the full range of the digital converter (F_S), and the digital converter resolution (N). The formula calculates the probability by finding the difference of two arcus sine functions, which represent the probability of a sinusoidal signal having a specific amplitude level within the full range of the digital converter. The numerator of each arcus sine function represents the deviation of the amplitude level from the mid-range value of the digital converter, while the denominator represents the range of the digital converter divided by the number of possible amplitude levels. This equation is used to determine the accuracy of the digital

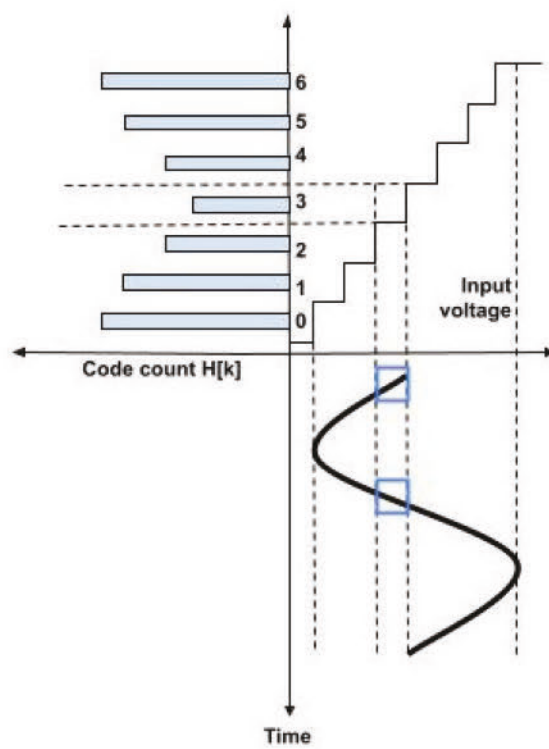


Fig. 3.5 Sinusoidal histogram test mechanism

converter in representing analog signals, and the difference between the two arcs sine functions can be used to calculate the differential non-linearity (DNL), which measures the deviation of the digital converter's step size from its ideal value. DNL can be calculated as follow

$$DNL = \frac{\text{actual } P(n^{\text{th}} \text{ code})}{\text{ideal } P(n^{\text{th}} \text{ code})} - 1 \quad (26)$$

As previously mentioned, INL can be derived by knowing DNL as shown in equation 16.

Fig 4.3 is an illustration for the difference in sinusoidal PDFs of an actual and ideal digital converter. The deviation is what gives rise to DNL and INL.

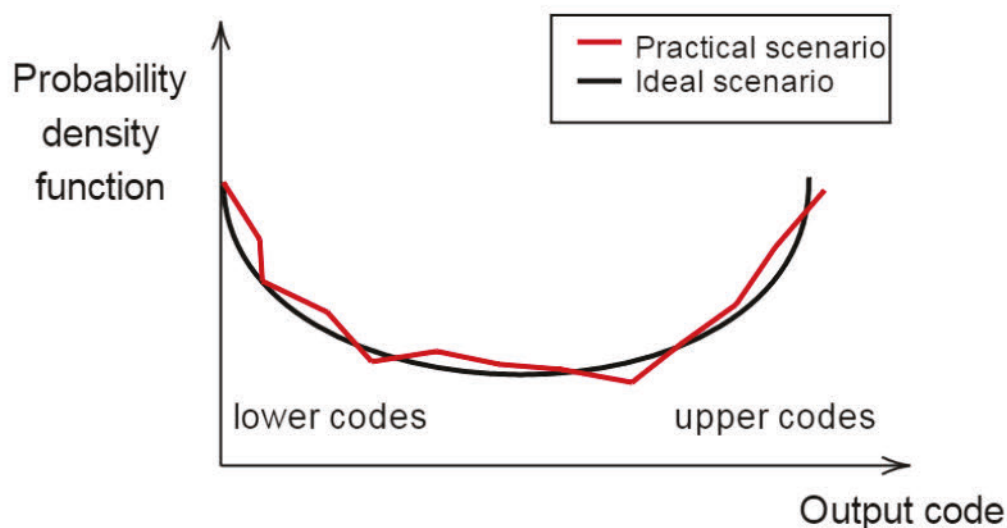


Fig. 3.6 Illustration for sine wave PDF difference of actual and ideal digital converter

3.2.2 Experimental measurements

The importance of quantifying INL in a high speed digital converters for coherent optical communication systems arises from their potential effect on high modulation formats such as 256 QAM and higher. The small euclidean distances between adjacent constellation points, by sustaining the average power and increasing the modulation order as shown in fig 3.7, increases the susceptibility against noises and distortion significantly. Thus, it's very crucial to anticipate any source of distortion and noise which might cause a performance degradation by careful characterisation and in-depth study of all components of the optical transceiver.

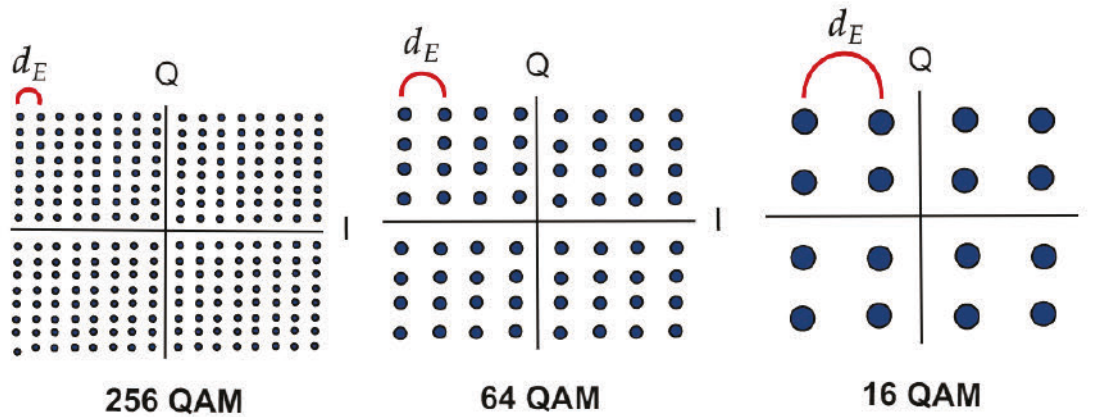


Fig. 3.7 A comparison of the euclidean distance between two adjacent constellation points in 256, 64 and 16-QAM

INL has been studied in a real case scenario with an electrical B2B setup as shown in fig 3.8. The setup is consisted of 8 bits, 92 GSamples pair of DAC/ADC. High speed digital converters for coherent optical communication systems are made up of 4 timely interleaved sub DAC/ADC pairs, therefor. 4 separate sinusoidal signal with identical frequencies are generated and uploaded to each sub DAC. The sinusoidal signal frequency is chosen to be 533.2662 MHz for two reasons. Firstly, in order to meet the asynchronous sampling criterion as previously explained. Secondly, to minimise the effect of frequency response and sampling jitter since 533.2662 MHz is considered relatively low comparing to the overall bandwidth of a high speed digital converter. Each sinusoidal signal is later captured by a corresponding sub ADC and SHT is applied to each sub ADC individually. The resultant is a combined INL of the DAC/ADC pair.

Fig 3.9 indicates the measured INL for each sub DAC/ADC pair identified by different colour. SHT has been applied to the all $2^8 = 256$ codes. Noticeably, INL curves for all sub DAC/ADC pairs are nearly identical which indicates that all sub DAC/ADC pairs have similar circuit structure and mismatches.

3.2.3 Modelling

INL is an intrinsic feature in digital converters. Therefore, the capability of conducting a comprehensive study on the effect of different INL values on transmission is limited to the availability of multiple digital converters with different INL characteristics. Obtaining a digital converter with specific INL requires introducing circuit mismatches deliberately which is not commonly practiced in industry. Hence, introducing an INL model which can

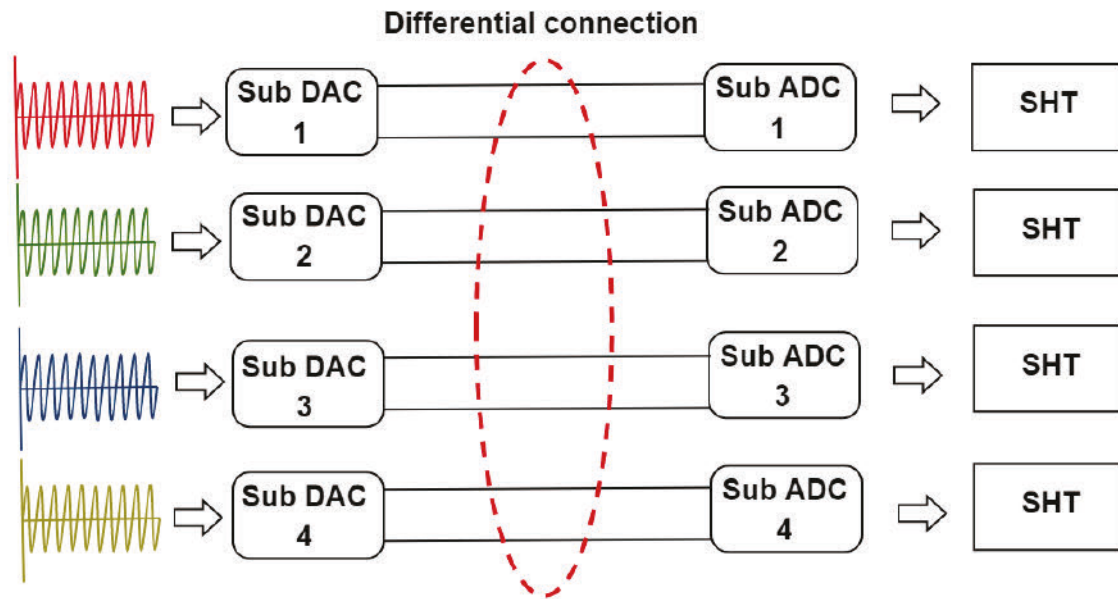


Fig. 3.8 Block diagram for SHT applied on Electrical back to back 8 bits/ 92 GSamples/s DAC/ADC setup

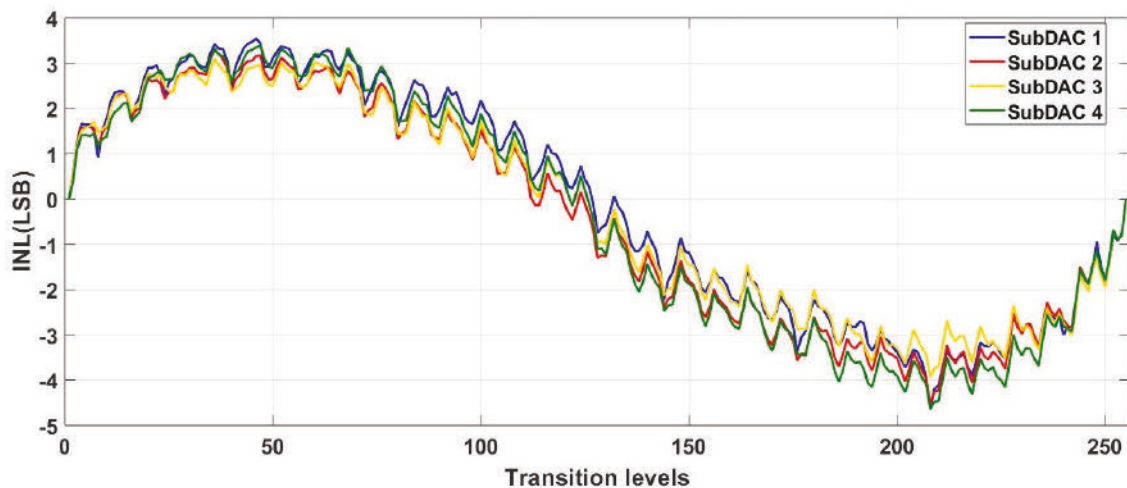


Fig. 3.9 INL measured for all codes in a real commercial 8 bits/ 92 GSamples/s DAC/ADC using SHT

easily be applied and adjusted accordingly in analytical investigations and experimental setups is immensely beneficial. Similar digital models have been introduced to manipulate the jitter [62] and limit down DAC's resolution [63], however, no model has been introduced to manipulate the INL.

Using simple curve fitting methods, a general INL "S" shaped model has been constructed based on the experimental work discussed in subsection 3.2.2. For the sake of simplicity, it has been assumed that sub DACs and ADCs have identical INL. Hence, the INL can be presented as shown in fig 3.10. The model is not restricted to 8 bits resolution as it can be altered to higher or lower resolution by adjusting the LSB voltage. LSB is calculated as $LSB = \frac{V_{fs}}{2^N}$ where f_s is the full converter scale and N is the resolution. Any change in the resolution will directly reflect on LSB . Moreover, any change in resolution will likely not affect the overall shape of INL since the circuit topology will remain the same but the number of current sources will be reduced.

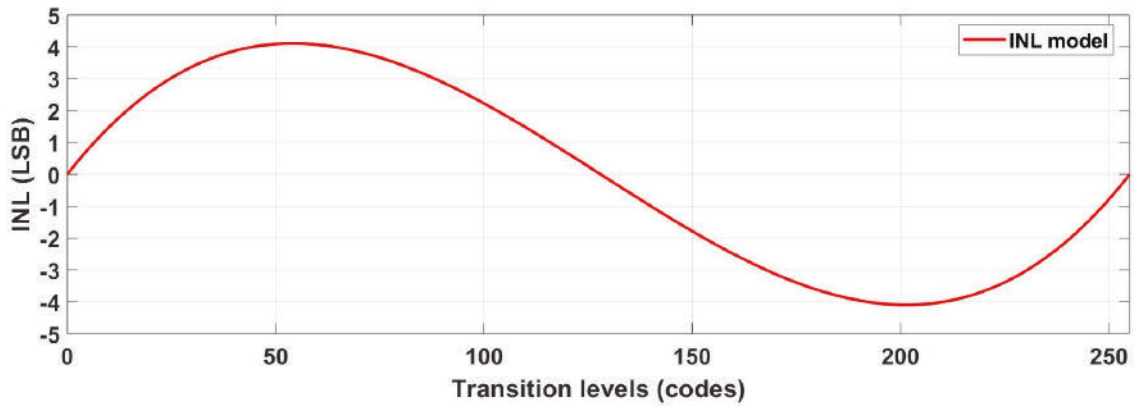


Fig. 3.10 INL model constructed based on experimental results

To justify the proposed model, a numerical test has been applied where a sinusoidal signal is inserted to the INL model then an 8 bits DAC/ADC pair. The output signal is then tested for linearity using SHT. INL has been swept from 0 to 7 and the SHT results are plotted against an ideal INL addition. As can be seen, the maximum deviation from the ideal INL mode is 0.28 LSB. The model demonstrates a 95% accuracy according to the test.

3.3 INL effect on ENOB

INL is one of the major $ENOB_{DC}$ contributors which reflects on the output spectrum of a digital converters in a form of harmonics. The magnitude and power of those harmonics rely on the severity and shape of INL. For instance, quadratic shaped INLs, eg. bow shaped

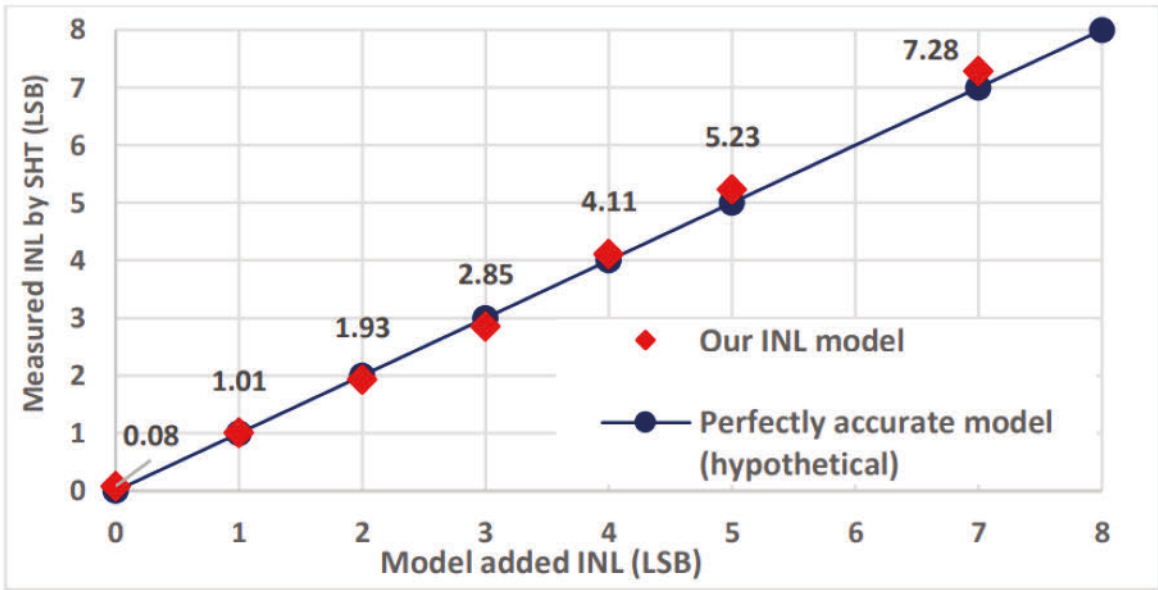


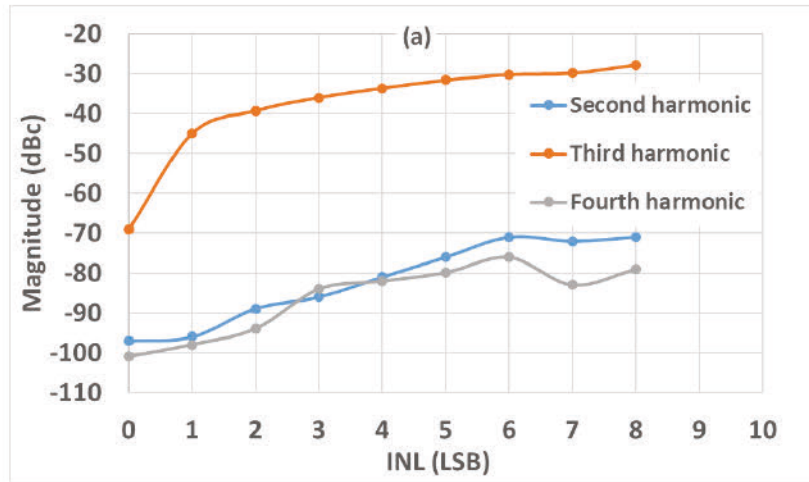
Fig. 3.11 A comparison between model added INL and measured INL by applying SHT

INL, boost even order harmonics especially 2^{nd} harmonic while cubic shaped INLs, eg. "S" shaped INL, boost odd order harmonics especially 3^{rd} harmonic. Thus, INL shape can be predicted by looking at dominant harmonics. Harmonics with relatively large magnitude indicates severe non linearity which result into a low SINAD and low ENOB.

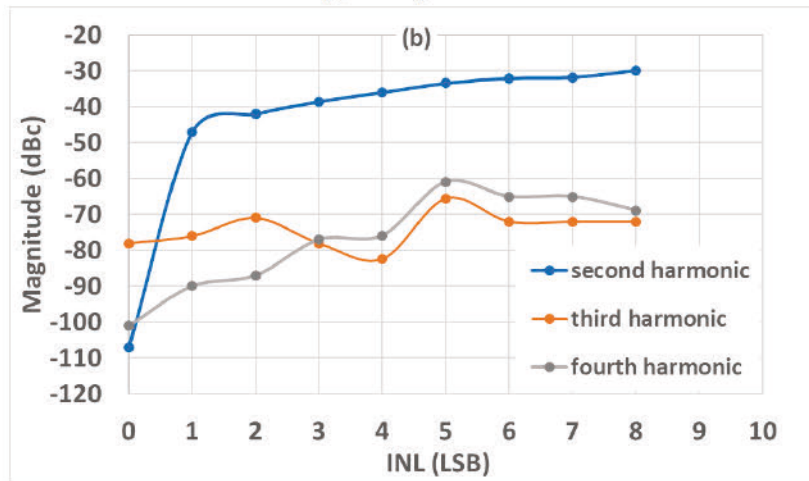
The effect of sweeping INL on harmonics has been numerically studied using the INL model. The model has been set to test two INL shapes, S shaped and bow shaped. INL shape is directly related to the internal architecture of the digital converter and can suppress specific harmonics and boost other harmonics as explained. A 1.3 GHz sinusoidal signal has been applied and harmonics magnitudes have been measured. All magnitudes have been measured in dB_c (decibel relative to carrier) as expressed in the following equation

$$P_S(dBc) = 10\log\left(\frac{S}{C}\right) \quad (27)$$

Where S refers to the signal power and C refers to the carrier power. As can be seen in fig 3.12a, every LSB increment of a S shaped INL increases the 3rd harmonic magnitude by 3 dB approximately while doesn't affect other harmonics. Similarly, every bow shaped INL increases the 2nd harmonic magnitude by 3 dB approximately while doesn't affect other harmonics as can be seen in 3.12b. The stronger the INL is, the higher harmonic magnitudes are and higher distortion is which reflects negatively on ENOB. This relationship is illustrated in fig 3.13 where INL has been swept from 0 to 8 LSB and ENOB calculated for each INL



(a) S shaped INL



(b) Bow shaped INL

Fig. 3.12 A comparison of different harmonics magnitudes for different INL variations

value in a DAC/ADC electrical back to back configuration. Every additional 1 LSB of INL degrades ENOB by 0.2 bits approximately.

3.4 INL effect on coherent transmission

To study the effect of INL on 256-QAM, an optical back-to-back setup was implemented as shown in fig 3.14. The setup included an arbitrary wave generation (AWG) at the receiver side which generates 23GBaud, 256-QAM. A 5% QPSK pilot symbols for synchronization and aiding carrier recovery algorithms at receiver side. A pulse shaping with 0.2 roll off factor was applied, followed by an INL model to control the added INL. Symbols are inserted into

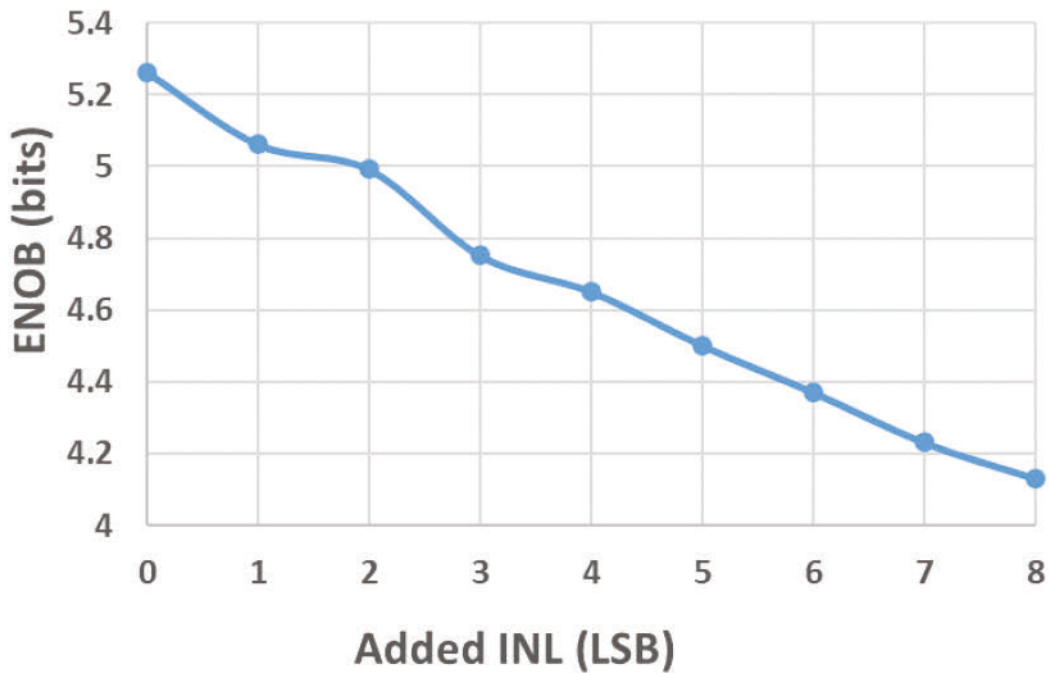


Fig. 3.13 ENOB degradation for different INL values

an 8 bits and 92 GSa/s DAC then optically converted using a CFP2 optical transponder. At the receiver side, an 8 bits, 92 GSa/s ADC captures the traces and convert the samples into a digital form. Subsequently, all samples undergo conventional processing via pilot-based DSP algorithms with a decision directed least mean square algorithm for adaptive filtering and pilot aided phase noise compensation DSP. The DSP sequence ends with mutual information (MI) estimation, which provides a good estimate of BER after FEC decoding is applied.

INL is swept along a range of 0 to 10 LSBs at different signal to noise ratio (SNR) levels. MI has been estimated and plotted on fig 3.15. As can be seen, an increment of 2 LSB of INL causes a 0.15dB of SNR degradation. It can be seen that the degradation difference is constant over the whole SNR range.

3.5 Conclusion

The non-linearity presence in optical and electrical subsystems poses a significant challenge for high-speed coherent optical communication systems. The complexity of non-linearity stems from the fact that conventional linear DSP methods cannot effectively compensate for

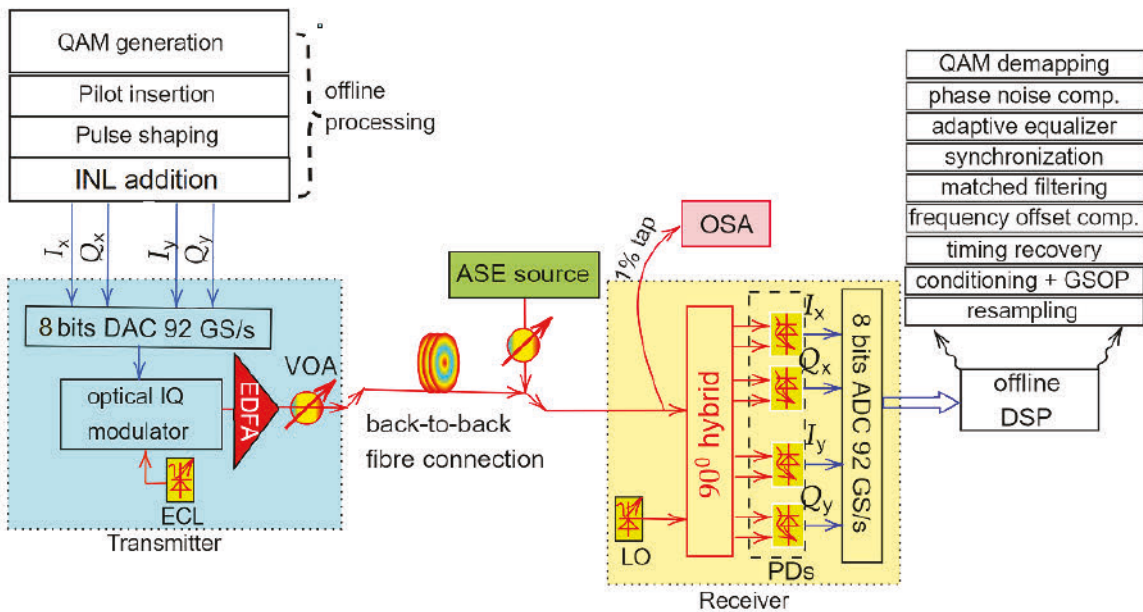


Fig. 3.14 An experimental optical back to back setup for a coherent optical transmission system

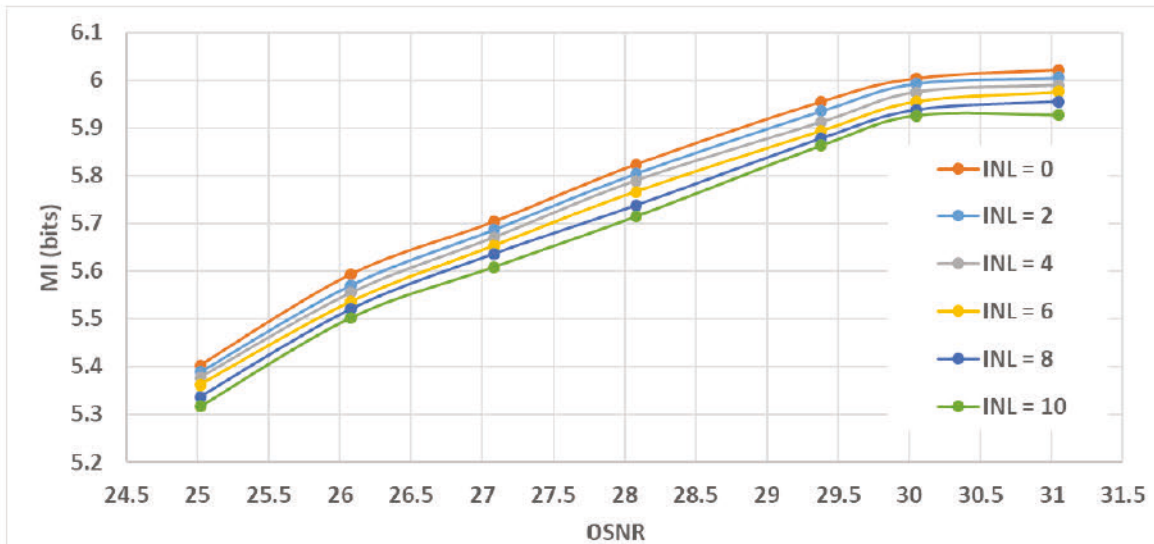


Fig. 3.15 The effect of different INL values on OSNR vs mutual information performance for a 256-QAM configuration

most forms of non-linearity, making it difficult to deal with and computationally expensive to solve.

Studies have focused on different forms of non-linearity such as IQ-MZM transfer function non-linearity, overdriven RF amplifier induced non-linearity, and Kerr non-linearity. However, digital converters have their own form of non-linearity that has been largely neglected despite its potential impact on future generations of coherent optical transceivers, which may rely on higher modulation formats to maximize their spectral efficiency.

Digital converters are known to have unique behavioral characteristics that can be classified into two main categories: signal-dependent or frequency dependent and signal-independent or frequency independent. Time jitter and digital converter frequency response are the main examples of the first category while INL and thermal noise are the main examples of the second one.

The existence of non-linearity in digital converters manifests itself in two distinct forms: INL and DNL. INL and DNL are caused by mismatches in the circuit-level structure, and it is crucial to comprehend these mismatches to fully grasp the distinction between INL and DNL. In the field of optical transmission, high-speed digital-to-analog converters (DACs) are widely implemented using a current-steering architecture. The current output for a given digital input code is computed as the result of the aggregation of all activated current sources in the circuit. Mismatches cause output deviation which results in non-linearity.

The magnitude and power of harmonics in a digital converter's output spectrum is largely influenced by INL. The shape of INL, either bow-shaped or S-shaped, directly impacts the dominant harmonics and results in a low SINAD and ENOB if the INL is high. A numerical study showed that every additional LSB of INL degrades ENOB by 0.2 bits. Similarly, an optical back-to-back setup was implemented to study the effect of INL on 256-QAM. The results showed that INL has a significant impact on the BER (Bit Error Rate) of the system. The strong relationship between INL and ENOB highlights the importance of reducing INL in digital converters to improve their performance.

Chapter 4

Neural networks for digital converters non-linearity compensation

ANNs are a category of deep learning which falls under a broader set of mathematical algorithms called machine learning. The term "machine learning" has been popularized by the engineer Arthur Samuel in 1959 [64] as he quoted describing the program he designed "A computer can be programmed so that it will learn to play a better game of checkers than can be played by the person who wrote the program". Considering the complexity of most real-life models which might incorporate numerous unknown parameters, ML manifests itself as an effective tool to approach a numerical solution through various ways of optimization using representative sets of data. This process can be perceived as an advanced level of programming where the program learns and improves from experience to perform certain tasks without being explicitly written to do so.

ML has been used in a variety of fields and for various applications such as natural language processing [65], speech and hand writing recognition [66] [67], stock market prediction [68] and medical cancer diagnosis [69]. Despite the faced challenges and obstacles to translate the fast-paced theoretical advancements in the field of ML into real-life utilization over the last few decades, a renewed interest among researchers and engineers is prominent [70]. This interest is ignited by the exponential growth of computational power which is considered as one of the pivotal pillars of any real-life application for ML [71]. Additionally, the attainability of storing big sets of data and the ease of accessing them through cloud services or on-site storage units make it easier to apply ML to real-life problems.

Undoubtedly, the complexity of numerous telecommunication problems which can not be solved by traditional engineering solutions or accurately modeled to capture all underlying physical properties will require advanced data-driven methods to solve. Hence, this qualifies the field of telecommunications to be one of the major beneficiaries of the aforementioned

renaissance of ML. For instance, signal detection [72], channel estimation [73], coding and encoding [74] and resource allocation [75] are a few of the investigated problems with ML-based solution proposals.

Optical telecommunication systems were not abandoned by this research and investigation movement. Incorporating ML in optical communication systems started by targeting non-linearity in optical links which arises from the intrinsic Kerr effect [76]. Non-linearity in coherent optical communication systems is considered as one of the prolonged limiting factors for the maximum achievable rates. Despite the existence of the well-known non-linear Schrodinger equation which models the light propagation over an optical fiber [77], a highly efficient equalizer to compensate for the effect of non-linearity is still challenging to design. This can be attributed to the reliance on multitude of channel intrinsic coefficients such as chromatic dispersion, attenuation and Kerr non-linearity coefficients and transmitted signal parameters such as launch power, bandwidth and occupied wavelength. Moreover, despite the deterministic nature of Kerr non-linearity, the interplay of multiple transmitted signal over WDM channels will result in a stochastic like problem which can not be predicted from the receiver standpoint. A technique called digital back propagation has been previously introduced to solve the non-linear Schrodinger equation, hence, compensates for the non-linearity induced by the fibre [78]. Digital back propagation is an iterative digital process which aims to invert the effect of non-linearity by dividing the fibre into segments and each segment is governed by a linear and non-linear component. Despite the significant gains achieved by applying digital back propagation on long transmission systems, the technique is considered computationally intensive especially with long distances, high launch powers and high baud rates. Moreover, digital back propagation does not account for amplification and other sorts of noise which extremely limits its capability to perform a full compensation. ML algorithms are known for their ability to perform regression and classification. Both of the processes can be used to estimate and compensate for non-linearity in coherent optical communication systems assisted by conventional DSP to compensate for all the other linear impairments and distortion. Hence, ML demonstrates itself as a strong, energy efficient and low complex candidate for non-linear compensation in long coherent transmission systems [79].

Non-linearity in coherent optical communication systems is not fibre exclusive. The optical transceiver is assembled of optical, electrical and electro-optical components which impose different forms of non-linearity on the signal. More severe effects are expected when utilizing high modulation formats such as 64-QAM and beyond. Due to its high peak to average power ratio comparing to uniform constellation, probabilistic constellation shaping (PCS) drives higher component non-linearity [80]. This results into higher non-

linearity effect on the transmission system. This chapter, will introduce a pre-compensation technique to compensate for digital converter's non-linearity, especially INL, based on indirect learning. Moreover, it will analytically study the performance improvement of applying the pre-compensation on a 64QAM/32 GBaud and 32QAM/32GBaud signal which suffers from the INL effect.

4.1 Machine learning

4.1.1 Learning algorithms

Learning in ML algorithms takes different forms and methods. However, they can be categorized into three main distinctive categories as follow

Supervised learning

Supervised learning is a ML task in which the algorithm attempts to classify or predict future values based on a set of labeled data fed into it by an external source. The key feature of supervised learning is the established knowledge of an output for each input of the training set. One of the common examples for supervised learning is image recognition. For instance, a computer can be trained to identify a certain type of fruits by feeding it million images labelled by the name of that fruit. Thereafter, the machine uses those labelled images to extract unique attributes and apply them on future predictions to distinguish any image of that certain fruit from any other fruit. If the training data comes from a discrete set of data the task is named "classification" as described in the example. If the training data comes from a continuous set of data the task is called "regression". Regression is when the algorithm extrapolates a correlation between two variables or more based on previous data. For instance, weather forecasting heavily depends on regression to predict future outcomes based on a number of variables which showed dependency in the past. Classification and regression are both visually illustrated in fig. 4.1. In this chapter, ANN based regression will be used to estimate DAC's non-linearity and design compensation block for it [81].

Unsupervised learning

Unsupervised learning is a ML task which aims to uncover hidden patterns from unlabeled data. One of the greatest examples of unsupervised learning is clustering. Clustering is the process of categorizing massive amount of unlabeled data to natural subgroups or clusters.

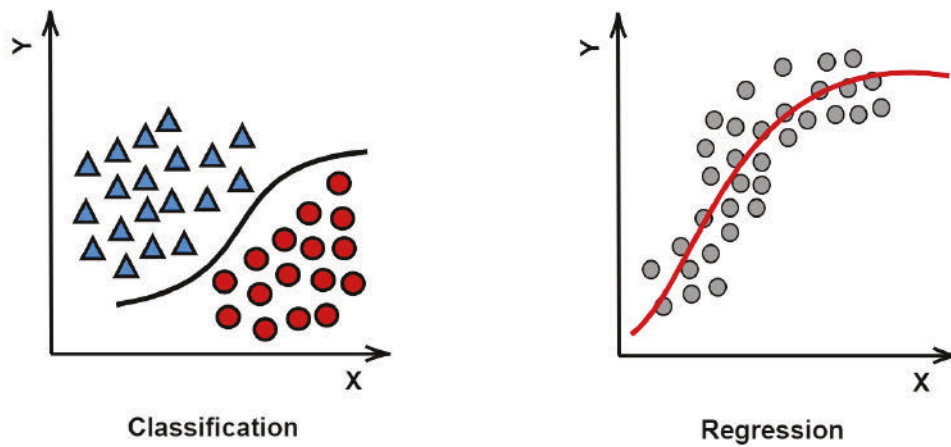


Fig. 4.1 Visual illustration for two types of supervised learning: classification and regression

Clustering is solely based on similarity with no pre-defined feature. One of the most common clustering algorithms is K-means clustering. In K-means clustering, the algorithm attempts to partition N number of points into K number of clusters. The algorithm assigns centroids to those clusters which would be the mean of the clustered points. Dimensionality reduction is another example for unsupervised learning. Assuming a massive training data set of N number of data points with K number of features. Thereby, the set is represented as a matrix with dimensions $N \times K$. The problem of processing large amount of data and reducing its dimensionality can be addressed by utilizing unsupervised learning techniques such as Principal Component Analysis and Linear Discriminant Analysis. These methods are designed to reduce the number of features in the data set while retaining the most important information, making it easier to process and analyze [81]. .

Reinforcement learning

Reinforcement learning is a ML technique which aims to train the algorithm to take decisions based on a trial and error approach. Reinforcement learning doesn't demand a set of samples fed into the system to train the algorithm as noted in supervised and unsupervised learning. Rather, the algorithm trains itself by evaluating the current state, taking an action and receiving a feedback from its surroundings to "reinforce" better future decisions. In other words, the algorithm navigates its way to perform a certain task in the best possible way solely by utilizing its gained knowledge from its own experience. Whilst, supervised and unsupervised learning can be considered as simple, myopic and singular solution oriented,

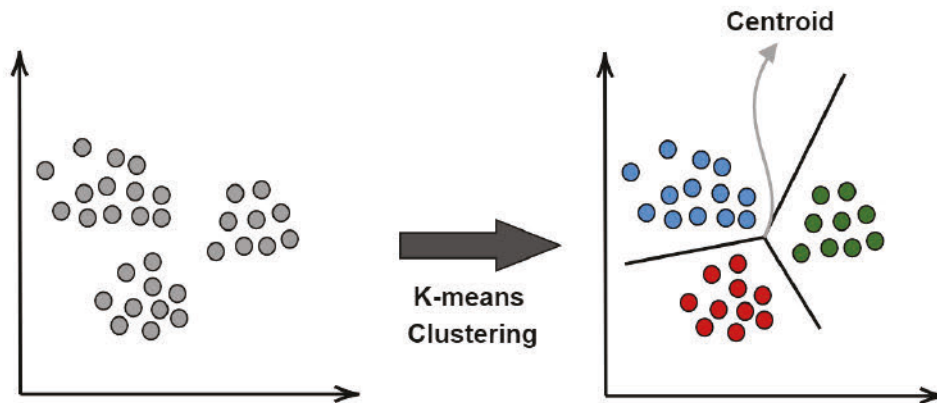


Fig. 4.2 Visual illustration for K-means clustering method

reinforcement learning is complex, farsighted and focused on optimizing a sequential set of decisions with broader objective. A computer learns how to play chess by competing against itself or against human chess players is an example for reinforcement learning. A self driving car learning how to drive in urban cities is another example for reinforcement learning. In both of the examples, the algorithm aims to perform a certain task by taking a sequence of optimized decisions. No single decision is correct, however, a sequence of decisions can lead to the best possible performance and that can be navigated by the algorithm through positive and negative feedback [82].

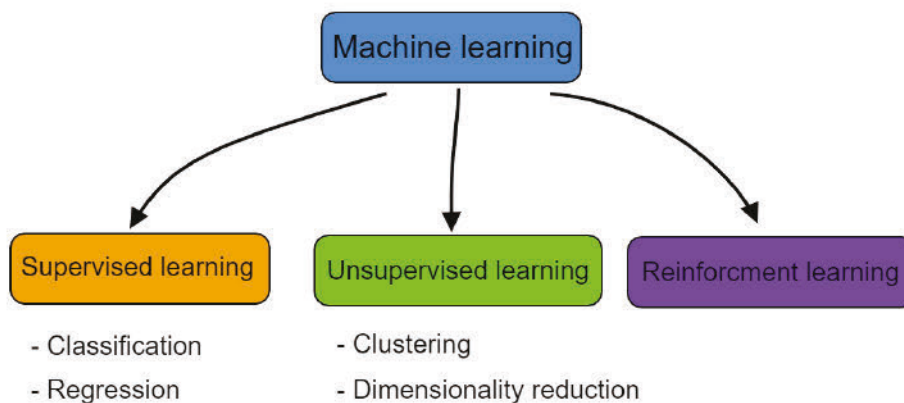


Fig. 4.3 Illustration for sine wave PDF difference of actual and ideal digital converter

Deep learning, multilayered neural networks consists of at least three layers, is one of the common methods used to perform reinforcement learning due to its capability to predict events and approximate complex functions. Neural networks are often dealt with as black-box models due to the lack of insight on the structure of approximated functions and exact route of convergence. This vagueness is a double edged sword. It eases the need for an in-depth mathematical knowledge to employ neural networks from a user stand point. However, it turns power optimization into a more challenging problem due to the one-solution-for-all approach neural networks take.

4.1.2 Artificial neural networks

ANNs are computer architectures which are modeled after human brains. They are built by a series of “neurons” (or “nodes”) and structured in layers. Those layers are connected in a consecutive manner and interplay to approximate a complex function. The structure of an ANN consists of an "input" layer, "output" layer and multiple layers in between performing most of the computation required by the network and called "hidden" layers. Each layer is consisted of n number of neurons. Those neurons are activated or deactivated by an activation function α which can be either a linear or non-linear. Hence, the signal propagates through those layers while being modified and altered by neurons to obtain a certain output at the end of the network.

Fig 4.4 depicts the structure of an artificial neuron with n inputs and single y output. Each one of those inputs is emitted by neuron from a previous layer. Each input is assigned a weight w_i which dictates its influence on the neuron’s output. An associated numerical value to the neuron called "bias" b controls the activation threshold by shifting. As previously mentioned, the neuron is activated or deactivated accordingly by an activation function. The operation can be mathematically represented as

$$y = \alpha \left(\sum_{i=1}^n w_i x_i + b \right) \quad (28)$$

where x_i is the i^{th} input of neuron and w_i is its weight. As described in the aforementioned mathematical representation, a vector of $x = (x_1, \dots, x_n)$ is weighted by a vector of weights $w = (w_1, \dots, w_n)$ through multiplication and summation then shifted by adding the bias b . The outcome passes through an activation function α afterwards to produce the neuron’s output.

During the training phase of neural networks, initial weights are often randomized. Forward propagation is the first step of training in which the data propagates from the input

layer to the output layer. During this stage, the weights are adjusted to generate a desired output at the output layer. The actual output would typically deviate from the desired output in the first few rounds of training. Hence, an optimization stage called back propagation is needed. Back propagation aims to minimize the cost function. The cost function in neural networks is an indicator of how well the ANN is performing its task and how accurate its predictions or approximations are. Generally, the cost function is the difference between the desired output and the actual output. Cost function calculation can be as simple as a mean square error or as complex as a cross entropy. Clearly, the smaller the cost function the better performing an ANN. As the name implies, back propagation is performed in the opposite direction of forward propagation. The back propagation process calculates the cost function and changes weights and biases by an optimization process such as gradient descent to find the the set of weights and biases which corresponds to global minimums of the cost function.

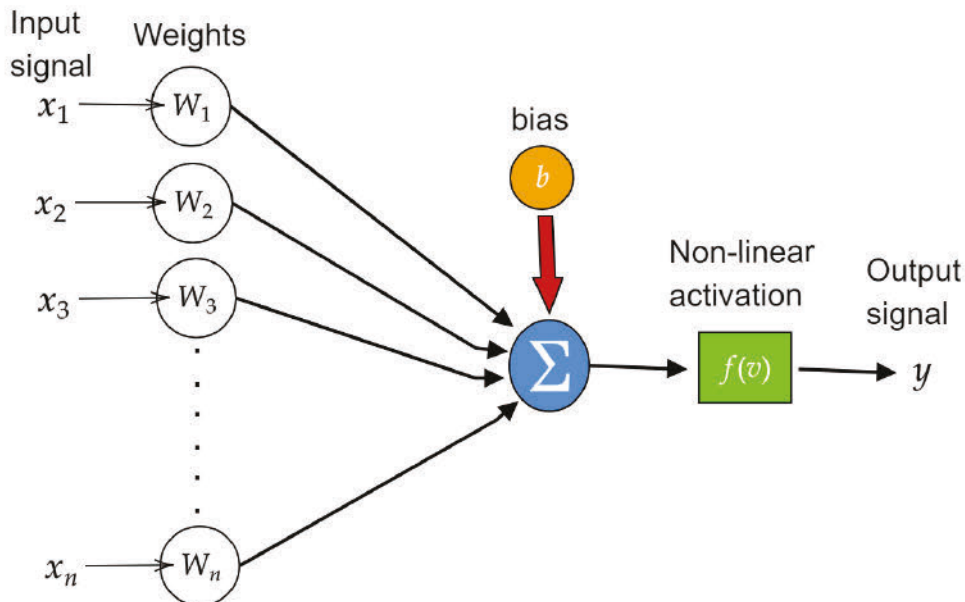


Fig. 4.4 Schematic of an artificial neuron with n inputs

. Activation functions are one of the most important features to characterize neurons in a neural network. As previously explained, the activation function can be linear or non-linear. Non-linear activation functions allow neural networks to perform more sophisticated tasks and provide a higher degree of freedom to approximate wide variety of functions with higher degrees of complexity. For instance, the difference between an ANN with linear activation function and non-linear activation function performing a classification task is illustrated in fig 4.5. The ANN with linear activation function is limited to a straight line to separate the

elements while the non-linear activation function provides a more complex and sophisticated solution. In this chapter, a few of the common linear and non-linear activation functions are discussed and plotted for elaboration [83]. .

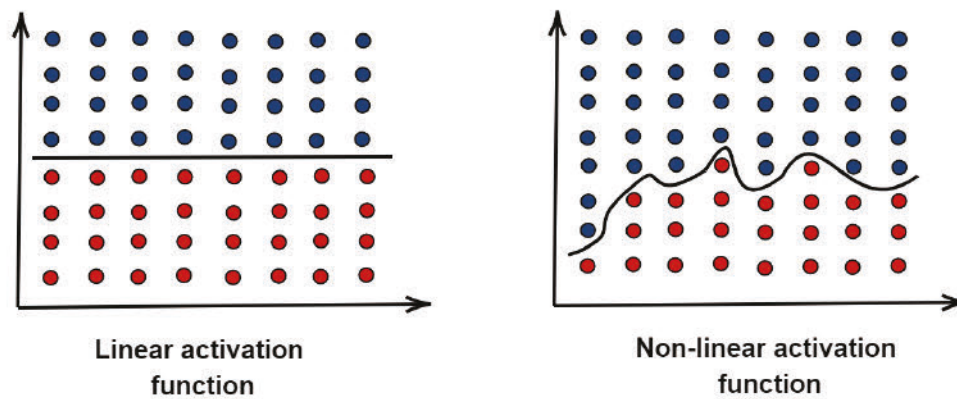


Fig. 4.5 Performing classification by an artificial neural network with linear and non-linear activation function

Linear activation functions

The linear activation function is usually called identity function. It can be considered as one of the simplest forms of activation functions in which the activation is proportional to the input as illustrated in Fig 4.6. The identity function can be mathematically described as

$$a_{identity} = f(x) = x \quad (29)$$

Where x is the input and $f(x)$ is the activation function. Linear activation functions put a great constraint on the type of functions neural networks can approximate. It's impossible to scale up the complexity of the neural network, notwithstanding the number of layers, since all layers will collapse into one layer if a linear activation function is used. Moreover, enabling gradient-based optimization is impossible in this case since differentiating a linear function will always result into a constant. Consequently, back propagation is impossible to apply on a neural network with linear activation function. Due to all the aforementioned reasons, linear activation functions aren't widely used in most of the applications. .

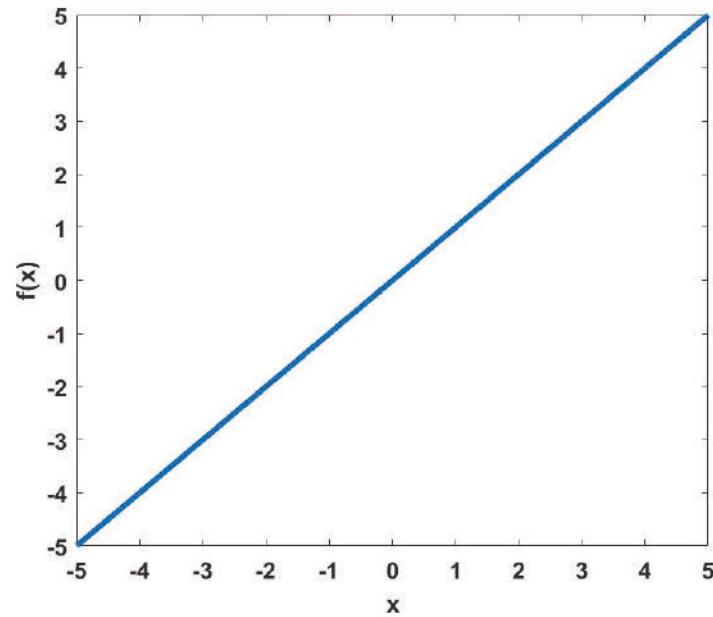


Fig. 4.6 Linear activation function

Non-linear activation functions

According to the universal approximation theorem, an ANN with a single hidden layer consisted of a finite number of neurons is capable of approximating any continuous function within a specific range. In order for this theorem to hold, the ANN should have a non-linear activation function. A few examples for non-linear activation functions are sigmoid, hyperbolic tangent and rectified linear activation unit (ReLU). Those functions are discussed briefly as follows:

- **Sigmoid** : the sigmoid function is sometimes called the logistic function. It's commonly used in ANNs which predict probability as an output. The function domain, all input values at which the function is defined, is all the real numbers belong to the interval $[-\infty, \infty]$ and the range is bounded to the interval $(0, 1)$ which explains why the sigmoid function is preferred for probability prediction applications. Looking at fig 4.7 it can be observed that the sigmoid function converges to 1 for high positive input values and converges to 0 for low negative input values. The mathematical representation of the sigmoid activation function is as follows

$$\alpha_{Sigmoid} = f(x) = \frac{1}{1 + e^{-x}} \quad (30)$$

The function is monotonic and differentiable which makes it suitable for gradient-based optimizations and capable of approximating complex functions.

- Hyperbolic tangent : the hyperbolic tangent activation function is referred to by "tanh". Similar to the sigmoid function, the domain extends from $[-\infty, \infty]$. However, the range is bounded to the interval $(-1, 1)$. As shown in fig 4.7, the larger the input the closer the output value is to 1, whereas, the smaller the input, the closer the output value is to -1. The hyperbolic tangent function is mathematically presented as

$$\alpha_{Tanh} = f(x) = \frac{e^x - e^{-x}}{e^x + e^{-x}} \quad (31)$$

The hyperbolic tangent activation function is differential and suitable for gradient based optimizations. Employing this activation function allows the neurons to have three output states negative, positive and neutral. A visual comparison between the sigmoid and hyperbolic tangent activation functions are depicted in 4.7

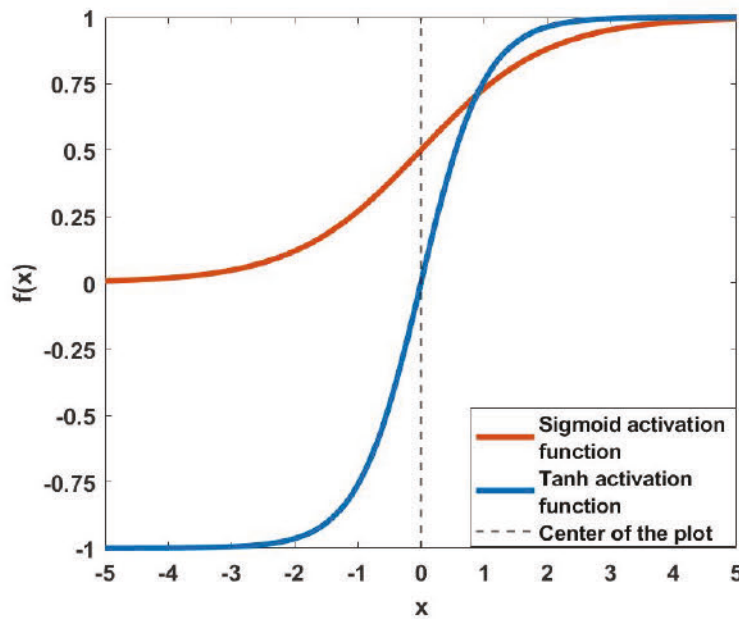


Fig. 4.7 Sigmoid and hyperbolic tangent activation functions

- ReLU : the ReLU function as shown in 4.8 is known for its high computational efficiency and fast convergence. Hence, it's one of the most used activation functions especially in hidden layers. As shown in fig 4.8, the ReLU function can be thought of as two combined functions. The function output will always be zero for any negative

input while the function acts like an identity function to any positive input. the function is presented as

$$\alpha_{ReLU} = f(x) = \max(0,x) \quad (32)$$

ReLU combines the simplicity of a linear activation function and the ability to build a universal approximator, which is a non-linear activation function feature, since it has a gradient of 0 or 1 depending on the sign of the input. This binary gradient allows an easy and fast back propagation optimization, thus, shorter training time [84].

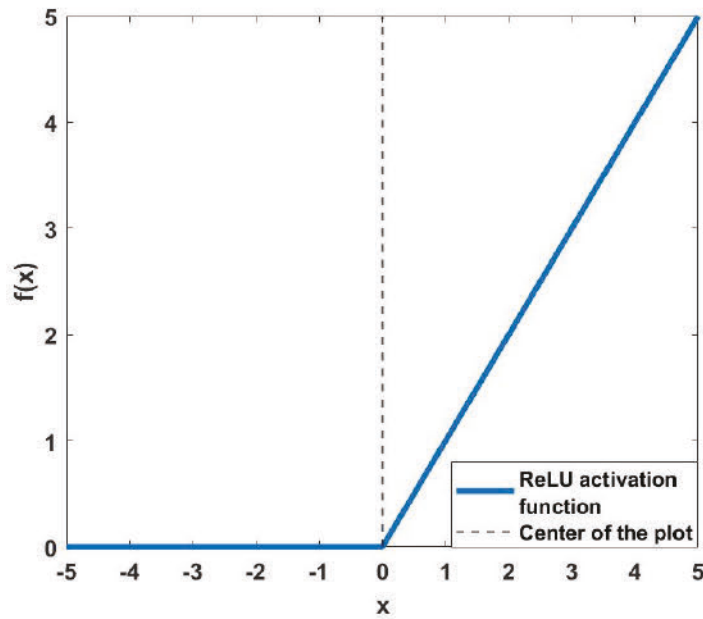


Fig. 4.8 ReLU activation function

4.2 Artificial neural networks for INL compensation

As previously discussed in chapter 3, INL is one of the static ENOB contributors which affects the performance of coherent optical transmission especially when utilizing high modulation formats such as 256-QAM or employing low resolution digital to analogue converters (eg. 4 or 5 bits). INL has been experimentally measured and a reliable model has been constructed and tested accordingly. Despite the fact that INL's function can be easily anticipated since most of the high speed digital to analogue converters are known for their "S" INL shape, accurate INL measurement and characterization are not easy to be

performed in real life scenarios where monitoring and analyzing equipment are not available. Hence, compensating for its effect requires ML or DSP based methods which are able to adapt to different INL values. ANNs are well-known for their adaptability and ability to learn and approximate variety of complex functions, therefore, they demonstrate themselves as one of the promising candidates to minimize the INL effect in modern coherent optical communication systems. In this chapter, an ANN is trained using an indirect learning technique to approximate the inverse of the INL function and apply it at the transmitter side as a pre-distorter. This pre-distorter reverses some of the INL effect on transmitted samples and improves the performance of the optical transmission system as will be shown.

4.2.1 Indirect learning

Indirect learning is a learning technique in which the algorithm is trained at a different position of where it would be used. This can be due to the lack of training samples or the ambiguity of desired output at the operation point. Therefore, the algorithm is trained at a position where more clarity is presented. Thereafter, transferred to where it needs to operate after the training is completed [85].

Indirect learning has been proposed to construct pre-distorters in telecommunication systems with a non-linear channel using Volterra series [86]. Since channel's outputs aren't known in advance at the transmitter side, it's impossible for the algorithm to train itself unless it's trained at the receiver side. Hence, the algorithm will be trained then deployed as a pre-distorter later on.

In our investigation, indirect learning is used to train an ANN to approximate the INL function and inverse it as a pre-distorter. This process is visually illustrated in fig 4.9. As can be noted, the pre-distorter is firstly trained to minimize the cost function $e(n)$ which is mathematically presented as

$$e(n) = \sqrt{(Z'(n) - Z(n))^2} \quad (32)$$

where $Z(n)$ is the transmitted sample and $Z'(n)$ is the received sample affected by DAC's non-linearity. The training phase requires a very low noise channel to ensure a accurate approximation. Hence, an optical back to back configuration is recommended during the training phase. Once the training is completed, the ANN converges to an inverse function of the INL. Then, all ANN parameters are copied and deployed at the trasnmmitter side as a pre-distorter. .

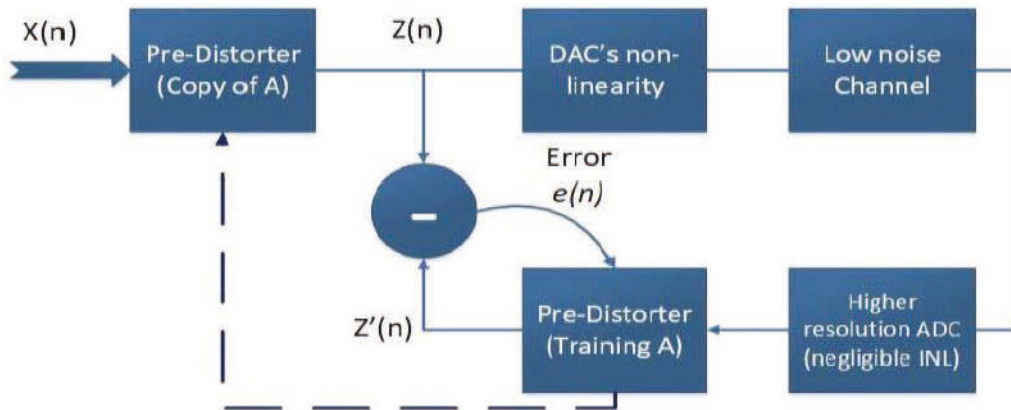


Fig. 4.9 The INL pre-distorter's indirect learning structure

4.2.2 Analytical study and results

An analytical study using the INL model and indirect learning technique has been conducted to investigate the feasibility of utilizing ANNs for INL compensation. The simulation setup is illustrated in the block diagram presented in fig 4.10. At the transmitter side, a sequence of PRBS-31 truncated to 10^6 bits is generated by the PRBS generator. All the bits are then mapped to either 32 QAM or 64 QAM by the mapper accordingly. A pulse shaping of 0.2 roll off factor is applied to all generated samples. Thereafter, an ANN based pre-distorter is applied to compensate for DAC induced INL. The applied ANN is a simple static feed forward neural network with 6 layers (4 hidden layers consisted of 10 neurons per layer accompanied with input and output layers). The training is based on Levenberg-Marquardt learning algorithm operating in a batch mode [87]. The Levenberg-Marquardt learning algorithm is known for its utility of extracting parameters of semiconductor devices. The utilized activation function is hyperbolic tangent due to its ability to approximate complex functions. DAC is modeled as a 5 bits quantizer with a 64 GSamples/s sampling rate. The INL model is incorporated into the DAC to introduce "S" shaped INL. Both CW laser and LO are modeled with 100 KHz linewidth each. At the receiver side, a 300MHz frequency offset between LO and the optical carrier is presented. ADC is modeled as a 8 bits quantizer with a 64 GSamples/s sampling rate. The DSP algorithm is consisted of a DD-LMS adaptive filtering, GSOP for I/Q imbalance compensation, Gardner timing recovery and conventional carrier recovery as discussed in **chapter 2**.

The OSNR has been swept between 23 and 37 and BER is captured at each OSNR point and the results are plotted in fig 4.11. The 7% FEC threshold is highlighted as a benchmark level for comparison. The results depicted in fig. 4.11(a) show that the 2 LSB INL introduced

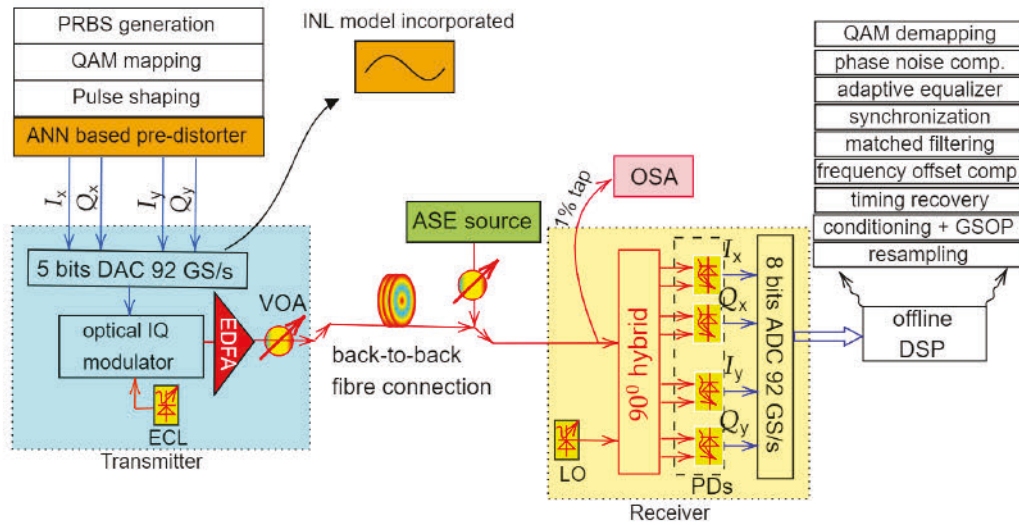


Fig. 4.10 Block diagram for the optical back to back transmission system used the simulation study including pre-distorter and INL model

a relatively small penalty of approximately 0.3dB for 32-quadrature amplitude modulation (QAM) and 1dB for 64-QAM. The pre-distorter provided a gain of 0.6dB for 64-QAM, but showed insignificant improvement for 32-QAM. The uncompensated penalty is due to the low DAC resolution which constrains the pre-distorter's choices of codes and thus voltage outputs, and thereby restricts its capability to fully compensate for the INL effect. Doubling the INL to 4 LSB resulted in an increase in penalties, with the pre-distorter recovering approximately 75% of the penalty for both 32-QAM and 64-QAM as seen in fig. 4.11(b). It also worth noticing that the 64-QAM with INL of 4 LSB curve would never go below 10^{-3} BER threshold without applying pre-distorter by interpolating the points shown in the figure.

Fig. 4.12 is a visual illustration for the significant improvement obtained by using ANN pre-distorter by comparing constellation diagrams. Fig 4.12a represents a Constellation diagram of a 64 QAM, 32 GBaud signal under INL of 4 LSB after DSP recovery. The OSNR in which the signal has been captured is 36 dB. As can be seen, the constellation points are compressed towards the corners of the constellation due to the INL effect. On the other hand, fig 4.12b show the same 64 QAM, 32 GBaud signal under INL of 4 LSB after DSP recovery with ANN pre-distorter. As seen, the ANN pre-distorter significantly improves the constellation.

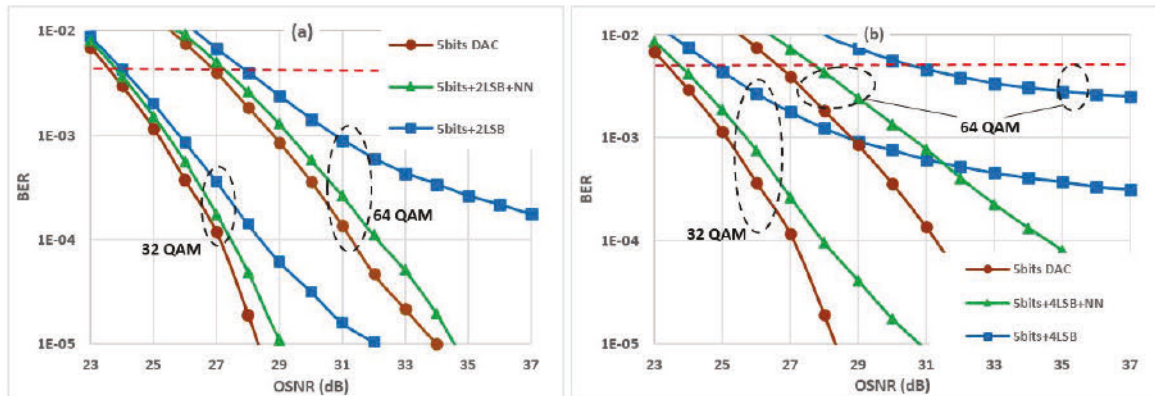
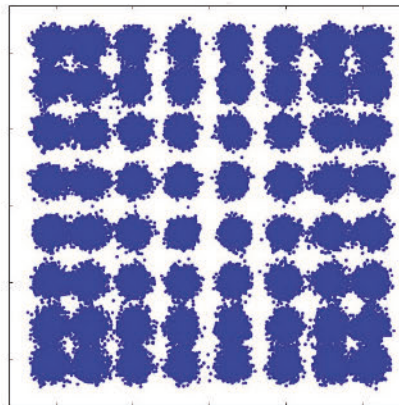
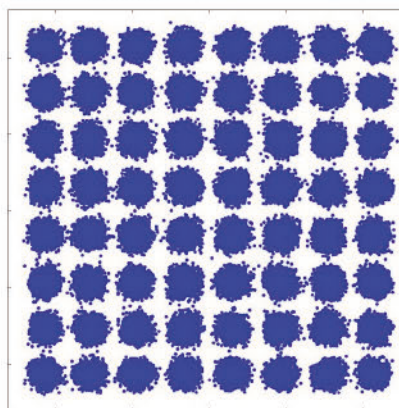


Fig. 4.11 BER vs OSNR curves for 64 QAM, 32 GBaud and 32 QAM, 32 GBaud with 5 bits resolution DAC in two scenarios (a) INL = 2 LSB (b) INL = 4 LSB



(a) Constellation diagram of a 64 QAM, 32 GBaud signal under INL = 4 LSB effect at OSNR = 36 dB



(b) Constellation diagram of a 64 QAM, 32 GBaud signal under INL = 4 LSB effect at OSNR = 36 dB after applying ANN pre-distorter

Fig. 4.12 Constellation diagram comparison to illustrate the effect of applying ANN pre-distorter to 64 QAM, 32 GBaud signal under INL = 4 LSB

4.3 Conclusion

ML algorithms, particularly ANNs, have the potential to be a valuable solution for non-linearity compensation in digital converters and coherent optical communication systems. The field of telecommunications can benefit from the renewed interest in ML due to the exponential growth in computational power and the availability of large amounts of data. The ability of ML to perform regression and classification makes it a strong candidate for non-linear compensation in long transmission systems, providing a low-complexity, energy-efficient solution. Additionally, ML algorithms can also be used to compensate for non-linearity induced by digital converters and optical transceiver components in shorter distances, especially with high modulation formats such as 64-QAM.

This chapter investigated the use of Indirect Learning in combination with Artificial Neural Networks (ANNs) for INL compensation in coherent optical communication systems. Indirect learning was used to train an ANN to approximate the INL function and invert it as a pre-distorter.

An analytical study was conducted to investigate the feasibility of the method. The simulation setup consisted of a back to back optical transmission system that includes a pre-distorter and an INL model. The pre-distorter was a simple static feedforward neural network and the training was based on the Levenberg-Marquardt learning algorithm.

The results of the analytical study showed that the 2 LSB INL introduced a relatively small penalty of approximately 0.3dB for 32-QAM and 1dB for 64-QAM. The pre-distorter provided a gain of 0.6dB for 64-QAM, but showed insignificant improvement for 32-QAM. Doubling the INL to 4 LSB resulted in an increase in penalties, with the pre-distorter recovering approximately 75% of the penalty for both 32-QAM and 64-QAM. The results were visually illustrated by comparing constellation diagrams, which showed significant improvement by using the ANN pre-distorter.

The results of the analytical study showed that the ANN pre-distorter was capable of compensating for INL in the DAC and improving the BER performance in optical transmission systems. The use of Indirect Learning and ANNs for INL compensation could potentially lead to the development of new and more efficient compensation techniques for digital converters non-linearity.

Chapter 5

Digital resolution enhancer to enable low resolution digital to analogue converters

The introduction of digital to analogue converters (DACs) in optical communication systems accompanied by digital signal processing (DSP) in 2005 has revolutionized the sector and accelerated its advancement [88]. Despite the modest DAC specifications back then, the 6 bits, 20 GSamples/s DAC implemented using 130 nm bipolar CMOS semiconductor technology strongly demonstrated its capability to accommodate a new generation of DSP-assisted transceivers. The first proposal to integrate DAC in an optical transceiver was introduced to perform a pre-compensation for the chromatic dispersion in a long intensity modulation direct detection (IMDD) transmission system. It has been followed later by introducing a 6 bits, 20 GSamples/s analogue to digital converters (ADCs) at the receiver side of a 40 Gbit/s dual-polarization coherent QPSK transmission system [89]. Incorporating DACs and ADCs allowed for post and pre-digital compensation not only for chromatic dispersion but also for polarization-dependent loss (PDL) and polarization mode dispersion (PMD). Thereupon, evolving into more sophisticated transceivers adequate for dual-polarization , phase and in-phase transmission by employing standard QAM formats. Multiplying the spectral efficiency, reducing the cost per transmitted bit and enhancing the power efficiency are a few of the benefits arose from the newly proposed architecture of DAC, ADC and DSP. Hence, digital converters established themselves as a cornerstone of all future high speed coherent optical communication systems.

Over the past 15 years, a great emphasis has been put on DSP algorithms to ameliorate the performance and increase the throughput by digitally compensating and mitigating against noise and linear and non-linear distortion imposed by the channel or optoelectronic components impairments. As a result, DSP algorithms has matured in a rapid pace with increased complexity and sophistication to solve more complex transmission problems. This

has been reflected on a significant increase in the maximum achievable bit rate which lately has arrived at 1.6 Tb/s per channel in a commercial system over 1600 Km [21]. This surge has resulted in stringent requirements on digital converters accompanied by expectations to continuously provide broader bandwidth, higher ENOB, higher sampling rate and better power efficiency. Table 5.1 shows the digital converter evolution over the last decade as updated from [90]. A few trends can be clearly perceived from tracing the progress. For instance, a steady increase in the 3-dB bandwidth to accommodate higher baud rates without sacrificing the SNR due to excessive frequency response pre-compensations has been one of the main goals to achieve in every new generation of digital converters. As previously mentioned in **Chapter 2**, scaling up the spectral efficiency of a single channel can be achieved by either increasing modulation format or baud rate. As shown in table 5.2, assuming a zero overhead, a single-channel coherent dual polarization transceiver can deliver 1.6 Tb/s by employing one of the following (modulation format, baud rate) pairs of configuration:

1. High modulation format and low baud rate pairs such as (1024QAM,50 GBaud) or (256QAM, 100 GBaud) are possible candidates [91]. In essence, employing high modulation formats will ease the pressure on the transceiver to support broader bandwidth. Moreover, enabling better exploitation of the available fiber capacity by more WDM channels occupying the same set of frequencies. Alternatively, sustaining the same throughput by reducing WDM channels and relaxing wide band amplifiers requirements is also possible to cut down the cost per bit. However, high modulation formats require relatively high SNR. As shown in fig 5.1, upgrading the transmission system by an extra 1 bit per symbol requires a transceiver with at least 3 dB better characteristic SNR. The practical SNR limit in a coherent transceiver is governed by DACs, ADCs and the fixed-point DSP. Thermal noise, cross talk and low ENOB are a few of the SNR degradation factors which should be carefully dealt with in the system. High modulation formats are also sensitive against noise and distortion which increases puts extra load on the DSP to recover the signal.
2. Low modulation format and high baud rate pairs such as (OOK,800 GBaud) or (QPSK, 400 GBaud) are less desirable due to their broad bandwidth which consumes more of the available fiber capacity compared to a high modulation format and low baud rate configuration. Extremely broad bandwidth optoelectronic components (> 50 GHz bandwidth) such as DACs, ADCs and MZMs are still not available which makes this configuration unpractical to construct in reality. Moreover, digital converters' sampling rates have not yet reached an adequate rate for such high baud rates unless advanced

multiplexing schemes have been used to amalgamate the bandwidths of multiple DACs and ADCs [92].

3. Medium modulation format and baud rate pairs such as (16QAM, 200 GBaud) and (64QAM, 133.3 GBaud) can be considered as optimum for high-speed transmission considering that the nominal SNR of current commercial coherent transceivers can vary from 19 to 24 dB. Methods such as PCS can assist to make the most of the provided SNR, especially when employing 64QAM. Moreover, extensive research has been conducted on DSP algorithms to recover 16QAM and 64QAM [40] which makes it easier to implement.

One of the observable trends in digital converters evolution is power consumption reduction. Power consumption is directly related to the operating expenses (OPEX) which determine the viability of deploying a transmission system in reality. A transmission system with lower power consumption is, beyond any doubt, preferable, especially, when dealing with short-haul and data center interconnect (DCI) applications with a high volume of transceivers. A previous study has addressed the power distribution over the main functions of DSP in a C Form-Factor Pluggable (CFP2) module with a 64QAM, 64 GBaud configuration. According to the study, digital converters consume around 40% of the total power. One of the ways to minimize the power consumption is by following the single DAC/DSP/ADC chip approach built on CMOS or FinFET ASICs. This approach aims to limit the need to Serializers/Deserializers (SerDes) which are not only complicated to implement to serve a high-speed digital converter but also, power inefficient and a potential source for cross-talk and distortion. Another approach is to select power-efficient architectures. For instance, successive approximation register (SAR) ADCs are well known for their power efficiency and segmented DACs are known for their easier high-resolution implementation. Furthermore, each new semiconductor process node technology reduces the voltage supply needed for transistors operation and increases transistors density on the chip, thus, reducing power consumption and chip size. However, this comes at the cost of design difficulties due to an increased number of mismatches and crosstalk.

Despite the significant improvement digital converter manufacturers have achieved in the last decade, next generations of digital converters will be harder to design and more challenging to manufacture. Each new generation requires a more advanced lithography equipment which drives the higher costs and expenses to manufacture ASIC chips.

Table 5.1 Digital converters evolution from 2010 to 2021 decade [90]

Year	2010	2012	2014	2015-17	2018-21	Future
	DAC/ADC Parameters					
Power	<2W channel	<1.5W channel	~1W channel	<1W channel	«1W channel	TBC
Resolution	6-8 bit [93] [94]	8 bit [95] [96]	8 bit [97]	6-10 bit [98]	6-10 bit [99]	6-10 bit
Bandwidth	> 16 GHz	> 19 GHz	> 26 GHz	> 35 GHz	> 42 GHz	> 49 GHz
ENOB	> 5.5 bit	> 5.7 bit	> 6 bit	5.5 to 6.5 bit	5.5 to 8.5 bit	5.5 to 8.5 bit
Sampling rate	Up to 56 GSamples/s	Up to 65 GSamples/s	Up to 92 GSamples/s	Up to 128 GSamples/s	Up to 140 GSamples/s	Up to 160 GSamples/s
Semiconductor technology	65 nm CMOS	40 nm CMOS	28 nm CMOS	16 nm FinFET	7 nm FinFET	5 nm FinFET

Table 5.2 The baud rate to modulation format trade off in a 1.6 Tb/s single channel dual polarization coherent system assuming no overhead

Modulation format	Bit rate Tb/s	Number of polarization	Baud rate Gbaud/s	Bits per symbol
OOK	1.6	2	800	1
QPSK	1.6	2	400	2
16QAM	1.6	2	200	4
64QAM	1.6	2	133.3	6
256QAM	1.6	2	100	8
1024QAM	1.6	2	50	10

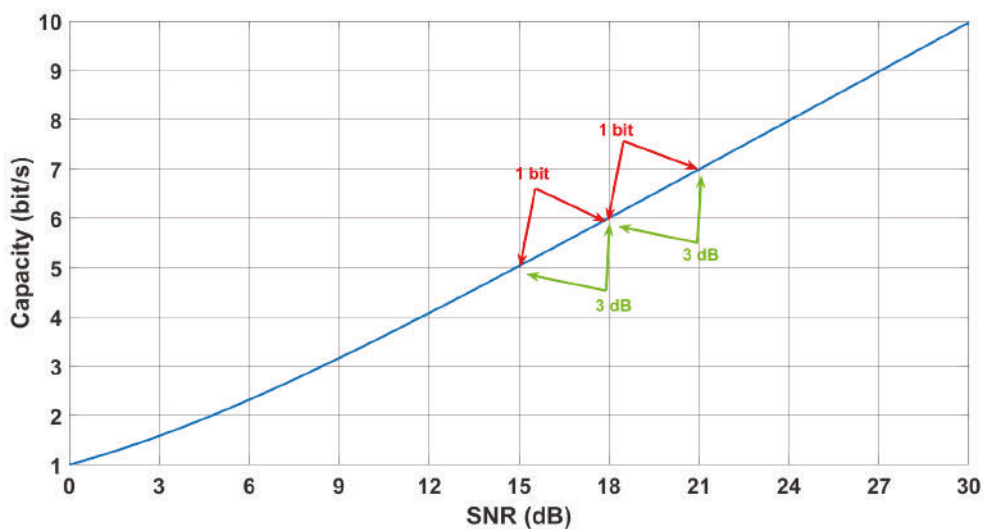


Fig. 5.1 The theoretical channel capacity vs SNR relationship

Additionally, transistors are approaching their atomic physical limit which requires new technologies such as nanowire transistors [100].

DSP techniques can ease some of the pressure on digital converters to slight extent. For instance, bandwidth requirements can be relaxed by applying adequate pre-emphasis and frequency response post-compensation which are capable of extending transceiver's bandwidth by a few GHz, hence, suppressing the ISI effect [101]. Relaxing DAC's resolution requirements has been one of the hot topics to investigate lately. This research interest has started by introducing a new DSP block termed digital resolution enhancer (DRE) for

the first time in 2018 [102]. DRE is a dynamic quantizer applied prior to DACs as an extra layer of compensation. It reshapes the quantization noise of a low resolution DAC by manipulating input samples and assigning them to one of the quantization possibilities generated by the dynamic quantizer. Those new quantization levels are selected to minimise a cost function derived from the so called "effective quantization noise" which differs from their instantaneous counterpart. Applying DRE to a low resolution DAC (e.g. 3 and 4 bit) based transmission system allows for employing high modulation formats such as 64QAM with minimum SNR penalty.

In this chapter, A comprehensive and in-depth analysis of the mathematical principles behind DRE is performed. This study is supported by simulation investigation to illustrates the expected performance enhancement of combining DRE with PCS to a 64QAM/64 GBaud configuration. Then, the results are verified by an experimental investigation imitating the set-up and parameters defined in the analytical study.

5.1 Digital resolution enhancer

5.1.1 Effective quantization noise

The quantization process is a non-linear process which introduces error to the signal due to representing its infinite set of values by a finite discrete set of values. The deviation of the output signal shape comparing to the input introduces a wide range of harmonics which can be approximated to a white Gaussian noise [25]. This approximation is practically valid and very close to reality when two main conditions are satisfied:

1. Assuming the distance between two quantization levels is Δ , the quantizer's input is $x(n)$ and the quantized output is $x_q(n)$, the quantization error is the difference between the input value and the output quantized value $e(n) = x(n) - x_q(n)$. All of the error values should be equally likely to occur between any two adjacent quantization levels $[-\frac{\Delta}{2}, \frac{\Delta}{2}]$ to validate the white Gaussian noise assumption. In other words, all the possible inputs between two adjacent quantization levels should equally likely appear.
2. The values of quantization error sequence $e(n)$ are uncorrelated to each other. In other words, the input should be randomized.

If the aforementioned conditions were satisfied, quantization error sequence can be modelled as a white Gaussian noise uncorrelated to the input. In a real transmission system, those conditions are satisfied when dealing with DAC as an isolated system without including the channel effect. However, DAC output samples pass through a channel consisted of DACs,

ADCs and electrical and optical interface such as amplifiers, MZM modulators and RF cables as shown in fig 5.2. Thereafter, the samples are match filtered prior to undergoing a chain of DSP recovery. Looking at the samples from a receiver standpoint, they are all a product of convolution with the impulse response of all the forenamed components and can be mathematically presented as

$$y_q(n) = h_c(n) * x_q(n) = \sum_{l=0}^{L-1} h_c(n) x_q(n-l) \quad (1)$$

where $y_q(n)$ is the discrete received time sample after MF, $*$ is the convolution operator, $h_c(n)$ is the combined channel impulse response, $x_q(n)$ is the quantized DAC output sample and L is the length of the channel impulse response. This convolution enforces a correlation between successive quantized samples which invalidates the second condition of white gaussian noise approximation and transforms the quantization problem from a stochastic insolvable to a deterministic problem with an attainable optimized solution.

Any optimization process requires a cost function to minimize. The objective in a low resolution DAC transmission system is to reduce the quantization error to mitigate its effect on the signal. To approach a full understanding for the problem, a clear distinction should be drawn between the two types of quantization errors in the system. The first quantization error the so called "instantaneous quantization error". This error is the difference between the sample $x(n)$ prior to being quantized by the DAC and the sample $x_q(n)$ after being quantized by the DAC. Instantaneous quantization error is written as

$$q(n) = x_q(n) - x(n) \quad (2)$$

And it complies with white Gaussian noise approximation conditions so it should not be regarded as a part of the optimization process. The second type of quantization error is the difference between the quantized sample $y_q(n)$ after passing through CIR and its ideal counterpart $y(n)$ with no quantization. This error is the one which affects the performance from a receiver standpoint and it is referred to by effective quantization error q_{eff} .

effective quantization error can be written as

$$q_{eff}(n) = y_q(n) - y(n) \quad (3)$$

and the cost function for a sample n is the mean square-error of q_{eff} . It can be derived from equation 1, 2 and 3 and written as

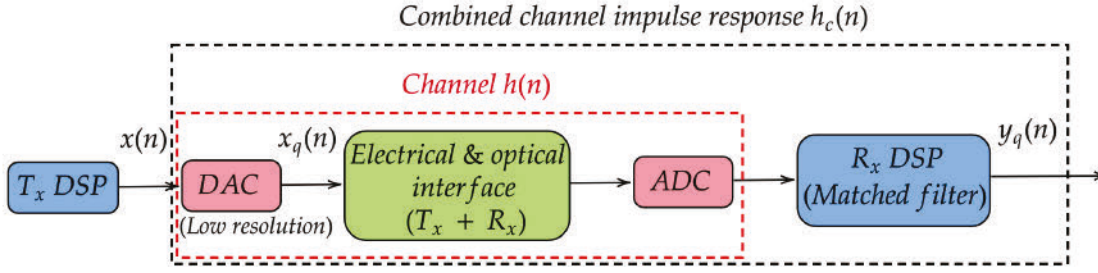


Fig. 5.2 Simplified block diagram for an optical transmission system to illustrate the combine channel impulse response $h_c(n)$ components

$$J(n) = |q_{eff}(n)|^2 = |h_c(n) * q(n)|^2 = \left| \sum_{l=0}^{L-1} h_c(n) q(n-l) \right|^2 \quad (4)$$

where L is the number of channel taps. It can be clearly noticed from equation 4 that the quantization error is not memoryless anymore. The convolution with CIR causes dependency on past quantization error values to calculate present and future values. Hence, optimizing the quantization process is not limited to minimizing the euclidean distance between ideal and quantized samples but it should take into account the effective quantization noise over the whole sequence of samples.

5.1.2 Dynamic quantization

Optimizing the quantization process can be performed by replacing the conventional round-off quantizer by a dynamic quantizer (DQ) as visually illustrated in fig 5.3. The dynamic quantizer doesn't assign quantization levels for incoming samples based on the closest available value to exact value. Alternatively, it makes a structured decision to choose the best quantization level out of a predefined number of options to minimize the effective quantization noise. DQ error is written as

$$q_{dq}(n) = q_{ro}(n) + u(n) \cdot \Delta, \quad (5)$$

where $q_{ro}(n)$ is the round-off error, $u(n)$ is the integer control parameter and Δ is quantizer step size, the output difference between two successive digital inputs, and it is usually set to 1 LSB. To ensure complying with DAC's dynamic range constrain, the following condition should be satisfied

$$c_{\min} \leq q_{ro}(n) + u(n) \cdot \Delta \leq c_{\max}, \quad (6)$$

where c_{\min} and c_{\max} are the maximum and minimum values of the DQ corresponding to DAC's dynamic range, respectively.

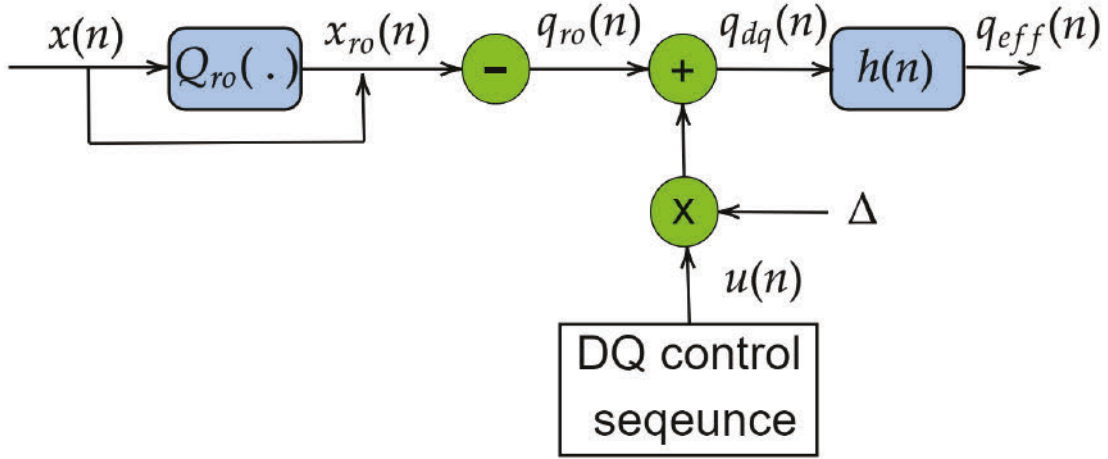


Fig. 5.3 Schematic diagram to illustrate the dynamic quantization problem

Assuming an input sequence of length N , the DQ control sequence is expected to be a vector of values $u_{opt} = \{u_{opt}(0)u_{opt}(1)u_{opt}(2)\dots u_{opt}(N-1)\}$ with the same length N to minimize the mean square error over the whole input sequence

$$J_{\text{avg}}^{(N)} = \frac{1}{N} \sum_{n=0}^{N-1} J(n) = \frac{1}{N} \sum_{n=0}^{N-1} |q_{eff}(n)|^2 \quad (7)$$

The trellis diagram depicted in fig 5.4 illustrates the process of extracting an optimum DQ control sequence out of a N input samples. It should be noted that calculating the optimized DQ control sequence can easily turn into a computationally intensive problem. Assuming a DAC with 4 bits resolution which translates into $M = 16$ quantization levels and input sequence of $N = 5$ samples, DQ's different combinations will be $M^N = 16^5$ which is slightly over 1 million different variations. Thus, calculating the average cost function for each of the combinations is impractical and extremely complex in a real system. The main problem here is the exponential relationship between computational complexity and number of input samples which sets the greatest obstacle to implement it in reality. This problem can be considered as a dynamic programming problem which can be formulated using a hidden

Markov Model (HMM). HMMs are very common in natural language processing which faces problems with similar complexity to the DQ problem. HMMs aim to find a sequence of states which satisfies a certain criteria such as maximizing a probability or minimizing an error function. Viterbi algorithm is a searching algorithm which explores the hidden states of HMM to find the most likely state sequence by a process of systematic elimination based on a path metric. Any path which diverges from the optimum path at any state will automatically be eliminated even if it reemerges later. Calculations are only performed on paths which extend from previous states and have a high likelihood of continuation.

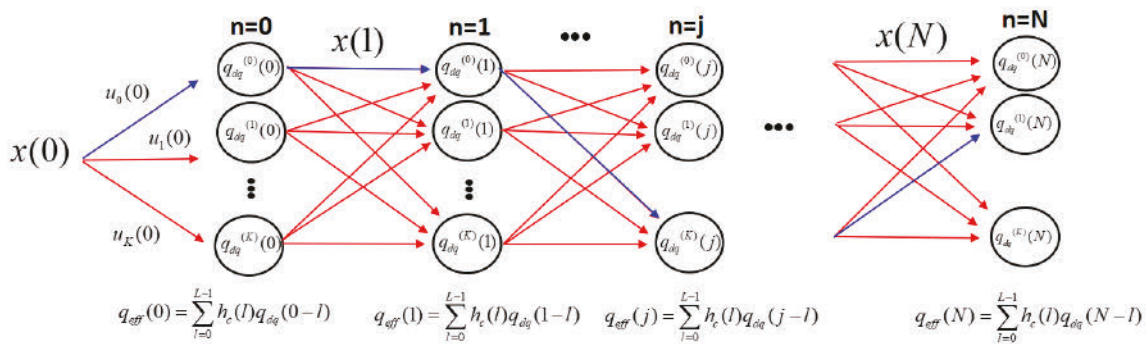


Fig. 5.4 Trellis diagram for a dynamic quantization problem

Viterbi decoders are well-known for their excellent error rate performance, feasible implementation and fast convergence. Due to all of the aforementioned features, Viterbi is considered as one of the most promising algorithms to solve this HMM problem. Hence, it has been chosen as a primary decoding algorithm in the DRE block.

5.2 Probabilistic constellation shaping

The technological evolution in the field of internet applications and mobile communication systems has resulted into a significant growth in data traffic and caused an unprecedented pressure on coherent optical core network to keep up with the demand, Deploying new fibre cables and upgrading the network is not the most cost effective solution especially that the capacity of legacy fibre infrastructure is not fully exploited. variety of DSP algorithms have been introduced to compensate for the linear and non-linear effect, therefore, facilitating the way to improve capacity utilization. DSP algorithms has been improved and enhanced throughout the years to bridge the inherent gap to Shannon capacity. One of the new techniques introduced in the last few years to further fill this gap is probabilistic constellation

shaping. Conventional QAMs lack the granularity which makes them not optimum under many SNR and non-linearity conditions. PCS demonstrates itself as an effective and practical DSP based solution to achieve better optimization. This can be performed by manipulating the probability of occurrence of constellation points to achieve the best achievable information rate. The flexible PCS provides in term of the rate adaptivity with iterative FEC decoding and demodulation makes it more attractive to be implemented in practical transmission systems.

5.3 Analytical studies

The simulation is for an optical B2B transmission system over AWGN channel as shown in fig 5.5. The transmitter side begins with QAM generation followed by a distribution matcher to apply PCS to generated symbols. A 5% pilot overhead is used for synchronization and carrier recovery aid. This is followed by a pulse shaper with a pulse-shaping factor of 0.1. Subsequently, an optimized pre-emphasise stage is applied to compensate for transmitter's side frequency response followed by DRE to compensate for quantization noise. To minimize the complexity, the filter representing channel impulse response taps has been shortened to three taps and number of possible DQ levels are limited to three levels. All symbols will pass through 4 bits DAC for digital to analogue conversion then optically converted. At receiver side, 8 bits ADC convert the signal again to digital form to undergo a conventional of pilot-based DSP algorithms with a decision directed least mean square algorithm for adaptive filtering and pilot aided phase noise compensation. The DSP ends up with a mutual information (MI) estimation.

5.3.1 Probabilistic shaping optimization

PCS factors can be optimized for different SNR levels to maximize the MI. As a first step, this relationship has been numerically investigated to explore the optimum PCS factors for different scenarios to be applied later. As shown in fig 5.6, the received SNR was swept from 13 dB to 25 dB and the PCS factor was tested over a range of 0 (no shaping) to 0.046. The MI is normalized for each SNR to the maximum achievable MI at that SNR, M_{maxSNR} . The heat map scale bar ranges from zero to unity, where 0 and 1 correspond to the lowest and highest achievable MI for a given SNR, respectively. It can clearly be seen that higher PCS factors achieve higher MI at low SNR levels and vice versa. Thus, for further investigation, $\kappa = 0.036$ and $\kappa = 0.016$ were chosen to be representative of strong and weak PCS factors respectively.

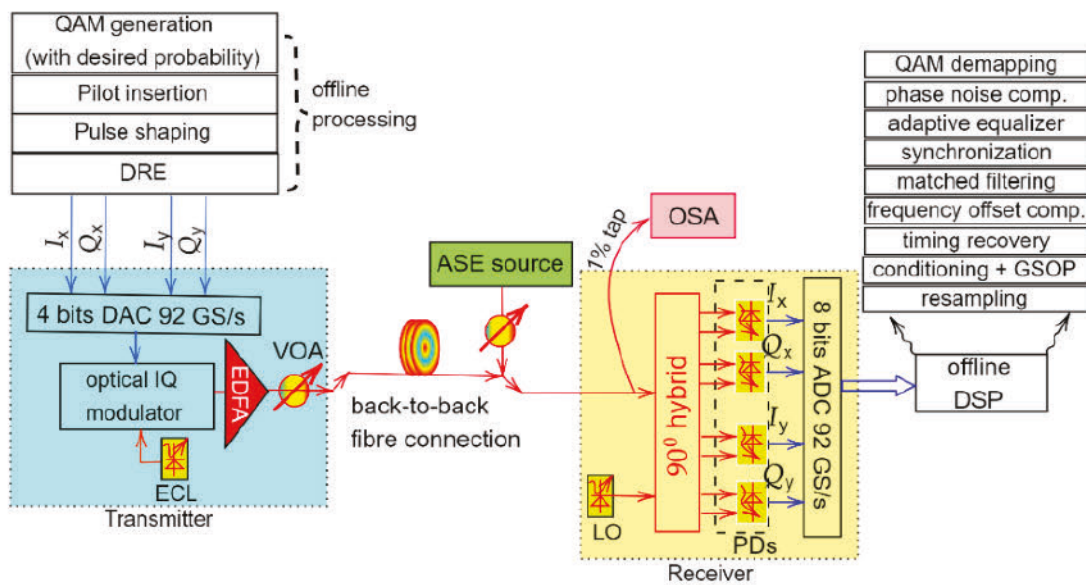


Fig. 5.5 Block diagram for the optical back-to-back transmission system used in the experimental and simulation study including probabilistic shaping and digital resolution enhancement

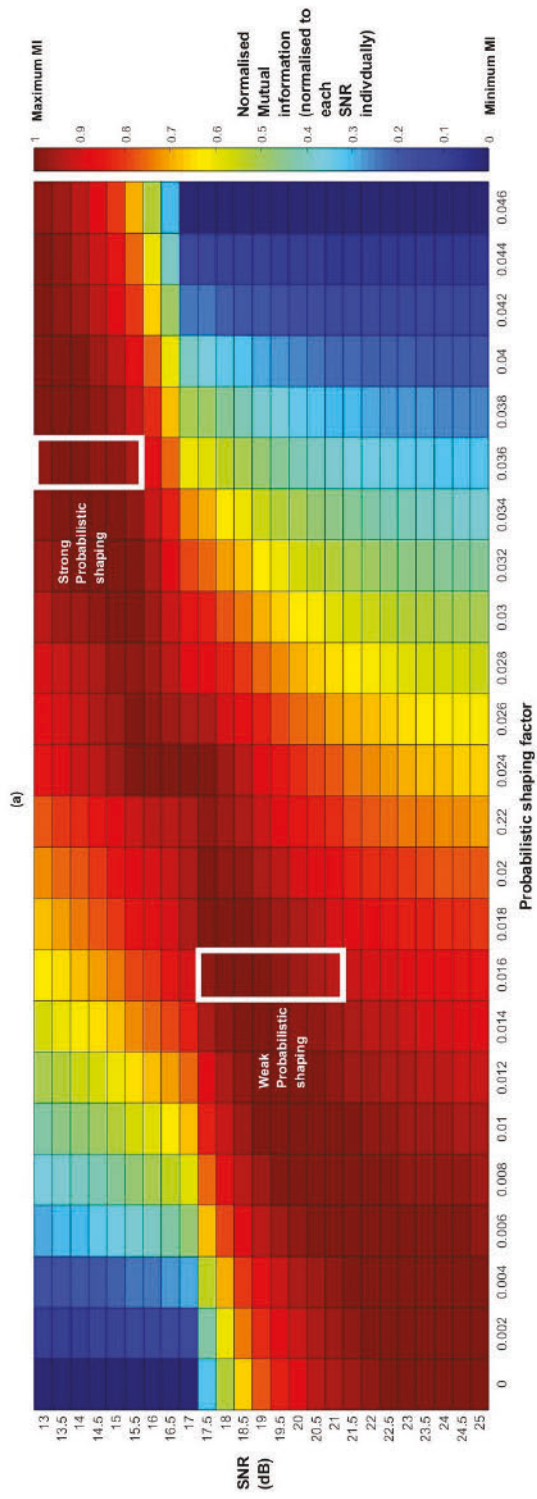


Fig. 5.6 A heat map shows the performance in terms MI for different SNR vs PCS factors. The scale bar ranges from 0 to 1 where 0 corresponds to lowest achievable MI and 1 corresponds to highest achievable MI at each SNR.

5.3.2 PCS gains for a 4 bit DAC with DRE

Fig 5.6 shows results of 64-Gbd/64-QAM signals tested for the two different selected scenarios. Firstly, comparing the performance of DRE alone with a 4 bit DAC (blue curve) to the same set-up using PCS with $\kappa=0.016$ (yellow curve) shows an improvement of up to 0.45 dB in required SNR at MI = 5.5 bits/symbol.

Secondly, the stronger PCS factor of $\kappa=0.036$ (purple curve) shows up to 0.75 dB of SNR gain at MI = 4.5 bits/symbol, compared to using DRE alone at the same MI level. These simulation results demonstrate that a combination of PCS and DRE is possible and can outperform the application of DRE alone when dealing with low resolution DACs. For illustration, Fig. 5.8 shows the recovered constellation after applying DSP for different scenarios. Fig. 5.8(a) and Fig. 5.8(b) show uniform 64-Gbd/64-QAM signals with and without applying DRE. It can be noticed that DRE reduces the noise in constellation which minimises the susceptibility to errors and improves the overall performance. Similarly, Fig. 5.8(c) and Fig. 5.8(d) show probabilistically shaped 64-Gbd/64-QAM signals with and without applying DRE. It can be noticed that applying DRE to the probabilistically shaped signal also reduces the noise in constellation and improves the overall performance.



Fig. 5.7 Performance in terms of MI versus channel SNR for simulated 64-Gbd/64-QAM modulation in different scenarios with DRE compared to Shannon's limit (black) and uniform modulation w/o DRE (red)

5.4 Experimental studies

In our corresponding experimental study, an optical B2B setup was established as shown in fig. 5.5, similar to the simulated setup. A pair of 92 GSa/s DAC/ADCs was used for digital conversion in which DAC resolution was digitally restricted to 4 bits. A C-form factor pluggable CFP2 transceiver was used as an optical transponder. At the transmitter side, QAM generation was followed by a distribution matcher to apply PCS to the generated symbols. As with the numerical simulations, 5% pilot overhead was used for synchronization and to aid carrier recovery and followed by a pulse shaper with a pulse-shaping factor of 0.1. Subsequently, an optimized pre-emphasis stage extracted separately and compensated for the transmitter's side frequency response.

Fig. 5.9 shows the same set of comparisons numerically studied in Fig. 5.7, confirming a good match between these experimental results and the simulations. Applying a weak PS factor of $\kappa = 0.016$ shows a 0.43 dB improvement (0.45 dB in simulations), taking a MI of 5.5 bits/symbol as a reference level of comparison. Moreover, applying a strong PS factor of $\kappa = 0.036$ shows a 0.65 dB improvement (0.75 dB in simulations) taking a MI of 4.5 bits/symbol.

In both figs 5.7 and 5.9, it is noticeable that different PCS factors enhance or degrade the performance at different SNR values. For instance, in the experimental data of Fig. 5.9 at a SNR of 19 dB, applying weak probabilistic shaping resulted in a 0.2 bit improvement in terms of MI compared to the case without probabilistic shaping, while applying strong probabilistic shaping resulted in a small degradation of order 0.1 bit. Note that similar differences at a SNR of 19dB are evident in the simulation data of Fig. 5, and optimum PCS factors for different SNR values can be easily realised from the numerical study summarised in fig. 5.6. For illustration, Fig. 5.8 shows the recovered constellation after applying DSP for different scenarios. Fig. 5.8(a) and Fig. 5.8(b) show uniform 64-Gbd/64-QAM signals with and without applying DRE. It can be noticed that DRE reduces the noise in constellation which minimises the susceptibility to errors and improves the overall performance. Similarly, Fig. 5.8(c) and Fig. 5.8(d) show probabilistically shaped 64-GBd/64-QAM signals with and without applying DRE. It can be noticed that applying DRE to the probabilistically shaped signal also reduces the noise in constellation and improves the overall performance.

.
.

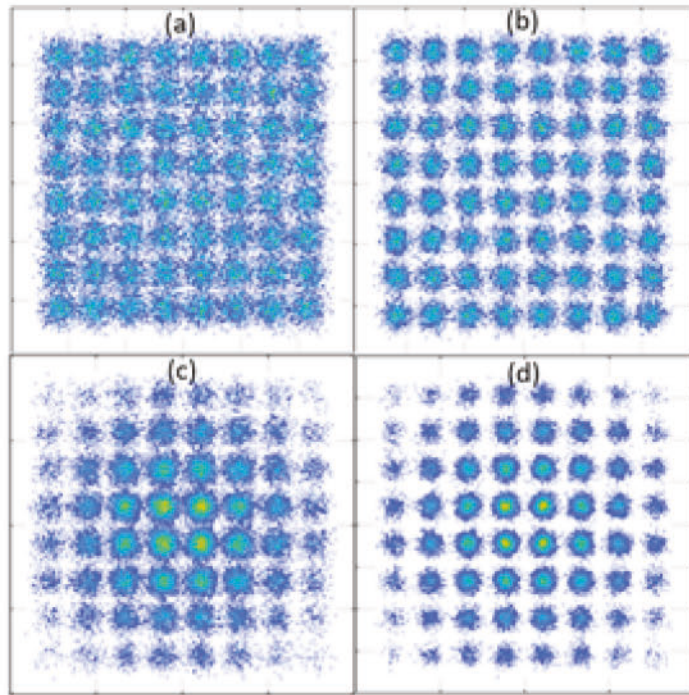


Fig. 5.8 Performance improvement reflected in recovered constellations after applying DSP at receiver side. The improvement is due to applying DRE in two different scenarios. (a) Uniform 64GBd/64-QAM without applying DRE, (b) Uniform 64-GBd/64-QAM with applying DRE, (c) Probabilistically shaped 64-GBd/64-QAM without applying DRE, (d) Probabilistically shaped 64-GBd/64-QAM with applying DRE.

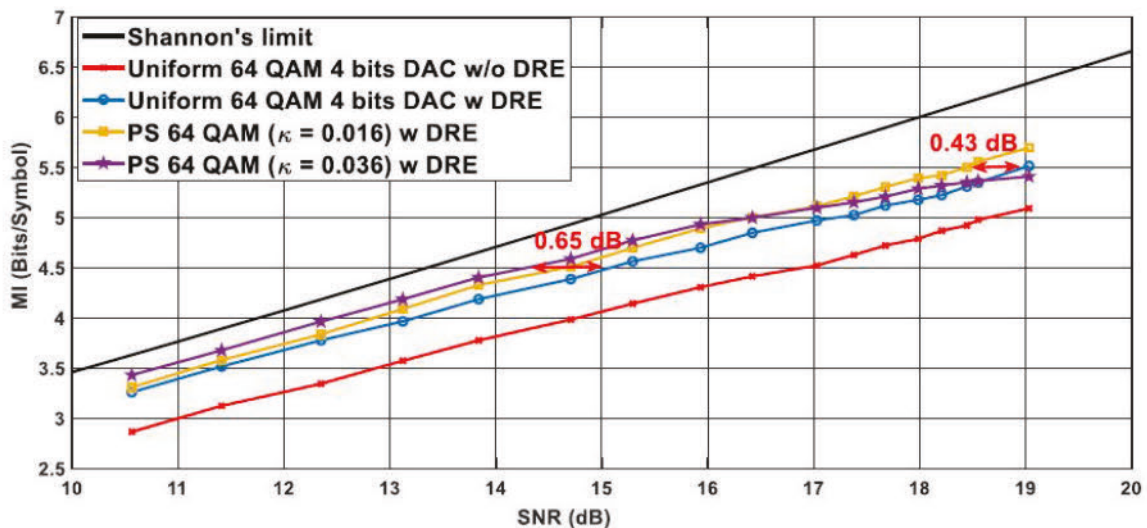


Fig. 5.9 Performance in terms of MI versus channel SNR for experimental 64-Gbd/64-QAM modulation in different scenarios with DRE compared to Shannon's limit (black) and uniform modulation w/o DRE (red)

5.5 Conclusion

The integration of DACs and DSP in optical communication systems in 2005 marked a significant milestone in the sector and has led to its rapid advancement [88]. This integration has enabled efficient digital compensation for various channel impairments, leading to significant increases in the maximum achievable bit rate. However, to keep up with the ever-growing demands of the high-speed optical communication sector, digital converters must continuously evolve and provide broader bandwidth, higher ENOB, higher sampling rate, and better power efficiency. The interplay between the modulation format, baud rate, and digital converters' specifications must be carefully considered to optimize the performance of a high-speed optical transceiver. As utilized modulation formats are expected to be higher than the ones currently utilized, the effect of quantization noise introduced by limited resolution DACs and ADCs are expected to be more dominant. Moreover, application specific digital converters with low resolution might be used for energy sensitive cases applications such as data center applications. Therefore, DRE demonstrates its importance as a DSP method to compensate for the effect of the quantization noise in coherent optical transceivers.

DRE relies on the fact that in a real transmission system, the received quantized samples pass through various components such as DACs, ADCs, amplifiers, MZM modulators, and RF cables, leading to a correlation between successive quantized samples and the channel impulse response. This correlation invalidates the assumption of white Gaussian noise and transforms the quantization problem from a stochastic to a deterministic problem. This process can be optimized by a pre-quantizer based on Viterbi algorithm. This chapter studies the feasibility of combining DRE with PCS to achieve the highest possible improvement. An analytical study followed by an experimental verification has been conducted with highly matching results. The results of PCS combined with a 4 bit DAC and DRE showed a significant MI improvement with gains up to 0.65 bits/symbol.

Chapter 6

Conclusion and future work

6.1 Conclusion

Digital converters are one of the pillars of modern coherent optical communication systems. They have been one of the key elements to enable DSP, hence, contributing to the exponential increase of transmission speed and capacity. However, they also contribute to the distortion and noise applied on transmitted signal which might limit transceiver's performance. To quantify this contribution, ENOB has been introduced as an assessment metric. As ENOB calculation has been explained in chapter 3, the thesis focused in one of the important ENOB contributors which affect the transmission of high modulation formats called INL. It has been shown that INL adds 0.15 dB loss for each 2 LSB increment in a B2B 256-QAM, 23 GBaud configuration.

Chapter 4 discussed applying machine learning algorithms to compensate for the INL effect. It has been analytically shown the artificial neural networks are able to achieve significant improvement if trained using indirect learning and operated as a pre-distorter. A simulation setup was established, consisting of a back-to-back optical transmission system, an INL model, and an ANN pre-distorter. The pre-distorter was trained using the Levenberg-Marquardt learning algorithm and was tested on two modulation formats, 32-QAM and 64-QAM. The results of the analytical study showed that the ANN pre-distorter was able to compensate for INL in the DAC and improve the BER performance in optical transmission systems. When the INL was 2 LSB, the pre-distorter provided a gain of 0.6dB for 64-QAM, while for 32-QAM, the improvement was insignificant. Doubling the INL to 4 LSB resulted in increased penalties, however, the pre-distorter was still able to recover 75% of the penalty for both modulation formats. The improvement was visually demonstrated by comparing constellation diagrams.

Chapter 5 studied the performance enhancement due to PCS in low resolution DAC and DRE based systems. For a 64-Gbd/64-QAM configuration, it was confirmed that PCS can add up to 0.75 dB on top of DRE gains in simulations, and up to 0.65 dB gain on top of DRE gains in a similar experimental setup. The study affirms the expected performance improvement when applying strong probabilistic shaping at low SNR levels and weak probabilistic shaping at high SNR levels. Combining DRE and PCS could be an effective solution to attain the maximum capacity using minimum DAC requirements hence saving power, chip/package size and cost.

In conclusion, the thesis studied digital converters in-depth and provided different solutions for its limitations and imperfections. A few aspects such as INL, ENOB and SINAD and their effect on optical communication systems performance have been addressed, studied and explained. New promising solutions such as ANN to compensate for INL and DRE to compensate for the quantization noise effect combined with PCS to further improve the performance have been studied, discussed and presented.

6.2 Future work

In this thesis, we have presented an in-depth analysis of digital converters in coherent optical transmission systems. The thesis studied different aspects such as digital converter non-linearities and its effect on high modulation formats, the potential solutions to compensate for non-linearities such as ANNs and DRE to compensate for the effect of high quantization noise. While our results provide new insights into the aforementioned topics, there are still many aspects that need to be explored further. Those are described as follow

Chapter three studied the effect of the combined INL in DAC/ADC pairs on the overall performance of optical communication systems. While the results provide a good insight into the relationship between INL and the overall performance, there is still room for further investigation. Future work should aim to study the effect of DAC's INL and ADC's INL individually on the system's performance. This would provide a more in-depth understanding of how each component affects the system's performance, which is essential for the design of future systems. Moreover, a more hardware-based technique rather than a software model to manipulate INL would be more accurate for experimental work. This would allow for a more precise measurement of the INL's effect, which would provide more reliable results. In this direction, future work could involve the development of a hardware platform to perform experiments and quantify the effect of DAC's INL and ADC's INL on the overall performance of optical transceivers.

Chapter four studied the utilisation of ANNs to compensate for INL in optical communication systems. While, ANNs presented themselves as a good solution to compensate for INL's effect on the overall performance, ANNs' complexity is still a major drawback which need to be reduced. Exploring ANNs with less number of layers or even studying other alternative solutions might potentially present a good area of research. Moreover, a supplementary experimental study to support the simulations is needed.

Finally, chapter five studied DRE combined with PCS. The results demonstrated a significant improvement in performance when DRE and PCS are used together.

However, the limitations of DRE must be acknowledged. Currently, DRE is limited in its ability to compensate for the effects of quantization noise in low-resolution DACs. Further research is needed to develop other techniques that can effectively compensate for low-resolution ADCs and provide a more complete solution for the whole system. Additionally, the potential of using DRE with high modulation formats such as 1024 QAM in combination traditional 8-bit DAC/ADC pairs, should be explored. These investigations may lead to further advancements in the field and uncover new, exciting results. Another area of future work is to study methods of compensating for quantization noise that do not require prior knowledge of the channel response. This could lead to a more effective and efficient solution, and provide a new direction for future research.

In conclusion, our study has shown promising results and has provided a foundation for further investigation. By exploring the limitations of digital converters and developing new techniques to compensate for their impairments, we can continue to advance the field and improve the performance of optical communication systems.

References

- [1] The Zettabyte Era:Trends and Analysis . Technical report, Cisco USA, 07 2016.
- [2] V Coffey. Sea change: The challenges facing submarine optical communications. *Optics and Photonics News*, 25(3):26–33, 2014.
- [3] Charles H. Townes. Theodore h. maiman (1927–2007). *Nature*, (447):654, 2007.
- [4] R. Maurer, D. Keck, and P. Schlutz. Method of producing optical waveguide fibers, US3711262A, May. 1970.
- [5] R.A. Griffin and A.C. Carter. Optical differential quadrature phase-shift key (odqpsk) for high capacity optical transmission. In *Optical Fiber Communication Conference and Exhibit*, pages 367–368, 2002.
- [6] Cisco. Cisco Annual Internet Report (2018–2023) White Paper, 2020.
- [7] S. Tsukamoto, D.-S. Ly-Gagnon, K. Katoh, and K. Kikuchi. Coherent demodulation of 40-gbit/s polarization-multiplexed qpsk signals with 16-ghz spacing after 200-km transmission. In *OFC/NFOEC Technical Digest. Optical Fiber Communication Conference, 2005.*, volume 6, pages 3 pp. Vol. 5–, 2005.
- [8] A Farbert, S Langenbach, Nebojsa Stojanovic, Claus Dorschky, T. Kupfer, and C Schulien. Performance of a 10.7 gb/s receiver with digital equaliser using maximum likelihood sequence estimation. page Th.4.1.5, 01 2011.
- [9] John Mcnicol, Maurice O’Sullivan, K Roberts, A Comeau, D McGhan, and L Strawczynski. Electronic domain compensation of optical dispersion. *Conference on Optical Fiber Communication, Technical Digest Series*, 4, 03 2005.
- [10] Seb J. Savory. Digital filters for coherent optical receivers. *Opt. Express*, 16(2):804–817, Jan 2008.
- [11] Robert W Keyes. Physical limits of silicon transistors and circuits. *Reports on Progress in Physics*, 68(12):2701–2746, sep 2005.
- [12] Michel Goossens, Frank Mittelbach, and Alexander Samarin. *Digital communications*. Pearson, Edinburgh, UK, 2003.
- [13] Md Asif Iqbal, Lukasz Krzaczanowicz, Ian D. Phillips, Paul Harper, Andrew Lord, and Wladek Forysiak. Ultra-wideband raman amplifiers for high capacity fibre-optic transmission systems. In *2020 22nd International Conference on Transparent Optical Networks (ICTON)*, pages 1–4, 2020.

-
- [14] Antonio Napoli, Nelson Costa, Johannes K. Fischer, João Pedro, Silvio Abrate, Nicola Calabretta, Wlodek Forysiak, Erwan Pincemin, Juan P.F-P. Gimenez, Chris Matrakidis, Gunther Roelkens, and Vittorio Curri. Towards multiband optical systems. In *Advanced Photonics 2018 (BGPP, IPR, NP, NOMA, Sensors, Networks, SPPCom, SOF)*, page NeTu3E.1. Optical Society of America, 2018.
- [15] Charles Laperle and Maurice O’Sullivan. Advances in high-speed dacs, adcs, and dsp for optical coherent transceivers. *Journal of Lightwave Technology*, 32(4):629–643, 2014.
- [16] Timo Pfau, Sebastian Hoffmann, and Reinhold Noé. Hardware-efficient coherent digital receiver concept with feedforward carrier recovery for M -qam constellations. *J. Lightwave Technol.*, 27(8):989–999, Apr 2009.
- [17] Antonio Napoli, Mahdi M. Mezghanni, Talha Rahman, Danish Rafique, Robert Palmer, Bernhard Spinnler, Stefano Calabrò, Carlos Castro, Maxim Kuschnerov, and Marc Bohn. Digital compensation of bandwidth limitations for high-speed dacs and adcs. *Journal of Lightwave Technology*, 34(13):3053–3064, 2016.
- [18] Antonio Napoli, Mahdi M. Mezghanni, Danish Rafique, Vincent A. J. M. Sleiffer, Talha Rahman, Bernhard Spinnler, Stefano Calabrò, and Marc Bohn. Novel dac digital pre-emphasis algorithm for next-generation flexible optical transponders. In *Optical Fiber Communication Conference*, page Th3G.6. Optical Society of America, 2015.
- [19] M. Ziari, V. Lal, P. Studenkov, H. Hodaei, T. Frost, C. Tsai, K. Hoshino, B. Behnia, R. Going, S. Wolf, S. Porto, M. Kuntz, T. Vallaitis, E. Sooudi, J. Lavrencik, R. Salvatore, N. Modi, P. Abolghasem, M. Fisher, S. Murthy, S. Buggaveeti, R. Brigham, D. Pavinski, J. Zhang, J. Zhang, S. Corzine, P. Evans, V. Dominic, R. Maher, P. Mertz, S. Sanders, H. Sun, J. Osenbach, and P. Kandappan. High-performance 100 gbaud coherent photonic modules. In *Optical Fiber Communication Conference (OFC) 2021*, page F2A.3. Optical Society of America, 2021.
- [20] Han Sun, Mehdi Torbatian, Mehdi Karimi, Robert Maher, Sandy Thomson, Mohsen Tehrani, Yuliang Gao, Ales Kumpera, George Soliman, Aditya Kakkar, Mohammad Osman, Ziad A. El-Sahn, Clayton Doggart, Weikun Hou, Shailesh Sutarwala, Yuejian Wu, Mohammad Reza Chitgarha, Vikrant Lal, Huan-Shang Tsai, Scott Corzine, Jiaming Zhang, John Osenbach, Sanketh Buggaveeti, Zulfikar Morbi, Miguel Iglesias Olmedo, Irene Leung, Xian Xu, Parmijit Samra, Vince Dominic, Steve Sanders, Mehrdad Ziari, Antonio Napoli, Bernhard Spinnler, Kuang-Tsan Wu, and Parthiban Kandappan. 800g dsp asic design using probabilistic shaping and digital sub-carrier multiplexing. *J. Lightwave Technol.*, 38(17):4744–4756, Sep 2020.
- [21] R. Maher, M.R. Chitgarha, I. Leung, A. Rashidinejad, B. Buscaino, Z. Wang, M. Torbatian, A. Kakkar, Z.A. El-Sahn, M. Osman, A. Kumpera, R.M. Nejad, A. Yekani, G. Soliman, C. Doggart, M.I. Olmedo, S. Kerns, J. Diniz, Z. Morbi, S. Koenig, L. Dardis, B. Ellis, A. Le Liepvre, M. Missey, S. Blakey, Y. Wu, P. Samra, V. Dominic, S. Makovejs, V. Lal, M. Ziari, H. Sun, K-T. Wu, S. Sanders, and P. Kandappan. Real-time 100.4 gbd pcs-64qam transmission of a 1.6 tb/s super-channel over 1600 km of g.654.e fiber. In *Optical Fiber Communication Conference (OFC) 2021*, page Tu6D.2. Optical Society of America, 2021.

-
- [22] Ian Glover and Peter Grant. *Digital communications*. Pearson, Edinburgh, UK, 2009.
- [23] Han Sun. Real-time measurements of a 40 gb/s coherent system. In *Frontiers in Optics 2008/Laser Science XXIV/Plasmonics and Metamaterials/Optical Fabrication and Testing*, page FWH3. Optical Society of America, 2008.
- [24] Yi Cai, Jin-Xing Cai, Alexei Pilipetskii, Georg Mohs, and Neal S. Bergano. Spectral efficiency limits of pre-filtered modulation formats. *Opt. Express*, 18(19):20273–20281, Sep 2010.
- [25] W. R. Bennett. Spectra of quantized signals. *The Bell System Technical Journal*, 27(3):446–472, 1948.
- [26] Cleveland W. First-order-hold interpolation digital-to-analog converter with application to aircraft simulation. Technical report, NASA, Washington DC, 1976.
- [27] J. Deveugele, P. Palmers, and M.S.J. Steyaert. Parallel-path digital-to-analog converters for nyquist signal generation. *IEEE Journal of Solid-State Circuits*, 39(7):1073–1082, 2004.
- [28] Chris R. S. Fludger, Thomas Duthel, Dirk van den Borne, Christoph Schullien, Ernst-Dieter Schmidt, Torsten Wuth, Jonas Geyer, Erik De Man, Giok-Djan Khoe, and Huug de Waardt. Coherent equalization and polmux-rz-dqpsk for robust 100-gb transmission. *Journal of Lightwave Technology*, 26(1):64–72, 2008.
- [29] T.L. Paoli and J.E. Ripper. Direct modulation of semiconductor lasers. *Proceedings of the IEEE*, 58(10):1457–1465, 1970.
- [30] J.C. Cartledge and G.S. Burley. The effect of laser chirping on lightwave system performance. *Journal of Lightwave Technology*, 7(3):568–573, 1989.
- [31] G.L. Li and P.K.L. Yu. Optical intensity modulators for digital and analog applications. *Journal of Lightwave Technology*, 21(9):2010–2030, 2003.
- [32] M. Doi, M. Sugiyama, K. Tanaka, and M. Kawai. Advanced linbo/sub 3/ optical modulators for broadband optical communications. *IEEE Journal of Selected Topics in Quantum Electronics*, 12(4):745–750, 2006.
- [33] Mian Zhang, Cheng Wang, Prashanta Kharel, Di Zhu, and Marko Lončar. Integrated lithium niobate electro-optic modulators: when performance meets scalability. *Optica*, 8(5):652–667, May 2021.
- [34] Kazuro Kikuchi. Fundamentals of coherent optical fiber communications. *Journal of Lightwave Technology*, 34(1):157–179, 2016.
- [35] Johannes K. Fischer, Mattia Cantono, Vittorio Curri, Ralf-Peter Braun, Nelson Costa, João Pedro, Erwan Pincemin, Philippe Doaré, Claude Le Bouëtté, and Antonio Napoli. Maximizing the capacity of installed optical fiber infrastructure via wideband transmission. In *2018 20th International Conference on Transparent Optical Networks (ICTON)*, pages 1–4, 2018.

-
- [36] Seb J. Savory. Digital coherent optical receivers: Algorithms and subsystems. *IEEE Journal of Selected Topics in Quantum Electronics*, 16(5):1164–1179, 2010.
- [37] Hwan Seok Chung, Sun Hyok Chang, and Kwangjoon Kim. Effect of iq mismatch compensation in an optical coherent ofdm receiver. *IEEE Photonics Technology Letters*, 22(5):308–310, 2010.
- [38] Pavel Skvortcov, Christian Sanchez-Costa, Ian Phillips, and Wladek Forysiak. Transmitter iq skew calibration in coherent transceivers based on dsp. In *Advanced Photonics 2018 (BGPP, IPR, NP, NOMA, Sensors, Networks, SPPCom, SOF)*, page SpW1G.6. Optical Society of America, 2018.
- [39] Wonzoo Chung. Transmitter iq mismatch compensation in coherent optical ofdm systems using pilot signals. *Opt. Express*, 18(20):21308–21314, Sep 2010.
- [40] Md. Saifuddin Faruk and Seb J. Savory. Digital signal processing for coherent transceivers employing multilevel formats. *Journal of Lightwave Technology*, 35(5):1125–1141, 2017.
- [41] Seb J. Savory. Digital coherent optical receivers: Algorithms and subsystems. *IEEE Journal of Selected Topics in Quantum Electronics*, 16(5):1164–1179, 2010.
- [42] Xiang Zhou and Chongjin Xie. *Enabling Technologies for High Spectral-efficiency Coherent Optical Communication Networks*. Wiley Blackwell, 2016.
- [43] J.C. Geyer, C.R.S. Fludger, T. Duthel, C. Schulien, and B. Schmauss. Efficient frequency domain chromatic dispersion compensation in a coherent polmux qpsk-receiver. In *Optical Fiber Communication Conference*, page OWV5. Optical Society of America, 2010.
- [44] Yuxin Chen, T. Le-Ngoc, B. Champagne, and Changjiang Xu. Recursive least squares constant modulus algorithm for blind adaptive array. *IEEE Transactions on Signal Processing*, 52(5):1452–1456, 2004.
- [45] Ziyad Ahmad Almatroudi, Amr Ragheb, Abdelouahab Bentrchia, and Habib Fathallah. Performance investigation of cma and rls based equalization for next generation long reach passive optical networks. In *2015 International Conference on Information and Communication Technology Research (ICTRC)*, pages 160–163, 2015.
- [46] F. Gardner. A bpsk/qpsk timing-error detector for sampled receivers. *IEEE Transactions on Communications*, 34(5):423–429, 1986.
- [47] ITU-T Rec. G.975.1 (02/2004) Forward error correction for high bit-rate DWDM submarine systems. Technical report, ITU-U, 04 2004.
- [48] Irshaad Fatadin, David Ives, and Seb J. Savory. Laser linewidth tolerance for 16-qam coherent optical systems using qpsk partitioning. *IEEE Photonics Technology Letters*, 22(9):631–633, 2010.
- [49] Claude Elwood Shannon. A mathematical theory of communication. *The Bell System Technical Journal*, 27:379–423, 1948.

-
- [50] Tobias Fehenberger, Alex Alvarado, Georg Böcherer, and Norbert Hanik. On probabilistic shaping of quadrature amplitude modulation for the nonlinear fiber channel. *J. Lightwave Technol.*, 34(21):5063–5073, Nov 2016.
- [51] G. Forney, R. Gallager, G. Lang, F. Longstaff, and S. Qureshi. Efficient modulation for band-limited channels. *IEEE Journal on Selected Areas in Communications*, 2(5):632–647, 1984.
- [52] D. G. Foursa, H. G. Batshon, H. Zhang, M. Mazurczyk, J.-X. Cai, O. Sinkin, A. Pilipetskii, G. Mohs, and Neal S. Bergano. 44.1 tb/s transmission over 9,100 km using coded modulation based on 16qam signals at 4.9 bits/s/hz spectral efficiency. In *39th European Conference and Exhibition on Optical Communication (ECOC 2013)*, pages 1–3, 2013.
- [53] Siddharth V., Jerrod Langston, Varghese A. Thomas, Sorin Tibuleac, and Stephen E. Ralph. Frequency dependent enob requirements for m-qam optical links: An analysis using an improved digital to analog converter model. *Journal of Lightwave Technology*, 36(18):4082–4089, 2018.
- [54] Tobias Ellermeyer, Rolf Schmid, Anna Bielik, Jörg Rupeter, and Michael Möller. Dac and adc converters in sige technology: Speed and resolution for ultra high data rate applications. In *36th European Conference and Exhibition on Optical Communication*, pages 1–6, 2010.
- [55] M.P. Kennedy. On the robustness of r-2r ladder dacs. *IEEE Transactions on Circuits and Systems I: Fundamental Theory and Applications*, 47(2):109–116, 2000.
- [56] Behzad Razavi. The current-steering dac [a circuit for all seasons]. *IEEE Solid-State Circuits Magazine*, 10(1):11–15, 2018.
- [57] Xi Chen, Sethumadhavan Chandrasekhar, Sebastian Randel, Wenjun Gu, and Peter Winzer. Experimental quantification of implementation penalties from limited adc resolution for nyquist shaped higher-order qam. In *2016 Optical Fiber Communications Conference and Exhibition (OFC)*, pages 1–3, 2016.
- [58] Ieee standard for terminology and test methods for analog-to-digital converters. *IEEE Std 1241-2010 (Revision of IEEE Std 1241-2000)*, pages 1–139, 2011.
- [59] J. Doernberg, H.-S. Lee, and D.A. Hodges. Full-speed testing of a/d converters. *IEEE Journal of Solid-State Circuits*, 19(6):820–827, 1984.
- [60] J. Blair. Histogram measurement of adc nonlinearities using sine waves. *IEEE Transactions on Instrumentation and Measurement*, 43(3):373–383, 1994.
- [61] Francisco Corrêa Alegria and Antônio Cruz Serra. The histogram test of adcs with sinusoidal stimulus is unbiased by phase noise. *IEEE Transactions on Instrumentation and Measurement*, 58(11):3847–3854, 2009.
- [62] Sylvain Almonacil, Philippe Jennev e, Petros Ramantanis, and Patricia Layec. Dac jitter requirements for high speed optical networks. In *2018 European Conference on Optical Communication (ECOC)*, pages 1–3, 2018.

-
- [63] Ginni Khanna, Yaron Yoffe, Erik De Man, Eyal Wohlger, Bernhard Spinnler, Stefano Calabrò, Antonio Napoli, Norbert Hanik, and Dan Sadot. Experimental verification of 400g 64qam using 4 bits dacs enabled by digital resolution enhancer. In *2018 European Conference on Optical Communication (ECOC)*, pages 1–3, 2018.
- [64] A. L. Samuel. Some studies in machine learning using the game of checkers. *IBM Journal of Research and Development*, 44(1.2):206–226, 2000.
- [65] Kyunghyun Cho, Bart van Merriënboer, Caglar Gulcehre, Dzmitry Bahdanau, Fethi Bougares, Holger Schwenk, and Yoshua Bengio. Learning phrase representations using RNN encoder–decoder for statistical machine translation. In *Proceedings of the 2014 Conference on Empirical Methods in Natural Language Processing (EMNLP)*, pages 1724–1734, Doha, Qatar, October 2014. Association for Computational Linguistics.
- [66] Chao Weng, Dong Yu, Shinji Watanabe, and Biing-Hwang Fred Juang. Recurrent deep neural networks for robust speech recognition. In *2014 IEEE International Conference on Acoustics, Speech and Signal Processing (ICASSP)*, pages 5532–5536, 2014.
- [67] Il-Seok Oh and Ching Y. Suen. A class-modular feedforward neural network for handwriting recognition. *Pattern Recognition*, 35(1):229–244, 2002. Shape representation and similarity for image databases.
- [68] Yuxuan Huang, Luiz Fernando Capretz, and Danny Ho. Neural network models for stock selection based on fundamental analysis, 2019.
- [69] R. Zemouri, N. Omri, B. Morello, C. Devalland, L. Arnould, N. Zerhouni, and F. Fnaiech. Constructive deep neural network for breast cancer diagnosis. *IFAC-PapersOnLine*, 51(27):98–103, 2018. 10th IFAC Symposium on Biological and Medical Systems BMS 2018.
- [70] Osvaldo Simeone. A very brief introduction to machine learning with applications to communication systems. *IEEE Transactions on Cognitive Communications and Networking*, 4(4):648–664, 2018.
- [71] Neil Thompson, Kristjan Greenewald, Keeheon Lee, and Gabriel Manso. The computational limits of deep learning. 07 2020.
- [72] Nariman Farsad and Andrea Goldsmith. Neural network detection of data sequences in communication systems. *IEEE Transactions on Signal Processing*, 66(21):5663–5678, 2018.
- [73] Muhammet Nuri Seyman and Necmi Taşpınar. Channel estimation based on neural network in space time block coded mimo–ofdm system. *Digital Signal Processing*, 23(1):275–280, 2013.
- [74] Tobias Gruber, Sebastian Cammerer, Jakob Hoydis, and Stephan ten Brink. On deep learning-based channel decoding. In *2017 51st Annual Conference on Information Sciences and Systems (CISS)*, pages 1–6, March 2017.

-
- [75] Mark Eisen, Clark Zhang, Luiz F. O. Chamon, Daniel D. Lee, and Alejandro Ribeiro. Learning optimal resource allocations in wireless systems. *IEEE Transactions on Signal Processing*, 67(10):2775–2790, 2019.
- [76] Toshiaki Koike-Akino, Ye Wang, David S. Millar, Keisuke Kojima, and Kieran Parsons. Neural turbo equalization: Deep learning for fiber-optic nonlinearity compensation, 2019.
- [77] Govind P. Agrawal. Nonlinear fiber optics: its history and recent progress "invited". *J. Opt. Soc. Am. B*, 28(12):A1–A10, Dec 2011.
- [78] Ezra Ip and Joseph M. Kahn. Compensation of dispersion and nonlinear impairments using digital backpropagation. *Journal of Lightwave Technology*, 26(20):3416–3425, 2008.
- [79] Valey Kamalov, Ljupcho Jovanovski, Vijay Vusirikala, Shaoliang Zhang, Fatih Yaman, Kohei Nakamura, Takanori Inoue, Eduardo Mateo, and Yoshihisa Inada. Evolution from 8qam live traffic to ps 64-qam with neural-network based nonlinearity compensation on 11000 km open subsea cable. In *2018 Optical Fiber Communications Conference and Exposition (OFC)*, pages 1–3, 2018.
- [80] Julian Renner, Tobias Fehenberger, Metodi P. Yankov, Francesco Da Ros, Søren Forchhammer, Georg Böcherer, and Norbert Hanik. Experimental comparison of probabilistic shaping methods for unrepeated fiber transmission. *Journal of Lightwave Technology*, 35(22):4871–4879, 2017.
- [81] Christopher Bishop. *Pattern Recognition and Machine Learning*. Springer, 2006.
- [82] Richard S. Sutton and Andrew G. Barto. *Reinforcement Learning: An Introduction*. MIT Press, 2018.
- [83] Yoshua Bengio Ian Goodfellow and Aaron Courville. *Deep Learning*. MIT Press, 2016.
- [84] Sebastian Raschka. *Python Machine Learning*. Packt Publishing, 2015.
- [85] C. Eun and E. J. Powers. A new volterra predistorter based on the indirect learning architecture. *IEEE Trans. Signal Process.*, 45(1):223–227, Jan. 1997.
- [86] Changsoo Eun and E.J. Powers. A new volterra predistorter based on the indirect learning architecture. *IEEE Transactions on Signal Processing*, 45(1):223–227, 1997.
- [87] Sapna Singh. Backpropagation learning algorithm based on levenberg marquardt algorithm. volume 2, pages 393–398, 10 2012.
- [88] J. McNicol, M. O’Sullivan, K. Roberts, A. Comeau, D. McGhan, and L. Strawczynski. Electrical domain compensation of optical dispersion [optical fibre communication applications]. In *OFC/NFOEC Technical Digest. Optical Fiber Communication Conference, 2005.*, volume 4, pages 3 pp. Vol. 4–, 2005.
- [89] Han Sun, Kuang-Tsan Wu, and Kim Roberts. Real-time measurements of a 40 gb/s coherent system. *Opt. Express*, 16(2):873–879, Jan 2008.

-
- [90] Tomislav Drenski and Jens C. Rasmussen. Adc/dac and asic technology trends. In *2019 24th OptoElectronics and Communications Conference (OECC) and 2019 International Conference on Photonics in Switching and Computing (PSC)*, pages 1–3, 2019.
- [91] Robert Maher, Kevin Croussore, Matthias Lauermann, Ryan Going, Xian Xu, and Jeff Rahn. Constellation shaped 66 gbd dp-1024qam transceiver with 400 km transmission over standard smf. In *2017 European Conference on Optical Communication (ECOC)*, pages 1–3, 2017.
- [92] Hiroshi Yamazaki, Munehiko Nagatani, Shigeru Kanazawa, Hideyuki Nosaka, Toshikazu Hashimoto, Akihhide Sano, and Yutaka Miyamoto. Digital-preprocessed analog-multiplexed dac for ultrawideband multilevel transmitter. *Journal of Lightwave Technology*, 34(7):1579–1584, 2016.
- [93] Ian Dedic. 56gs/s adc : Enabling 100gbe. In *2010 Conference on Optical Fiber Communication (OFC/NFOEC), collocated National Fiber Optic Engineers Conference*, pages 1–3, 2010.
- [94] Yuriy M Greshishchev, Jeorge Aguirre, Marinette Besson, Robert Gibbins, Chris Falt, Philip Flemke, Naim Ben-Hamida, Daniel Pollex, Peter Schvan, and Shing-Chi Wang. A 40gs/s 6b adc in 65nm cmos. In *2010 IEEE International Solid-State Circuits Conference - (ISSCC)*, pages 390–391, 2010.
- [95] Roman Dischler. Experimental study of 16-, 32- and 64-qam constellation sets in the 200-gb/s regime on a data rate flexible system. In *2013 Optical Fiber Communication Conference and Exposition and the National Fiber Optic Engineers Conference (OFC/NFOEC)*, pages 1–3, 2013.
- [96] Luke-es 55–65g saamples/s 8 bit adc. Technical report, Fujitsu Microelectronics Limited, 2012 <https://www.fujitsu.com/uk/Images/c63.pdf>.
- [97] J. Cho, X. Chen, S. Chandrasekhar, G. Raybon, R. Dar, L. Schmalen, E. Burrows, A. Adamiecki, S. Corteselli, Y. Pan, D. Correa, B. McKay, S. Zsigmond, P. Winzer, and S. Grubb. Trans-atlantic field trial using probabilistically shaped 64-qam at high spectral efficiencies and single-carrier real-time 250-gb/s 16-qam. In *2017 Optical Fiber Communications Conference and Exhibition (OFC)*, pages 1–3, 2017.
- [98] Socionext takes part in record-breaking transmission field trial of 38.4tbps over 762 kilometers. *socionext.com*, Jun 2015.
- [99] J. Cho, X. Chen, S. Chandrasekhar, G. Raybon, R. Dar, L. Schmalen, E. Burrows, A. Adamiecki, S. Corteselli, Y. Pan, D. Correa, B. McKay, S. Zsigmond, P. Winzer, and S. Grubb. Trans-atlantic field trial using probabilistically shaped 64-qam at high spectral efficiencies and single-carrier real-time 250-gb/s 16-qam. In *2017 Optical Fiber Communications Conference and Exhibition (OFC)*, pages 1–3, 2017.
- [100] Y Guerfi and G Larrieu. Vertical silicon nanowire field effect transistors with nanoscale gate-all-around. *Nanoscale Research Letter*, 11(210), 2016.

-
- [101] Antonio Napoli, Mahdi M. Mezghanni, Danish Rafique, Vincent A. J. M. Sleiffer, Talha Rahman, Bernhard Spinnler, Stefano Calabrò, and Marc Bohn. Novel dac digital pre-emphasis algorithm for next-generation flexible optical transponders. In *Optical Fiber Communication Conference*, page Th3G.6. Optical Society of America, 2015.
- [102] Yaron Yoffe, Eyal Wohlgemuth, and Dan Sadot. Digitally enhanced dac: Low-resolution digital pre-compensation for high speed optical links. In *2018 Optical Fiber Communications Conference and Exposition (OFC)*, pages 1–3, 2018.

